1990

Spontaneously adsorbed monolayer films: fabrication, characterization, and application of monolayers of alkanethiol and sulfur-bearing cyclodextrin derivatives

Chinkap Chung
Iowa State University

Order Number 9101341

Spontaneously adsorbed monolayer films: Fabrication, characterization, and application of monolayers of alkanethiol and sulfur-bearing cyclodextrin derivatives

Chung, Chinkap, Ph.D.

Iowa State University, 1990

U·M·I
300 N. Zeeb Rd.
Ann Arbor, MI 48106

Spontaneously adsorbed monolayer films : Fabrication, characterization, and application of monolayers of alkanethiol and sulfur-bearing cyclodextrin derivatives

by

Chinkap Chung

A Dissertation Submitted to the
Graduate Faculty in Partial Fulfillment of the
Requirements for the Degree of
DOCTOR OF PHILOSOPHY

Department : Chemistry
Major : Analytical Chemistry

Approved:

Signature was redacted for privacy.

Signature was redacted for privacy.

In Charge of Major Work

Signature was redacted for privacy.

For the Major Department

Signature was redacted for privacy.

For the Graduate College

Iowa State University
Ames, Iowa

1990

TABLE OF CONTENTS

ABSTRACT

Monolayers of *n*-alkanethiols ($CH_3(CH_2)_nSH$, n=1-17) and sulfur-bearing cyclodextrin derivatives spontaneously adsorbed on Ag and Au have been studied with a variety of surface characterization methods, such as infrared reflection spectroscopy, contact angle measurements, electrochemistry, optical ellipsometry, and scanning tunneling microscopy.

Long chain *n*-alkanethiols monolayers on Ag and Au are insulating to electron transfer and have contact angles indicative of well-ordered hydrocarbon terminated structures. Infrared and contact angle data indicate a different orientation of the methyl group with respect to the surface for chains with odd and even numbers of methylene groups. Compared to monolayers on Au, the alkanethiol monolayers on Ag are oriented more towards the surface normal. The observed odd-even effect of methyl group orientation for these monolayers on Ag is offset by a methylene group from that on Au. The relationships between the structure and packing of the monolayers on Ag and Au and the composition, roughness, and crystallinity of the substrate are also discussed.

Monolayers of sulfur-bearing cyclodextrin derivatives on Au and Ag are fabricated by spontaneous adsorption and characterized by the above techniques. Size-selectivity and molecular recognition of the α- and β-cyclodextrin cavity are shown with our monolayers. Because of molecular recognition, *p*-nitrophenol is retained preferrentially by the cyclodextrin monolayers over *o*-nitrophenol. Infrared spectroscopic evidence of the molecular recognition of monolayers is more reproducible than

electrochemical evidence. Potential applications of these monolayers are also discussed.

GENERAL INTRODUCTION

In recent years, electroanalytical chemists have become fascinated with the construction, characterization, and application of chemical microstructures at electrode surfaces. Efforts have also begun to explore the potential benefits of organized monolayer films. The main goal has been to manipulate the molecular architecture of the electrode surface, thereby controlling the rate and/or selectivity of a heterogeneous electron-transfer process.

The work described in this dissertation is a part of a larger effort to understand the structure-reactivity relationship of monolayers made by spontaneous adsorption process, and to apply this method to the fabrication of monolayers which will impart a specific chemical function to an interface. This dissertation is composed of two parts. The author was initially been involved with the fabrication of molecular recognition monolayers of cyclodextrin derivatives, which is described at Part II of this dissertation. In the process, we observed an intriguing difference in the apparent structure of various monolayers at Ag and Au as a substrate. We, therefore, undertook a detailed study to examine the structure and interfacial properties of monolayers of *n*-alkanethiols at Ag and Au, which is described in Part I. The monolayers of *n*-alkanethiols at Au have been studied before, although there are several intriguing differences in the observations of different research groups. As such, our work reexamined the structure and interfacial properties of *n*-alkanethiols monolayers on Au, and extended into a comparable effort for these monolayers at Ag. The detailed comparison

between of the monolayers on Ag and Au is also presented. We have used a variety of surface sensitive techniques to characterize the monolayers. The author of this dissertation was extensively involved in this effort, with part of the experimental data and interpretation obtained in collaboration with colleagues in our research group. Infrared reflection spectroscopy was mainly done by Scott Stole and scanning tunnelling microscopy was mainly done by Dr. Cindra Widrig; the data and discussions with Dr. Cindra Widrig, Dr. Mary Walczak and Scott Stole are vital to the development of Part I of this dissertation. Part II represents work performed solely by this author.

PART I. SPONTANEOUSLY ADSORBED MONOLAYERS OF ALKANETHIOLS ON GOLD AND SILVER SURFACES: FABRICATION, STRUCTURE, AND INTERFACIAL PROPERTIES.

ABSTRACT

Monolayers of *n*-alkanethiols ($CH_3(CH_2)_nSH$, n=1-17) spontaneously adsorbed on Ag and Au have been studied. A variety of surface characterization methods, such as infrared reflection spectroscopy, contact angle measurements, electrochemistry, optical ellipsometry, and scanning tunneling microscopy have been applied as probes of the structure of these monolayers.

Long chain *n*-alkanethiols monolayers on Ag and Au are insulating to electron transfer and have contact angles indicative of well-ordered hydrocarbon terminated structures. Infrared and contact angle data indicate a different orientation of the methyl group with respect to the surface for chains with odd and even numbers of methylene groups. Compared to monolayers on Au, the alkanethiol monolayers on Ag are oriented more towards the surface normal. The observed odd-even effect of the methyl group orientation for alkanethiol on Ag is offset by a methylene group from that on Au, which is indicative of a difference in the bonding of the thiolate head group to Ag relative to Au. The relationships between the structure and packing of the monolayers on Ag and Au and the composition, roughness, and crystallinity of the substrate surfaces are also discussed.

INTRODUCTION

Spontaneously adsorbed monolayers of organic molecules have been investigated extensively in recent years [1-7]. The formation of monolayers from organosulfur functionalized precursors continues to be examined as a rational approach toward the fabrication of interfaces with specific structural and interfacial properties. As illustrated in Figure I-1 for a *n*-alkanethiol at Au(111), these monolayers form spontaneously upon immersion of a metal substrate into dilute solutions of a sulfur-containing compound. *n*-Alkanethiol monolayers form highly ordered, densely packed structures at Au with the alkyl chains tilted ~30° from the surface normal [8-10]. These monolayers are not wetted by water or hexadecane [8] and are resistant to ion and electron transport [9]. Thiol adsorption kinetics at Au are fast, with only a few hours required to achieve limiting ellipsometric thicknesses [8]. The energy of the S-Au bond is estimated at ~28 kcal/mol [11]. As the length of the alkyl chain increases, the chemisorption bond strength also increases [10], confirming the importance of cohesive hydrophobic interactions between adjacent chains on the stability of the monolayer. The average (macroscopic) properties of the monolayers (e.g., chain tilt, orientation, and density) are well known. However, several fundamental questions regarding the microscopic structure of the monolayer remain. For instance, the bonding between the sulfur and gold is not well understood. The adsorption mechanism is frequently assumed to proceed with a loss of the proton of the thiol, resulting in a surface thiolate (i.e., R-S-Au). Although we agree with this mechanism, there is, as yet, no direct evidence of thiolate formation or

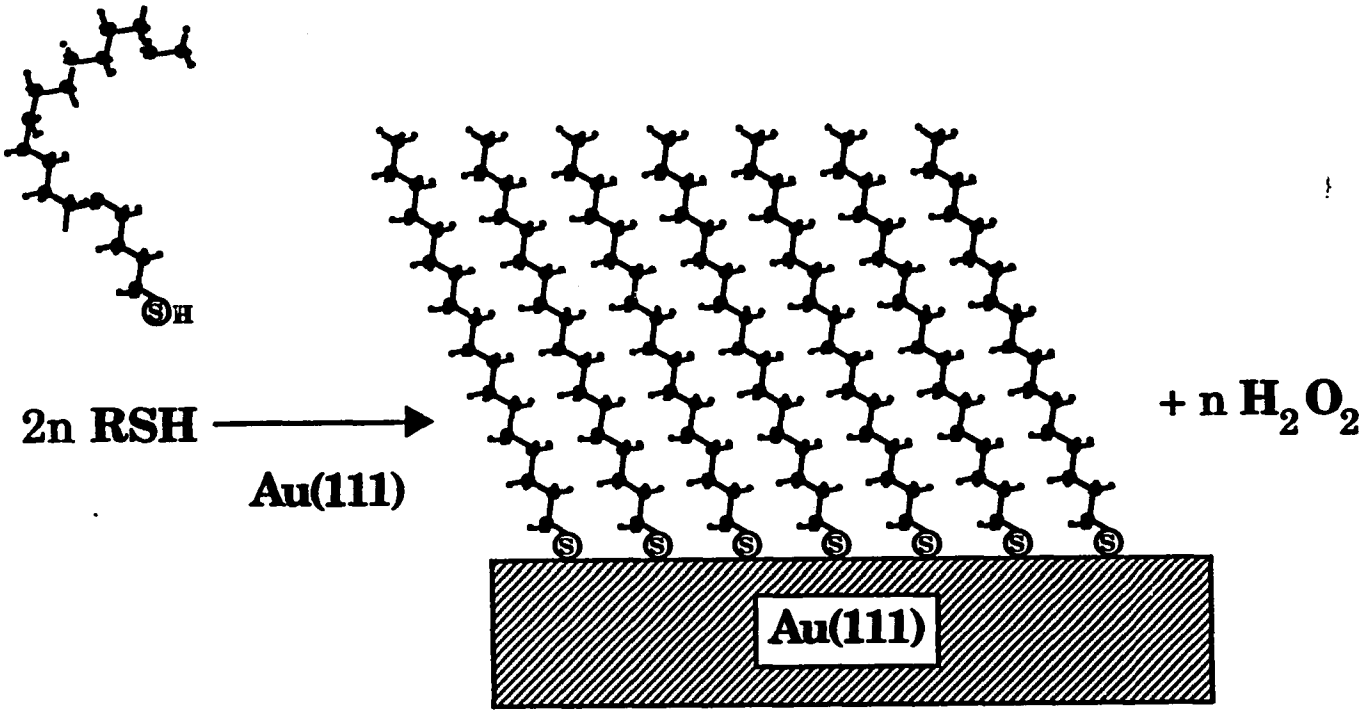

Figure I-1. Monolayer formation of an alkanethiol on Au(111) surface.

hydrogen loss in the literature. We have addressed this problem with electrochemical desorption experiments as a function of solution pH, and results will be discussed shortly [12]. Briefly, we find the thiol is oxidized to RS^- and O_2 is reduced to H_2O_2 during adsorption (i.e., $2RSH + {}^{\circ}2Au + O_2 = 2RSAu + H_2O_2$).

Another compelling issue about the microscopic structure of thiol monolayers is the two dimensional periodicity of the films. Surface characterization methods, such as infrared reflection spectroscopy and contact angle measurements, provide evidence for a densely packed array of molecules. Together, electron [13] and He [14] diffraction and scanning tunneling microscopy [15] studies have firmly established the presence of a hexagonally ordered surface phase that is consistant with a $(\sqrt{3} \times \sqrt{3})R30°$ overlayer at Au(111). Although likely, the $(\sqrt{3} \times \sqrt{3})R30°$ pattern has not been verified, since no measurement has been made which can index both the substrate and overlayer without sample repositioning.

As part of our interests in this area, we have explored the range and scope of the applicability of spontaneously adsorbed monolayers both as probes and modifiers of reactivity at liquid-solid interfaces. These efforts have focused in part on examining the molecular level details that control the attachment, spatial arrangement, and packing of these adsorbates, and in part on devising novel interfacial structures that provide for the selective control of heterogeneous reactivity. During the survey in which the potential utility of various metals as substrates for the formation of sulfur-containing monolayers was examined, we observed an intriguing difference in the apparent structure of *n*-alkanethiol monolayers at Ag and Au. We, therefore,

undertook a detailed study to examine the structure and interfacial properties of monolayers of *n*-alkanethiols at Ag.

This part of the dissertation reports our results of a detailed examination of the structure and interfacial properties of spontaneously adsorbed monomolecular films of *n*-alkanethiols ($CH_3(CH_2)_nSH$, n=1-17) at the surface of evaporated Ag films. We discuss a detailed comparison of monomolecular assemblies of the *n*-alkanethiols at the surfaces of evaporated Ag and Au films. The emerging importance of the identity, crystallinity, and roughness of the substrate on the structure and packing of the monolayer is of particular interest. Structural descriptions are deduced through the application of a variety of surface characterization methods: infrared reflection spectroscopy, optical ellipsometry, contact angle measurements, electrochemical measurements, and scanning tunneling microscopy. Infrared reflection spectroscopy, capacitance measurements, and optical ellipsometry are used to probe the average molecular structure of the monolayers. Contact angle measurements are used to assess the hydrophobicity of the surface. Underpotential metal deposition and scanning tunneling microscopy (STM) are used to examine both the roughness and crystallinity of the surfaces of Ag and Au films. Together, these data provide insights into thickness, packing density, spatial and conformational arrangement of the alkyl chains. Further, the importance of the identity, crystallinity, and roughness of the supporting metal is tractable.

EXPERIMENTAL

Reagent and Monolayer Preparation

Reagents

Deionized water was obtained from a Milli-Q purification system (Millipore Products, Bedford, MA). Absolute ethanol (Midwest Grain, Pekin, IL) and hexane (HPLC grade, Fisher Scientific, Pittsburgh, PA) were used as received. Prior to use, hexadecane (Aldrich Chemical Co., Milwaukee, WI) was repeatedly (usually twice) percolated through an activity 1 neutral α-alumina column until passing the Zisman test [16,17]. Liquid alkanethiols ($CH_3(CH_2)_nSH$ with n = 1-9, 11, 13, 15) were acquired from several sources (Alfa Products, n=1; Aldrich, n=2,4,6,7,8,15; Eastman Kodak, n=3,5,9,11; Pflatz and Bauer, Inc., n=13) and were purified by passage through an activity 1 neutral α-alumina (Aldrich) column just prior to use. Tridecanethiol, pentadecanethiol, and eicosanethiol were synthesized from 1-bromotridecane (Aldrich), 1-bromopentadecane (Aldrich), and 1-bromoeicosane (Sigma), respectively, with thioacetic acid (Aldrich) [8]. Deutrated thiols were synthesized with the same method for the perhydrido analog of corresponding thiols from starting material $CD_3(CH_2)_{19}Br$ (D 99%, Cambridge Isotope) and $C_{18}D_{37}Br$ (D 99%, Cambridge Isotope). The nuclear magnetic resonce spectra of the compounds synthesized were comparable with literature data [8]. *n*-Octadecanethiol (Aldrich) was recrystallized from ethanol. Undecanethiol and heptadecanethiol were gifts from Professor

George Whitesides (Department of Chemistry, Harvard University). All other chemicals were reagent grade unless otherwise specified.

Metal film preparation

Silver substrates were prepared by the resistive evaporation of 15-20 nm of Cr, followed by 250-300 nm of Ag or Au onto 2 inch diameter polished p-type silicon (111) wafers (Virginia Semiconductors, Inc., Fredricksburg, VA). The evaporation rates, which were measured with a quartz thickness monitor, were 0.2, 0.8, 2.5-3.0 nm/s for Cr, Au and Ag, respectively. The pressure in a cryopumped E360A Edwards Coating System during evaporation was $<9\times10^{-5}$ Pa (7×10^{-7} Torr). After ~45min. cooling time, the evaporator was back-filled with purified N_2 and the substrates were removed.

Metal film characterization

The surface composition was examined by Auger electron spectroscopy (AES) in a PHI Auger Multiprobe 600 system. In addition to evaporated Ag and Au, the evaporated metal surfaces are composed of sulfur, chlorine, carbon, and oxygen. Table I-1 summarizes the peak energies and normalized intensities of the prominent features: the intensities are normalized to Ag. Oxygen is attributed to a "native" oxide, resulting from exposure of clean Ag to oxygen. The observed O/Ag ratio, 0.02, is comparable to that for the (2x1) oxygen overlayer on Ag(110), corresponding to saturation surface coverage of 0.5 monolayers [18,19]. Sulfur, chlorine, and carbon are attributed to airborne impurities adsorbing upon the removal of the Ag substrates from the vapor deposition chamber.

Table I-1. Relative Auger intensities of adsorbates on bare Ag films. The ratios are the peak to peak height (differentiated spectra) of the adsorbate Auger peak divided by the peak to peak height of the Ag (356 eV) peak.

Element	Peak Energy (eV)	Relative Intensity (Normalized to Ag)
S	152	0.34
Cl	181	0.43
C	272	0.28
Ag	356	1.00
O	510	0.02

With further exposure to the ambient environment of the laboratory, the composition of the interface changes, as illustrated in Figure I-2. Upon increased exposure, the O/Ag Auger ratio increases, the C/Ag ratio remains essentially constant, and the Cl/Ag and S/Ag ratios decrease. Decreases in the Cl/Ag and S/Ag ratios are attributed to diffusion of Cl and S into the bulk Ag. The increase in the oxygen content of the films is consistent with the continued growth of the native oxide of Ag. The native oxide consists of both surface and subsurface oxygen [20-23] and is ~2-5 monolayers thick [24]. The predominant species comprising this thin oxide film is unknown, although studies have suggested a variety of possibilities (e.g., Ag_2O, AgO, AgO_2, and AgO_3) [25]. The highly basic nature of this oxide results in its hydration to a AgOH species in the presence of water [26]. Using contact angle titrations, we recently measured that this hydrated surface has an isoelectric point of ~10.2 [27].

The growth of the oxide layer has important implications with regard to sample preparation. We observed that monolayers prepared on substrates which were exposed to the ambient environment of the laboratory for different periods of time exhibited slightly different structures, as evidenced by IR spectral data. To minimize the variation in the substrate composition, the exposure to laboratory ambient was limited to 10-15 minutes before being placed in the thiol-containing solution. The data presented in this report are representative of this procedure.

Monolayer preparation

Alkanethiol monolayers were spontaneously adsorbed onto freshly evaporated Ag or Au substrates from dilute (0.1-1.0 mM) solutions in absolute

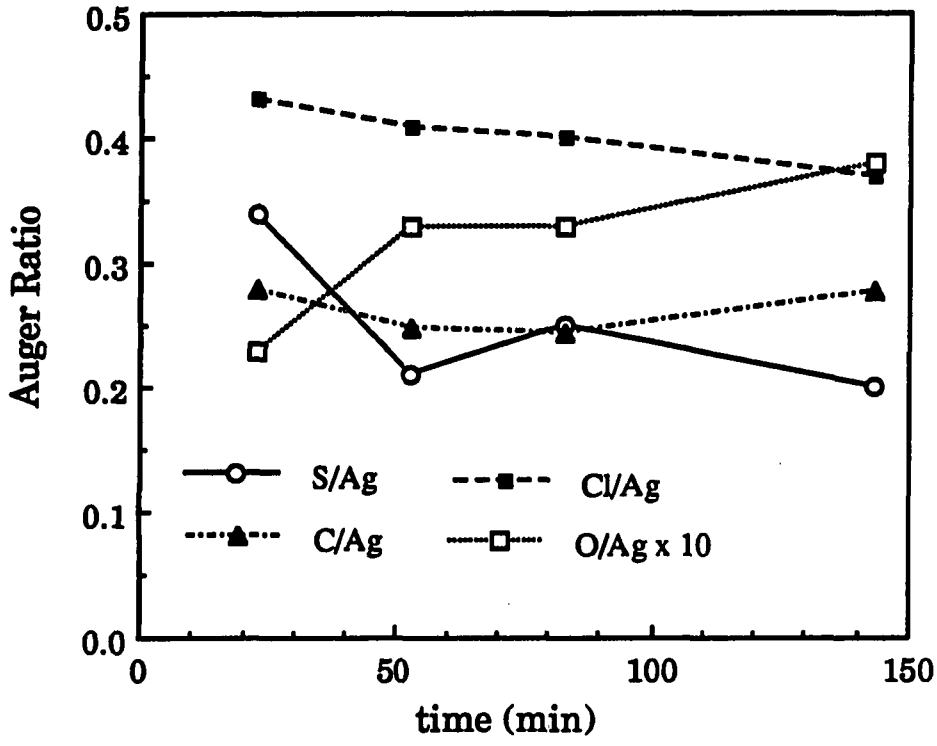

Figure I-2. Changes in the adsorbate/Ag Auger ratios on exposure to the ambient environment of the laboratory. The electron beam energy was 3kV, the current density was 0.6 mA/cm^2.

ethanol. After 12-24 hours, the samples were emersed, rinsed successively with absolute ethanol and hexane to remove residual solution, and dried on a photoresist spin-coater (Headway Research Inc., Garland, TX). Prior to solution preparation, the alkanethiols were purified by either recrystallization from absolute ethanol or by passage through an activity 1 neutral α-alumina column. The formation of monolayers is monitored by ellipsometry. These monolayers form quickly with no apparent differences in structure after an immersion of a few hours.

Silver films dissolve slightly when immersed in ethanolic solution. After soaking a Ag substrate ~20 hours in either absolute ethanol or ethanolic thiol-containing solutions, the solvent contains 5-8 ppm Ag, as determined in-house with Inductively Coupled Plasma Atomic Emission Spectroscopy (ICPAES). Surface roughening, which is emerging as an important factor in the structure of adsorbed monolayers, may occur as a result of this corrosion.

Characterization of Monolayers

Ellipsometric measurements of film thickness

The thicknesses of the monolayers were monitored and determined by optical ellipsometry with a computer-interfaced Gaertner Model L-116B Auto Gain ellipsometer at a wavelength of 632.8 nm (He-Ne laser).

The procedure consisted of two steps. First, the analyzer and polarizer angles for a reflected light beam from the uncoated substrates were measured at several spots immediately upon removal from the evaporation chamber. The complex refractive indices for the substrates were calculated with a two-phase parallel layer model from classical electromagnetic theory [28-30].

After monolayer formation, samples were again analyzed with the film thicknesses determined from a three-phase parallel layer model. The actual calculations of monolayer thicknesses were done with Gaetner SC6A automatic ellipsometric program provided with the ellipsometer. The real refractive index for the films was assumed to equal 1.45. This assumption neglects a consideration of the packing density of the alkyl chains. Densely packed chains may be more appropriately represented by the refractive index of polyethylene, which equals 1.5 [31]. A value of 1.45, however, permits a direct comparison with the thickness data that have been reported for a variety of other monolayer films. The influence of several possible refinements to our treatment of the ellipsometric data is deferred to a later section.

The growth of monolayers was monitored with ex situ and in situ ellipsometry. With ex situ measurements, the thicknesses of the monolayers were determined after removal from the thiol solution and extensive rinsing. After an immersion of 2 hours, there were no observable differences in film thickness for immersion times up to 96 hours.

In situ ellipsometry is performed with a home-made in situ ellipsometric cell with 70° incident angle of light. The basic design of the in situ cell can be found in the reference [32]. The substrate is immersed into the solution contained in the cell. After the substrate constant was measured, the thickness of the film was monitored in every 30 seconds. A drop of dilute thiol solution was added after 10 min. stabilization period. The thickness of the monolayers was calculated with the Gaetner GC4A in situ ellipsometry program provided by the Gaetner Scientific Co. When the

growth of *n*-octadecanethiol monolayers on Au was monitored with in situ ellipsometry, the film thickness increased to ~55Å in an hour, which is about twice that of the monolayer thickness measured after taken out of a solution. We think this difference is due to "bilayer" formation in the solution. Upon emersion from the solution and subsequent rinsing, the bilayer structure is destroyed leaving a monolayer.

Contact angle measurements

Contact angles of monolayers with hexadecane and deionized water as probe liquids were measured in air with a Rame-Hart Model 100-00 115 goniometer. Both advancing and receding contact angles were measured. When the boundary between the liquid drop and substrate starts moving, the contact angle is measured as an advancing contact angle, θ_a. Receding contact angle, θ_r, is measured when the boundary withdraws as the volume of the droplet decreases. A ~2μl droplet is formed on the substrate (with the needle of a syringe in the droplet) and the volume of the droplet slowly increases. The uncertainty in the angles, based on replicate experiments (sample to sample variation) is ±1° for hexadecane as the probe liquid; with water as the probe liquid, the uncertainty increases to a few degrees.

Infrared absorption spectroscopy.

Infrared spectra were acquired with a Nicolet 740 FT-IR (Nicolet Analytical Instruments, Madison, WI) spectrometer optimized for grazing angle reflection measurements. The p-polarized light was incident at 80°. An internally-designed sample holder was used to position reproducibly the substrates in the spectrometer. The spectrometer was purged with boil-off

from liquid N_2. Spectra were obtained by coaddition of 1024 sample scans to background scans at 2 cm^{-1} resolution (zero filled) with Happ-Genzel apodization. A liquid N_2 cooled InSb or MCT detector was used to monitor the intensity of the reflected beam. All spectra were reported as $-\log(R/R_0)$ where R is the reflectivity of the sample and R_0 is the reflectivity of a bare Au reference substrate.

Bare Au references [9] were prepared by immersion in 1:3 30% H_2O_2:con. H_2SO_4 solution for 5-10 minutes, and subsequent rinsing in deionized water and 30% H_2O_2. The references were then spun to near-dryness on a photoresist spin coater and placed immediately into the sample chamber of the spectrometer. After allowing the reference to dry in the N_2-purged chamber, the reference spectrum was recorded. ***Caution:*** *The oxidizing acidic solution reacts violently with organic compounds and should be handled with extreme care.*

In some cases, a monolayer of deutrated octadecanethiol ($C_{18}D_{37}SH$) spontaneously adsorbed on Au was used as a reference. As shown in Figure I-3, the infrared spectrum of the monolayer does not exhibit any features in the C-H stretching region, viz. 3200-2600cm-1 range. This reference monolayer was stable and could be used at least for 2 weeks without any further treatment. Furthermore, the use of 1:3 30% H_2O_2:con. H_2SO_4 solution for preparing a "bare" reference substrate can be avoided.

Electrochemical measurements

Cyclic voltammetry was performed with either a CV-27 potentiostat (Bioanalytical Systems, Inc., West Lafayette, IN) or a CYSY-1 Computer Controlled Electroanalytical System (Cypress Systems, Lawrence, KS). The

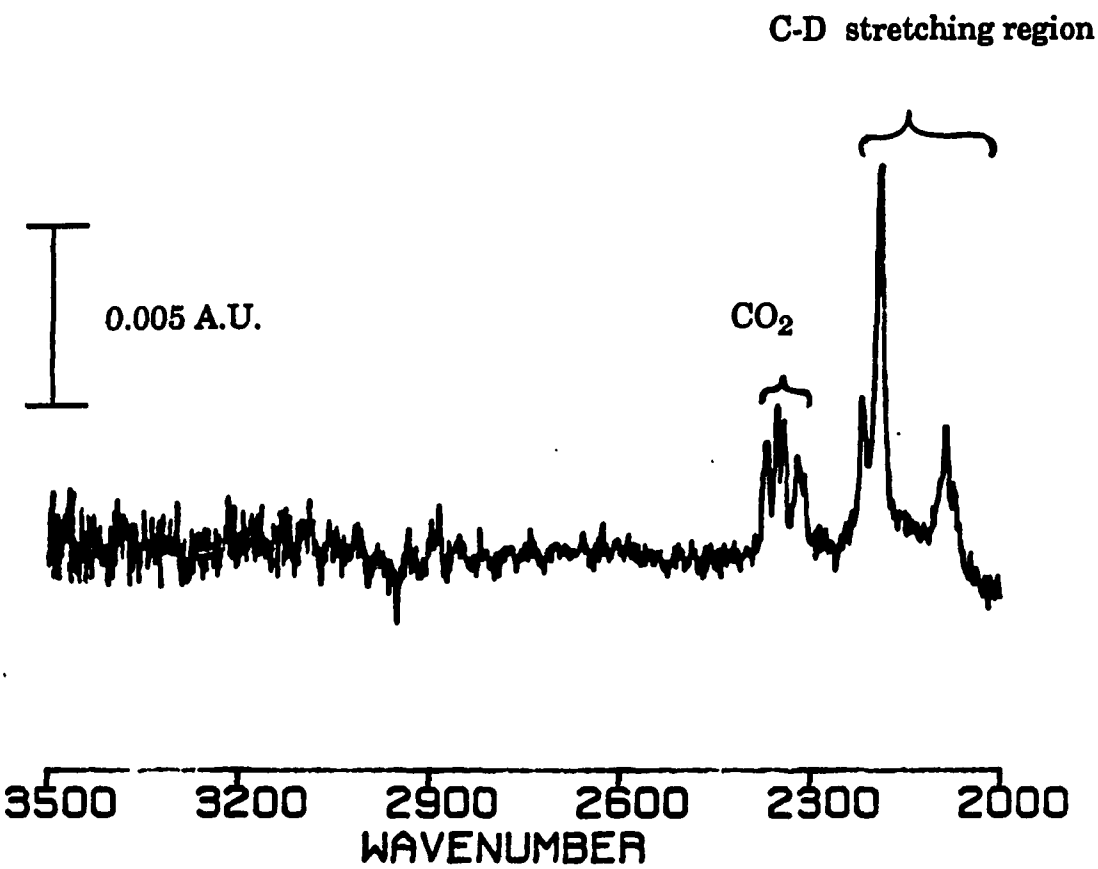

Figure I-3. Infrared reflection spectrum of $C_{18}D_{37}SH$ monolayer adsorbed on Au.

Ag or Au substrates were mounted in a conventional three-electrode cell with an exposed electrode area of 0.24 cm^2. Solutions were deoxygenated with water-saturated Ar (Air Products) or N_2 (Air Products) for 30 minutes. All potential measurements are reported with respect to a Ag/AgCl/ sat'd KCl electrode.

Scanning tunneling microscopy

The evaporated Ag and Au films were examined in air with a NanoScope II (Digital Instruments, Inc., Santa Barbara, CA) scanning tunneling microscope. The tips were prepared by electrolytically etching 0.25 mm diameter tungsten wire in 1 M KOH. The tips which did not image highly ordered pyrolytic graphite (HOPG) with 0.24 nm spacing were discarded. Lateral resolution, based on replicate measurements of the interatom spacing on HOPG, is estimated at ±0.04 nm. The microscope was operated in constant current mode with 1 nA tunneling current and 80 mV bias voltage.

RESULTS AND DISCUSSIONS

The first part of this section will discuss the average structure of the monolayers characterized with optical ellipsometry, contact angle measurements, electrochemical measurements, and infrared spectroscopy. Then, the microscopic aspects of monolayer formation, which deal with relationships between the composition, roughness, and crystallinity of the substrates and the structure of resulting monolayers, will be discussed, followed by scanning tunneling microscopic data and underpotential metal deposition results. Finally, the apparent differences and possible explanations of these differences for the structure of monolayers on Au and Ag will be discussed.

Average Structure of Alkanethiol Monolayers

There is no single experimental technique which can provide all the answers to the questions concerning the monolayer structure. We, therefore, employed a variety of complementary techniques, which together, provide us with a detailed structure picture of monolayers. Some of these techniques probe the *average* or bulk properties of monolayers; others provide information about microscopic defects, structural order, and binding interactions between a monolayer and a substrate.

Optical ellipsometry provides the average thickness of monolayers. Capacitive current measurements reveal the permeability of the monolayers to the small ions, as well as provide an estimation of the film thickness, which complements the ellipsometric data. Measurements of the contact angle between a probe liquid and a surface is a convenient approach for assessing

both the wettability and interfacial composition of an organic surface [33-35]. It also provides information about the exposed chain terminus. For example, a methylene group exhibits a lower contact angle than a methyl group, which means that contact angle of a less tilted alkyl chain is higher than that of a more tilted one. By measuring contact angle, we can estimate how the chain terminus is oriented on the exposed surface. Hysteresis in the contact angle measurement can also provide insights into the packing density of monolayer films. External reflection infrared spectroscopy is an extremely powerful approach for determining the chemical identity and average spatial orientation of monolayer films at metal surfaces. The chemical functionality of the organic surface structure can be deduced from the observed peak frequencies. The average spatial orientation of the structure can be deduced by virtue of the infrared metal surface selection rule [36]. Scanning tunneling microscopy and underpotential metal deposition data can provide information about crystallinity and roughness of surface as well as about defects in monolayer structures.

Optical ellipsometric characterization of monolayer film thickness

Optical ellipsometry is a convenient and accurate technique for the measurement of thicknesses and refractive indices of very thin films on solid surfaces [32]. Optical ellipsometry was used to determine the average thickness of the *n*-alkanethiol monolayers at Ag and Au. These thicknesses are plotted in Figure I-4 as a function of n, the number of methylene groups in the alkyl chain. These data are reasonably described by the solid line, which are linear regression fits with a slope of 1.3Å per CH_2 group and a y-intercept of 6.6Å for Ag, and a slope of 1.2Å per CH_2 group and a y-intercept

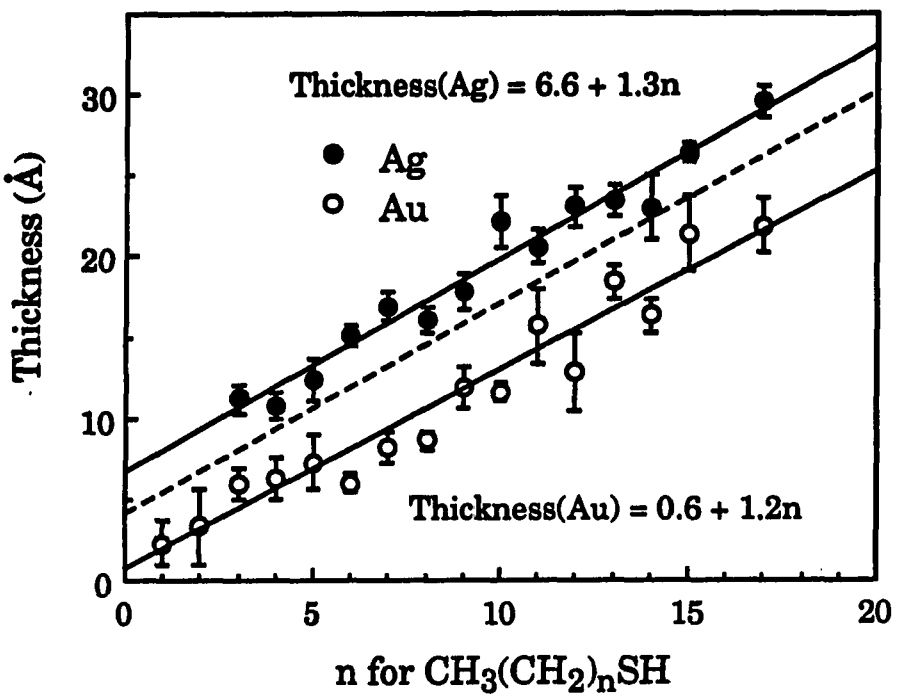

Figure I-4. Ellipsometric film thicknesses for *n*-alkanethiol monolayers ($CH_3(CH_2)_nSH$) adsorbed at Ag and Au. Uncertainties are standard deviations of measurements at 5-12 different samples with several locations on each. The dashed line represents the thickness of an all *trans*- alkyl chain extended normal to the surface (see text for details of the calculation).

of 0.6Å for Au. For comparison to a simple structural model, the dashed line represents the thicknesses for monolayers consisting of all *trans*- alkyl chains oriented with their molecular axes normal to the surface. This line has a slope of 1.3Å per CH_2 group and a y-intercept equal to 4.6Å. The intercept corresponds to the length methanethiolate (CH_3-S). Standard bond lengths and bond angles for the alkyl chains are used to calculate the thickness and it is assumed that the formation of the monolayer results in a silver (I) thiolate (S^- radius equal to 2.19 Å [37]).

The thickness data in Figure I-4 also provide a basis for a qualitative structural description of the monolayers. As noted, this Figure shows that the ellipsometric thicknesses increase linearly with chain length. This trend suggests a general consistency in both the conformation and spatial orientation of the alkyl chains that is independent of chain length. Further, a comparison of the slopes of the ellipsometric and calculated thicknesses suggests that the alkyl chains are oriented, within the uncertainty of the slope for the experimental data, close to the surface normal. We believe these thicknesses point to the presence of alkyl chains which contain all *trans*-conformational sequences, since the presence of disordered structures with a large number of gauche kinks is inconsistent with such small chain tilts. Such reasoning also implies that the alkyl chains exist as a densely packed structure. This interpretation does not, however, rule out the presence of disordered chain sequences in part of the monolayer structure. Disordered segments of the alkyl chains would most likely result from chains which are conformationally- or thermally-disordered [14] as a result of gauche kinks and/or weak cohesive interchain interactions. Extensively disordered chains

may also be present, however, we believe such structures are confined primarily to the regions of structural imperfections of the underlying substrate, *viz.* grain boundaries, which constitute only a small fraction of the surface area of the substrate.

Our treatment of the ellipsometric data is the same as described by others, allowing direct comparison to the growing body of ellipsometric data of ordered organic films. However, the limitations to this approach are evident from the fact that the *n*-alkanethiol monolayer thicknesses are consistently ~2 Å smaller than those calculated for the model structures in Figure I-4. These differences are not adequately accounted for by the experimental precision. Similar discrepancies with ellipsometric measurements have also been observed by both ourselves [9] and others [8] in recent studies of *n*-alkanethiol monolayers at Au, where the slopes and/or thicknesses were much larger than those predicted for fully extended chains normal to the surface. Although difficult to treat quantitatively, two factors stand out as major contributors to these differences. Both result from inadequacies in the three-phase isotropic structure used as a model of these interfaces: the refractive index of the adsorbed layer and the ubiquitous layer of adsorbed contaminants on the reference phase (i.e., the "bare" substrate).

Briefly, the ellipsometric measurements assume a chain length independent refractive index (n) of 1.45, a value which is representative of the adsorbate precursors [38] and facilitates comparison to thicknesses reported in the growing literature in this research area. More appropriate n's for the adsorbed monolayers may be 1.50 or 1.54, the values for polyethylene and an ordered hydrocarbon film in which the chains are tilted slightly from

the surface normal, respectively. The higher n's represent organic structures in which the chains are preferentially oriented with respect to one another, in a way similar to our emerging picture of the spontaneously adsorbed monolayers. Using larger n's to describe the organic film results in smaller thicknesses. Perhaps the most accurate representation is an n which varies with chain length and includes a consideration of the tensor nature of n. Since, by electrochemical evidence described later, short chain monolayers appear to be more disordered, long chain monolayers may have n's closer to 1.54, whereas the shorter chain monolayers may be adequately described by n~1.45 [36].

The inadequacies of the ellipsometric approach with respect to the reference phase arise directly from adventitiously adsorbed impurities from the ambient environment of the laboratory. Since the surface free energy of the bare Ag substrates is greater than that of the monolayer coated interfaces, greater amounts of impurities are likely present on the bare substrates. Further, as a result of the dependence of disorder on chain length described below, the difference in the amount of adsorbed contaminants may not be constant for all chain lengths. The inherently greater reactivity of Ag in comparison with the extensively studied substrate Au suggests this limitation in the ellipsometric model is a greater perturbation with Ag surfaces.

The effect of the adventitiously adsorbed contaminants is also to perturb the slope and intercept. However, it is not straightforward to estimate these effects quantitatively. To a first approximation, adsorbed

contaminants would have an effect similar to having a lower n (less hydrocarbon phase) so we would expect higher slopes and intercepts.

Irrespective of these quantitative limitations, ellipsometric thicknesses are useful for a qualitative assessment of monolayer structure. To summarize briefly, the ellipsometric thicknesses provide strong evidence for the formation of a film one molecular layer in thickness. Through a comparison with model calculations, these data support the presence of a densely-packed array of alkyl chains that are composed of all *trans*-conformational sequences with an average orientation along the surface normal. The aforementioned limitations in our ellipsometric treatment prohibit a description of more subtle features of structure.

Ellipsometric monitoring of the monolayer formation

To study the kinetics of octadecanethiol adsorption on Au, we used in situ ellipsometry. The cell is shown in Figure I-5. The growth of the layer on bare Au in ethanol is shown in Figure I-6. Upon injection of the thiol, the thickness increases with time, reaching a limit of ~55Å in less than 60 min., which is roughly twice of the thickness of the monolayer measured after taken out of solution and rinsed.

If the octadecanethiol forms a monolayer in the solution, the observed thickness should be around 25Å. To investigate the structure of octadecanethiol layer in the solution, we performed another experiment. If the octadecanethiol exists as a monolayer in the solution, the thickness of octadecanethiol layer will not change when we add octadecanethiol into ethanol in which an octadecanethiol monolayer has been immersed. Figure I-7 shows the thickness growth when we immersed an octadecanethiol

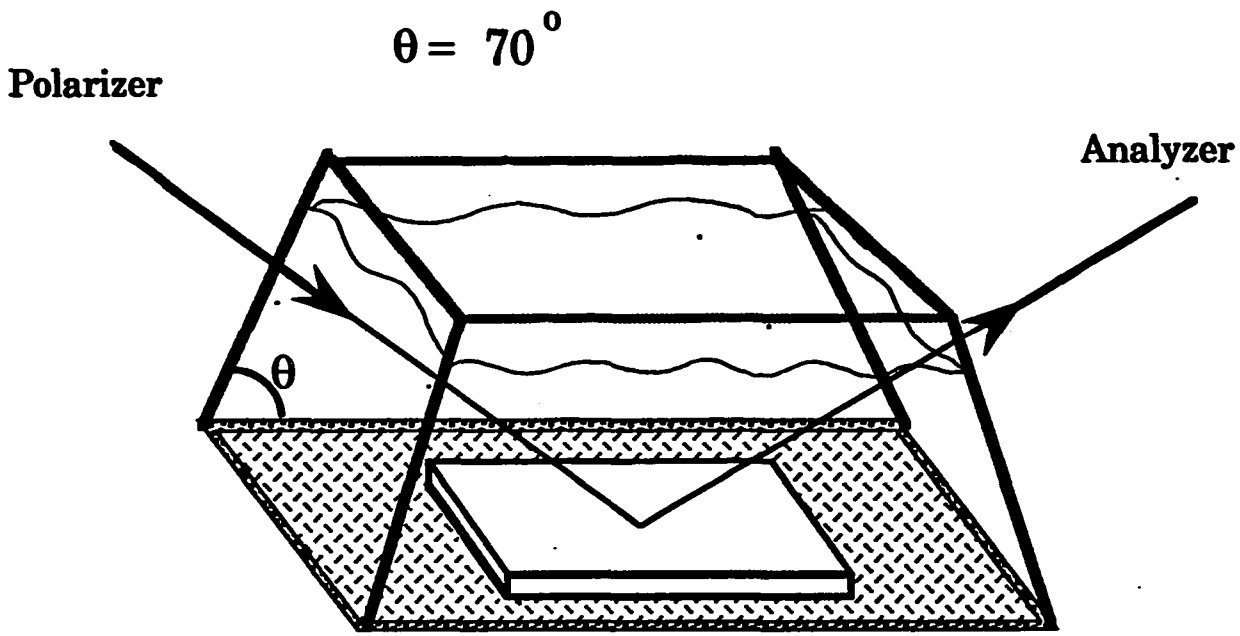

Figure I-5. **In-situ ellipsometric cell. The windows for light propagation are made of quartz and the rest of the cell is made of pyrex.**

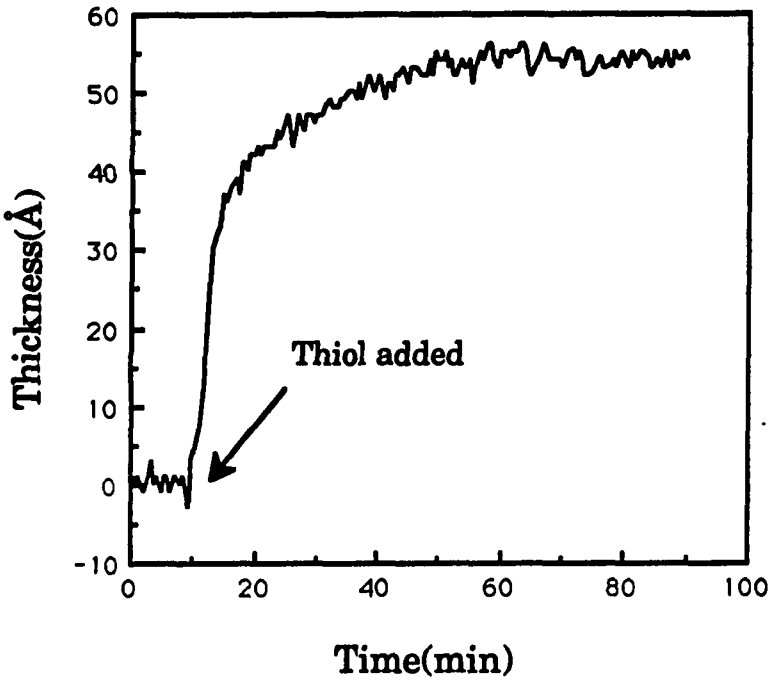

Figure I-6. Film thickness change of $C_{18}H_{37}SH$ monolayer adsorbed on Au. The substrate was bare Au. The thiol-containing solution was added 10 min. after the measurement was started. Data were acquired every 30 sec.

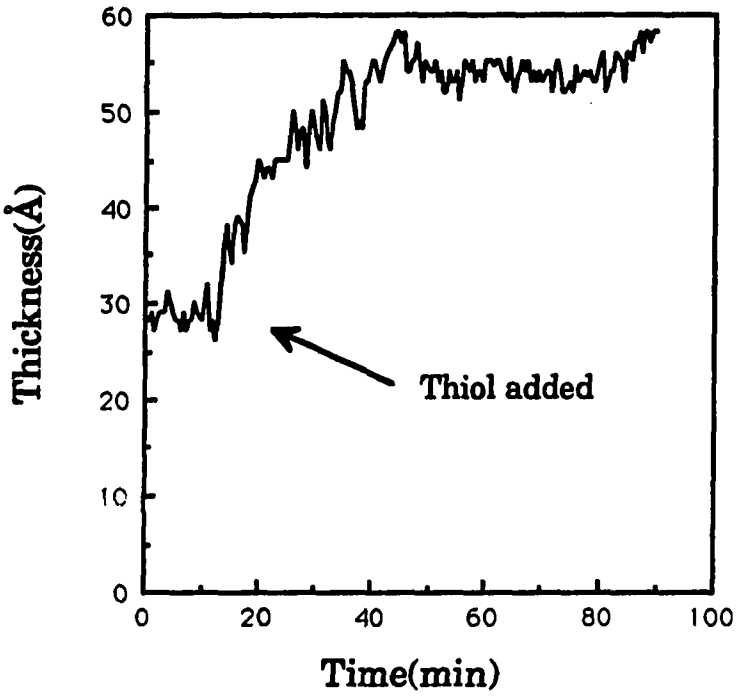

Figure I-7. Film thickness change of monolayer adsorbed on Au. Initial substrate has a monolayer of $C_{18}H_{37}SH$ adsorbed on top of Au. The thiol-containing solution was added 10 min. after the measurement was started.

monolayer into ethanol and added the same thiol to the solution. Before adding octadecanethiol, the thickness of monolayer remained constant in both the ethanol solution and air. However, the thickness increased by about 25Å upon addition of octadecanethiol to the ehtanol solution.

We believe that the alkanethiol exists as a bilayer in solution of alkanethiol. Upon removing from solution and rinsing with neat ethanol, the bilayer structure is destroyed, leaving only a chemisorbed monolayer on the substrate. If we immerse this monolayer into an octadecanethiol solution, an interdigitated bilayer is formed again with a total thickness of ~55Å. Figure I-8 is a conceptualization of the bilayer structure that we postulate.

Contact angle measurements of wetting characteristics and interfacial composition

The wetting characteristics of the *n*-alkanethiol monolayers were examined with contact angle measurements. The results for the advancing contact angles (θ_a) are given in Figure I-9 for the non-polar liquid hexadecane (HD) and the polar liquid water for Ag. The solid lines connect the θ_a's for the chains with an odd number of methylene groups and the dashed lines connect those for chains with an even number of methylene groups. For both probe liquids, θ_a's increase with n and approach limiting values. Limiting θ_a's are ~113° for water and ~44° for hexadecane. For both water and hexadecane, θ_a's are indicative of an extremely low surface free energy. Zisman plots, which were obtained with a series of probe liquids, yield a surface free energy of 16-17 dynes/cm for the long chain alkanethiol monolayers at Ag. These surface free energies are comparable to those

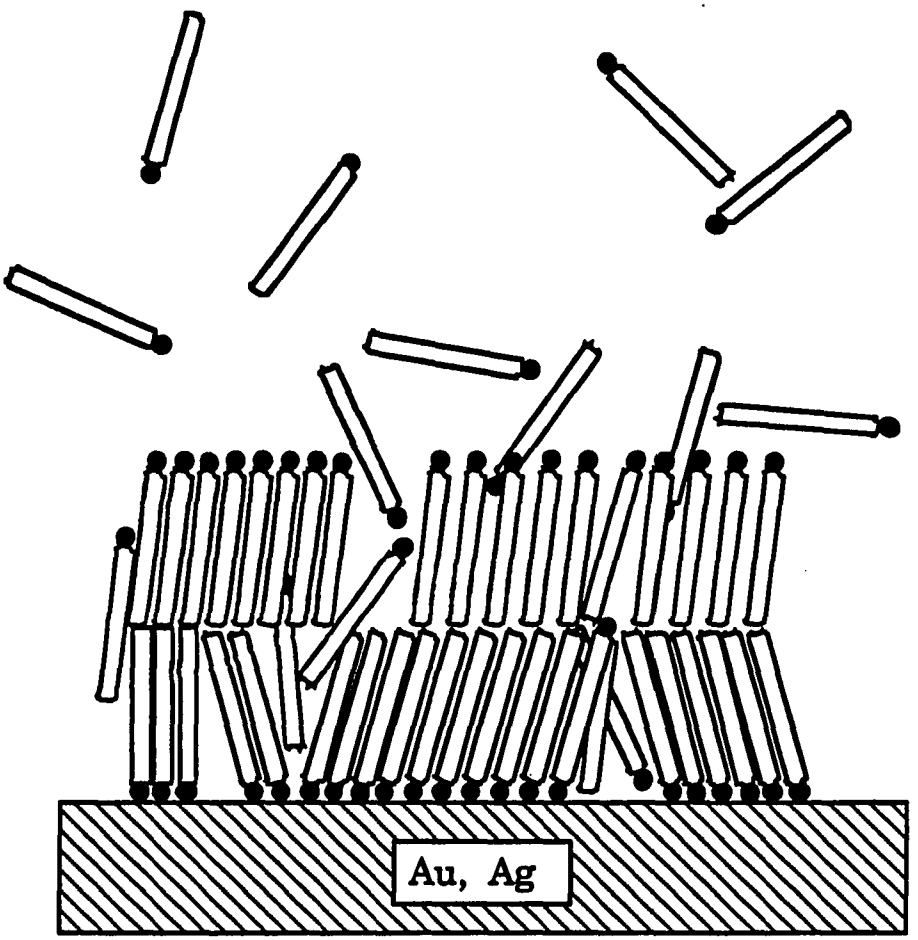

Figure I-8. Formation of a bilayer of alkanethiol in ethanol solution.

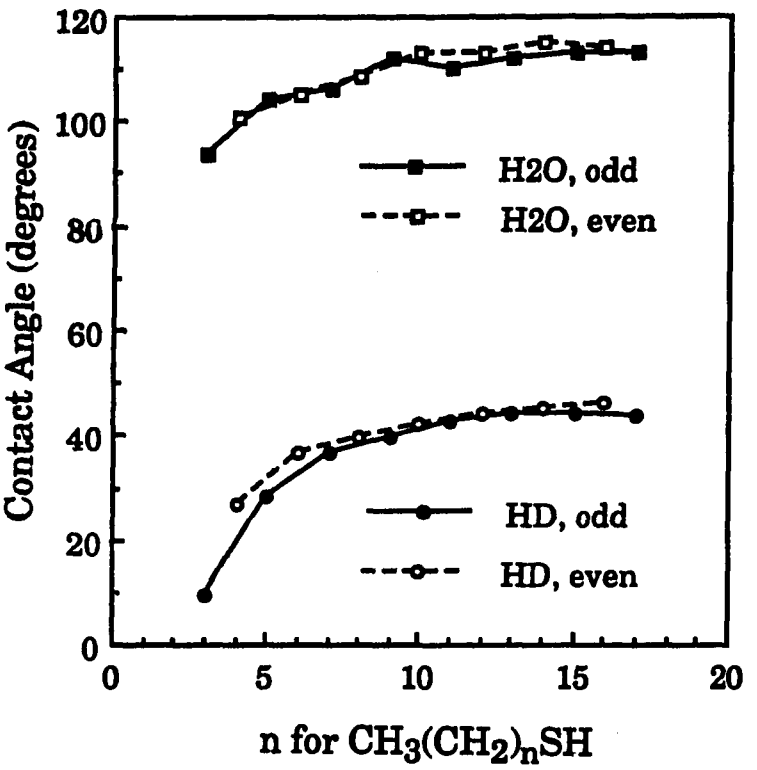

Figure I-9. Advancing contact angles of hexadecane and water versus n for $CH_3(CH_2)_nSH$ monolayers at Ag.

observed for other well-ordered closely-packed alkyl chain structures and are indicative of a methyl-terminated interface [8, 39-41].

The data in Figure I-9 point to important structural aspects of the monolayers at Ag, which are related to the change in θ_a with the odd-even variation of chain length. Changes in θ_a with the odd-even variation of chain length, which we will refer to hereafter as the "odd-even effect", arise from a difference in the chemical composition of the exposed portion of the chain terminus. For example, we have observed an odd-even effect in θ_a with both water and hexadecane at *n*-alkanethiol monolayers for n=1-17 on Ag. Our explanation of this observations is as follows. We believe that the monolayers are made up of molecules that are extended in the all trans zigzag configuration and tilted at 0° for Ag(100) or 32° for Ag(110) from surface normal. The portion of the molecules that are tilted at 32° give rise to the observed odd-even effect. As can be seen at Ag(110) case in Figure I-18 (b), the terminus of an alkyl chain with odd number of methylene groups on Ag presents a structure with slightly more methylene character to the contacting liquid. In contrast, chains with an even number of methylene groups on Ag exhibit an interface with less methylene character. This structural variation is manifested itself by an alteration in the surface free energy, with the odd-numbered alkyl chains exhibiting a lower θ_a. This is most evident for θ_a at monolayers with long alkyl chains. Such behavior is indicative of alkyl chain structures which are ordered and composed of all *trans-* conformational sequences.

The contact angle on monolayers on Au is also shown at Figure I-10 for comparison. Generally speaking, the contact angle data of monolayers of Au

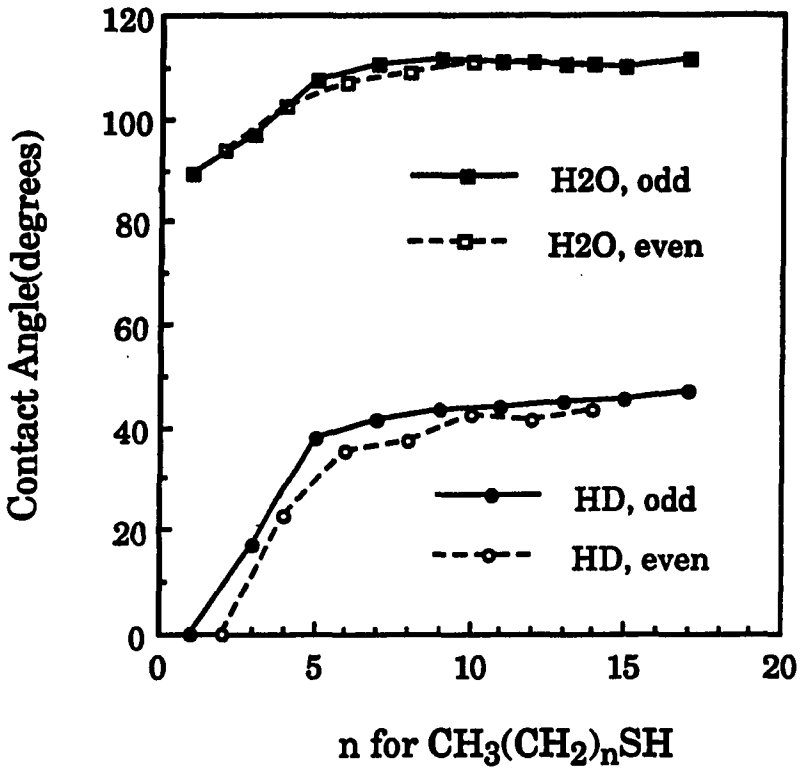

Figure I-10. Advancing contact angles of hexadecane and water versus n for $CH_3(CH_2)_nSH$ monolayers at Au.

show similar features as those on Ag, with low surface free energies for the long chain structures. However, we note that the observed odd-even effect for the monolayers on Au is offset by a methylene group from those on Ag. This might be due to the different head-group chemistry between Ag-S and Au-S and will be addressed later. Also, the odd-even effect is more pronounced on Au surfaces, which can be explained with the model system shown in Figure I-18. The Au surface is composed primarily of Au(111) [15] which gives the odd-even effect. However, Ag is a mixture of Ag(110) [15] which gives the odd-even effect and Ag(100) [15] which does not give the odd-even effect, and so the Ag surface will have, on average, less noticeable odd-even effect.

Contact angle hysteresis, $\theta_a - \theta_r$, has been attributed to several monolayer properties such as substrate roughness, chain packing density, and solubility of the adsorbate in the probe liquid. We measured differences in θ_a and θ_r of 12° for hexadecane and 15° for water. This effect arises from the penetration of solvent into the monolayer. Water, since it is smaller than hexadecane, is more effective at penetrating into the film. When θ_a is measured, defects in the film are empty. As the solvent passes over the defects, it permeates into the film. Thus, as the edge of the drop recedes across the surface, the drop interacts with a different surface: one which is a combination of monolayer and solvent. Since both water and hexadecane surfaces are expected to give lower contact angles than a methyl-terminated monolayer, θ_r is less than θ_a. Hysteresis depends on the substrate roughness if the crystallite size is smaller than the area probed by the drop because defects in the monolayer structure occur at the edges of small crystallites. Thus, the packing density at these locations may be lower, allowing solvent

penetration. Alternatively, some monolayers may exhibit hysteresis as a result of a slight solubility of the molecules in the solvent (e.g., alkanoic acids in H_2O). Thiols are probably not appreciably affected by dissolution because the Ag-S bond is very strong and they are relatively insoluable in H_2O.

Infrared spectroscopy as a probe of monolayer structure

Infrared spectroscopy provides us with informations of a functional groups present, an orientation of a functional group, and an environment of the functional group. In this section, we will examine the methyl and methylene mode of the alkanethiols and discuss the structure of the monolayers based on this infrared spectroscopic data. Infrared reflection spectra in the C-H stretching region for monolayers of *n*-alkanethiols at Ag are shown in Figure I-11 for n=3-17. For the long chain monolayers, five bands are observed. In descending energy, the bands are ascribed to $\nu_a(CH_3$, ip), $\nu_s(CH_3, FR_1)$, $\nu_a(CH_2)$, $\nu_s(CH_3, FR_2)$, and $\nu_s(CH_2)$. To verify the band assignments, the infrared spectrum of a monolayer of $CD_3(CH_2)_{19}SH$ on Au is shown in Figure I-12. Only those modes assigned to methylene stretches are observed. Table I-2 summarizes infrared data in terms of peak position and mode assignments [42] for the monolayers and for representative liquid and solid-phase alkanethiols. The liquid- ($CH_3(CH_2)_5SH$ and $CH_3(CH_2)_{11}SH$) and solid-phase ($CH_3(CH_2)_{17}SH$) alkanethiols are provided for comparative purposes. In an effort to deduce peak positions for $\nu_a(CH_2)$ for the short chain monolayers, we performed a deconvolution analysis of the spectral region between ~2950-2900 cm-1, and Table I-2 lists peak positions for the liquid- and solid-phase components of $\nu_a(CH_2)$ and $\nu_s(CH_3, FR_1)$. Transition dipoles for all the C-H stretching modes, assuming an all trans conformation

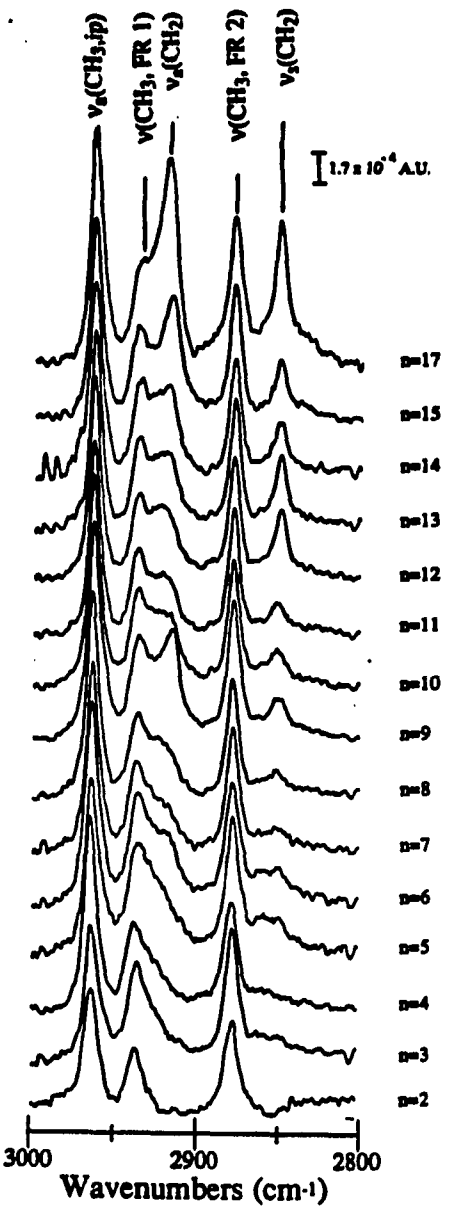

Figure I-11. Infrared external reflection spectra for *n*-alkanethiol monolayers ($CH_3(CH_2)_nSH$) adsorbed at Ag. The p-polarized light was incident at 80°.

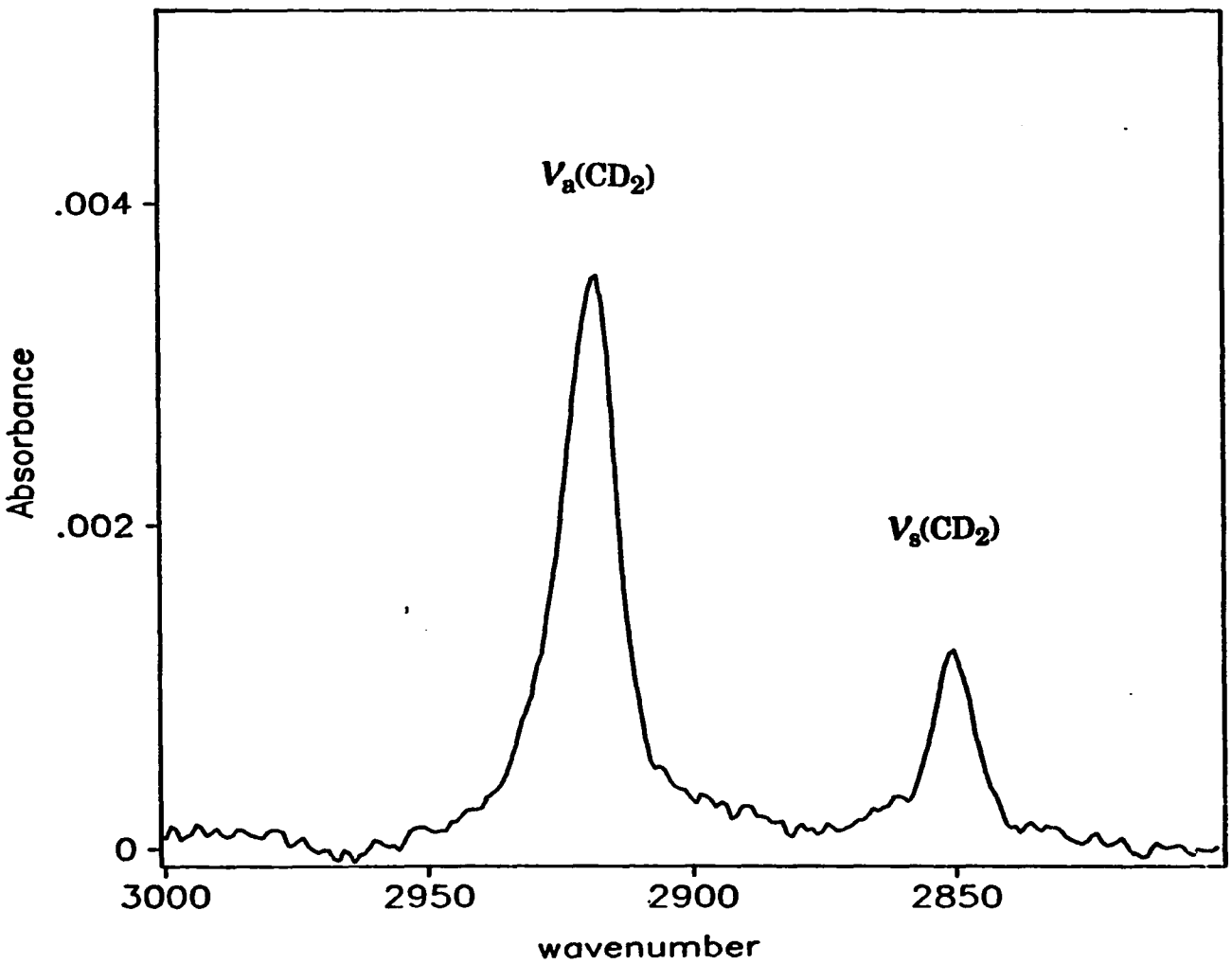

Figure I-12. Infrared external reflection spectra for a monolayer of $CD_3(CH_2)_{19}SH$ adsorbed at Au.

for the chain, are also listed. Peak positions for $\nu_a(CH_2)$ and $\nu_s(CH_2)$ are missing for some of the short chain monolayers because of insufficient absorbance (see Figure I-11) or overlap with $\nu_s(CH_3, FR_1)$. The $\nu_s(CH_3, FR_1)$ and $\nu_s(CH_3, FR_2)$ result from Fermi-resonance (FR) between $\nu_s(CH_3)$ and the first overtone of $\delta(CH_3)$ [43] where the subscripts 1 and 2 refer to higher and lower energy components, respectively. The $\nu_a(CH_3)$ is composed of two degenerate modes: the in-plane (ip) and out-of-plane (op), which are designated $\nu_a(CH_3, ip)$ and $\nu_a(CH_3, op)$, respectively. The absorbance maximum of the in-plane mode occurs at ~2964 cm^{-1} and that of the out-of-plane mode occurs at ~2956 cm^{-1} [44]. These two modes are perpendicular to each other. The $\nu_a(CH_3, ip)$ dipole is in the plane of the C-C-C axis and orthogonal to the CH_3-CH_2 bond; the $\nu_a(CH_3, op)$ dipole is orthogonal to both the C-C-C plane and CH_3-CH_2 bond. The remainder of this section examines information provided by the CH_2 modes about the structure of the monolayers. Later, structural insights derived from the CH_3 modes are discussed.

An examination of the peak positions and absorbances of the CH_2 stretching modes provides insights into the local environment and average tilt of the alkyl chains. Peak positions for the CH_2 modes are sensitive to intermolecular interactions and, therefore, provide an indication of the packing density of the alkyl chains. The dependence of the peak positions of the CH_2 stretching modes on intermolecular interactions is shown by the data in Table I-2 for the liquid ($CH_3(CH_2)_5SH$ and $CH_3(CH_2)_{11}SH$) and solid ($CH_3(CH_2)_{17}SH$) alkanethiols. The peak positions for $\nu_a(CH_2)$ and $\nu_s(CH_2)$ are 6 cm^{-1} higher in energy for the alkyl chains in a liquid-like phase.

Peak positions for the $\nu_a(CH_2)$ and $\nu_s(CH_2)$ for the n=15 and 17 monolayers suggest that a portion of the chains exists in a crystalline-like environment (all *trans-* conformational sequences). Evidence for crystallinity in the structure for chain lengths greater than n=10 comes from the peak positions of $\nu_s(CH_2)$. The sensitivity of $\nu_s(CH_2)$ to the local environment is not as sensitive as $\nu_s(CH_2)$. The CH_2 bands shift 8 and 6 cm^{-1}, respectively, on going from crystalline to liquid environments. A comparable interpretation for the $\nu_a(CH_2)$ is, however, more complicated because some of the peak positions in Table I-2 suggest liquid-like and others suggest crystalline-like environments. This variability is a result of the low absorbance of the band, its overlap with $\nu_s(CH_3, FR_1)$, and the possible presence of liquid-like *features*. The lack of progression from a liquid-like environment for short chains to a crystalline like environment for long chains is also inconsistent with (structural) observations of other alkyl chain monolayers. For example, for *n*-alkanethiol monolayers at Au as shown in Figure I-13, both $\nu_a(CH_2)$ and $\nu_s(CH_2)$ show a definite progression from a liquid to crystalline environment as chain length increases [9]. Such trends, which are also observed for Langmuir films at the air-water interface, arise from an increase in the hydrophobic interaction stabilization between chains as the chain length increases. Together, both of the above factors suggest the presence of liquid-like segments in the alkyl chains.

An examination of the absorbance of the methylene modes also provides information about the structure of the alkyl chains. As shown in Figure I-14 (a), both methylene bands increase with increasing chain length. These trends, within the uncertainty of the data, can be reasonably described

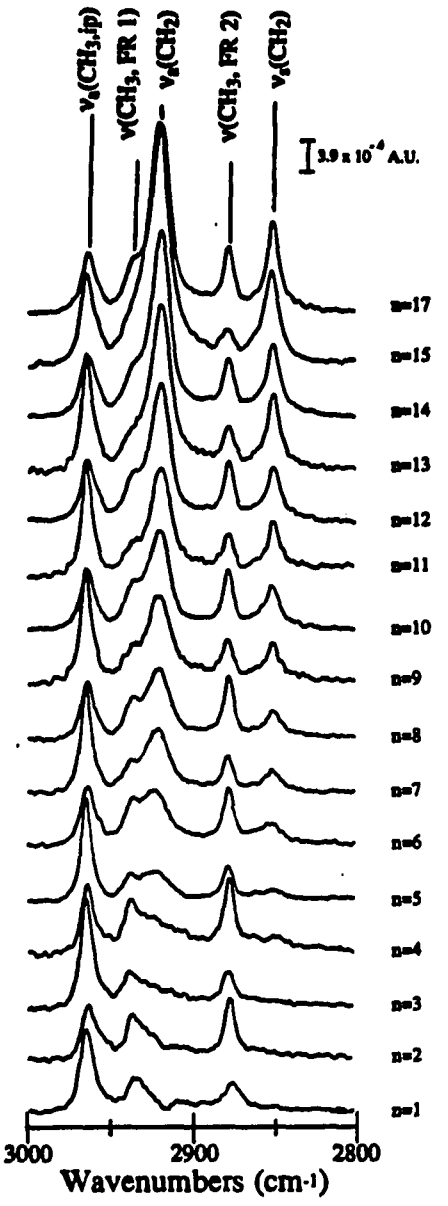

Figure I-13. Infrared external reflection spectra for *n*-alkanethiol monolayers ($CH_3(CH_2)_nSH$) adsorbed at Au. The p-polarized light was incident at 80°.

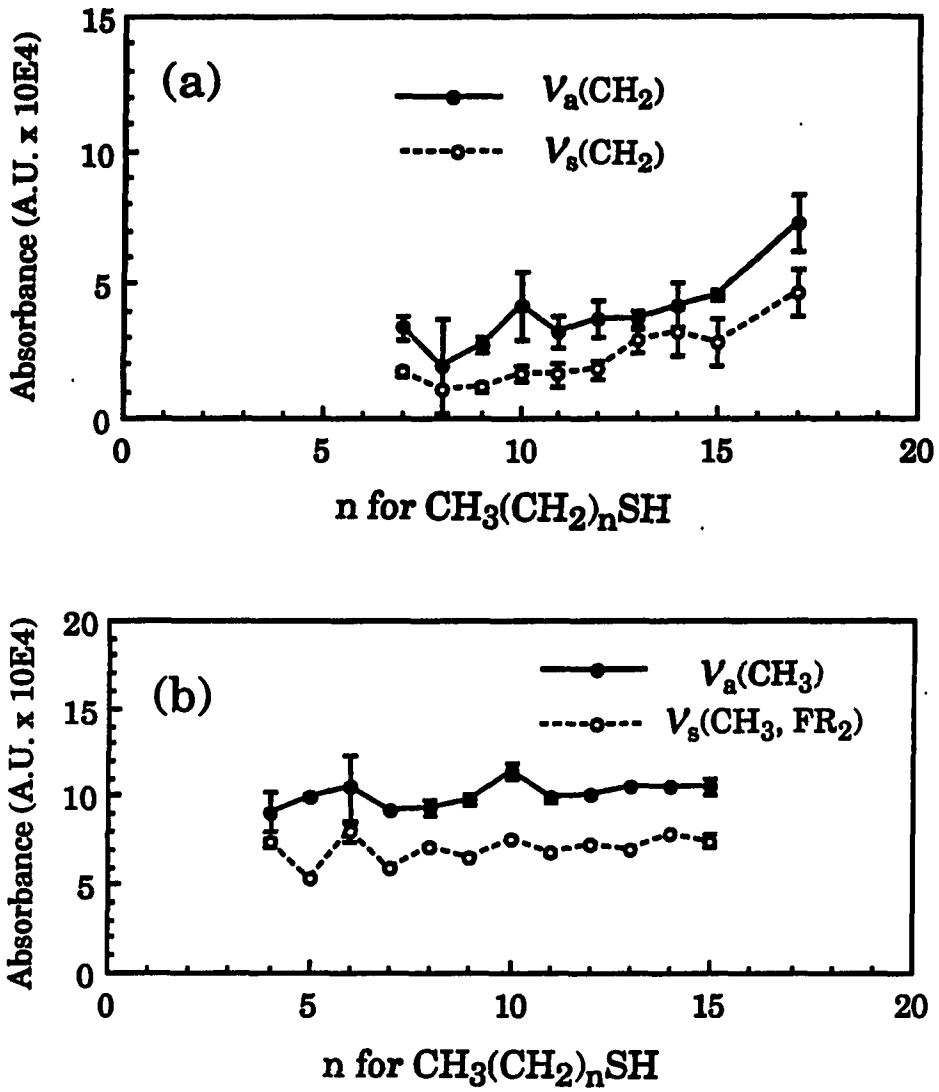

Figure I-14. IR absorbances vs. n for $CH_3(CH_2)_nSH$ monolayers at Ag. (a) Absorbances for the $\nu_a(CH_2)$ and $\nu_s(CH_2)$ bands. (b) Absorbances for the $\nu_a(CH_3)$ and $\nu_s(CH_3, FR_2)$ modes. The error bars are the absolute deviation of two measurements on separate wafers.

by straight lines. Figure I-14 (a) represents data obtained on a set of samples prepared within a 24 hour period. The error bars are the standard deviations of three separate samples. Since the $\nu_a(CH_3, ip)$ absorbance (see Figure I-14 (b)) remains relatively constant with n, the methylene band increase implies that the monolayers maintain the same approximate orientation on Ag for all chain lengths. These increases point to a comparatively constant orientation of the chains as a function of n, further substantiating the ellipsometry thickness data (Figure I-4) which show the monolayer thickness increases with chain length, and imply a consistency in structural order.

Compared to the intensity of CH_2 modes of monolayers on Au, which is shown in Figure I-15 (a), the absolute intensity of the same modes of monolayers on Ag is quite small, which suggests that the monolayers on Ag are, on average, less tilted from the surface normal. As previously described [3,4,45], the average tilt angle θ and twist angle ϕ of the adsorbed alkyl chains, as defined in Figure I-16 [46], were calculated. By comparing the measured intensities of $\nu_a(CH_2)$ and $\nu_s(CH_2)$ for monolayers with $n \geq 12$ with those calculated for a hypothetical isotropic monolayer, the angles θ and ϕ are determined. The calculated spectrum is based on a crystalline-phase alkyl chain film with the appropriate best-fit ellipsometric thickness measured on Ag. A hypothetical spectrum, shown in Figure I-17 (a), is calculated for a 29 Å isotropic film of a crystalline-phase alkyl chain. The experimental IR spectrum of an octadecanethiol monolayer at Ag is shown in Figure I-17 (b).

The equations involved in this orientational analysis are:

$$\frac{A_e^{\nu_s}}{3A_c^{\nu_s}} = \sin^2\theta \cos^2\phi$$

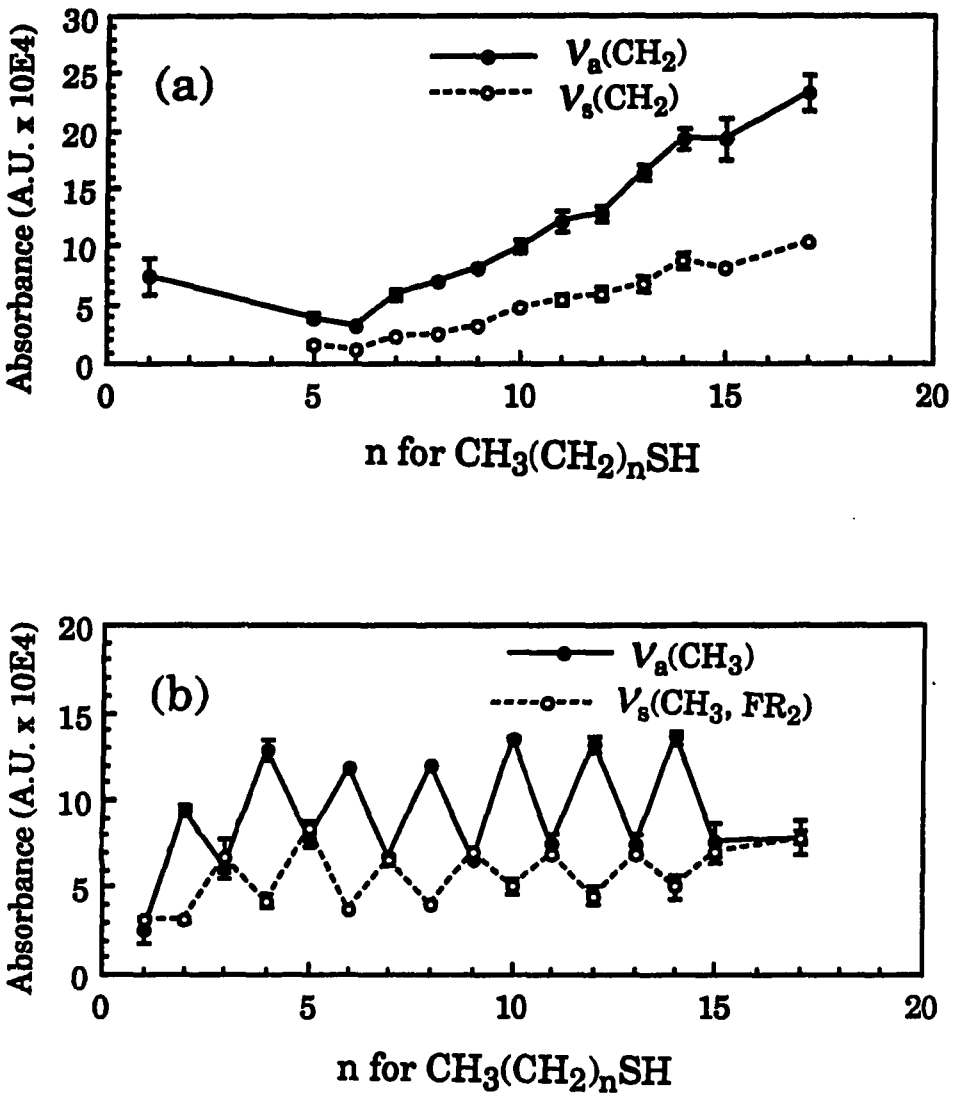

Figure I-15. IR absorbances vs. n for $CH_3(CH_2)_nSH$ monolayers at Au. (a) Absorbances for the $\nu_a(CH_2)$ and $\nu_s(CH_2)$ bands. (b) Absorbances for the $\nu_a(CH_3)$ and $\nu_s(CH_3, FR_2)$ modes. The error bars are the absolute deviation of two measurements on separate wafers.

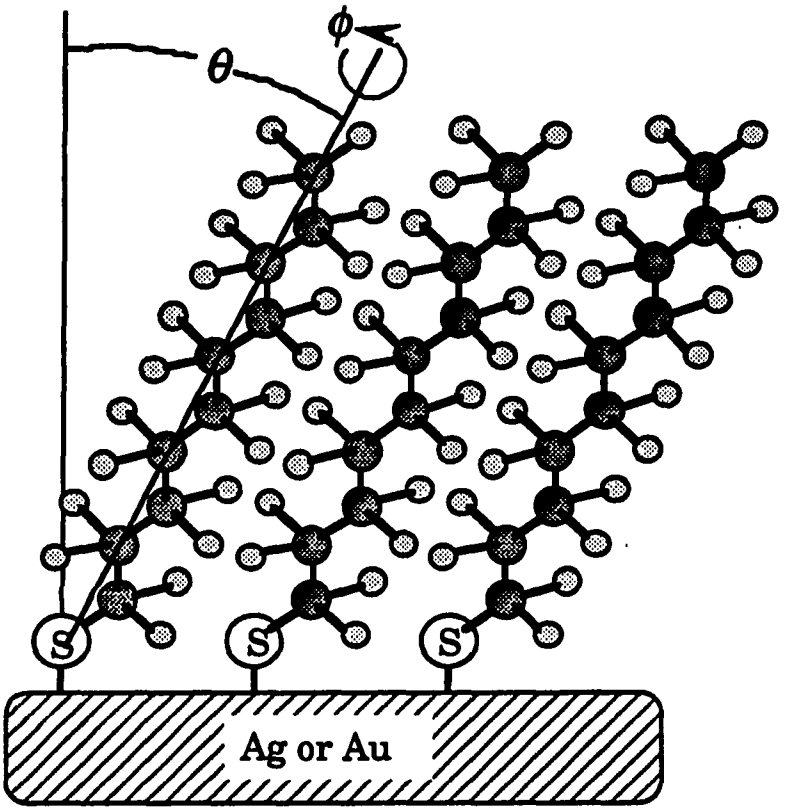

Figure I-16. The tilt angle θ and twist angle ϕ of a fully-extended *n*-alkanethiol molecule adsorbed at Ag or Au. See Table I-2 for a description of the directions of the transition dipoles of the methyl and methylene vibrations.

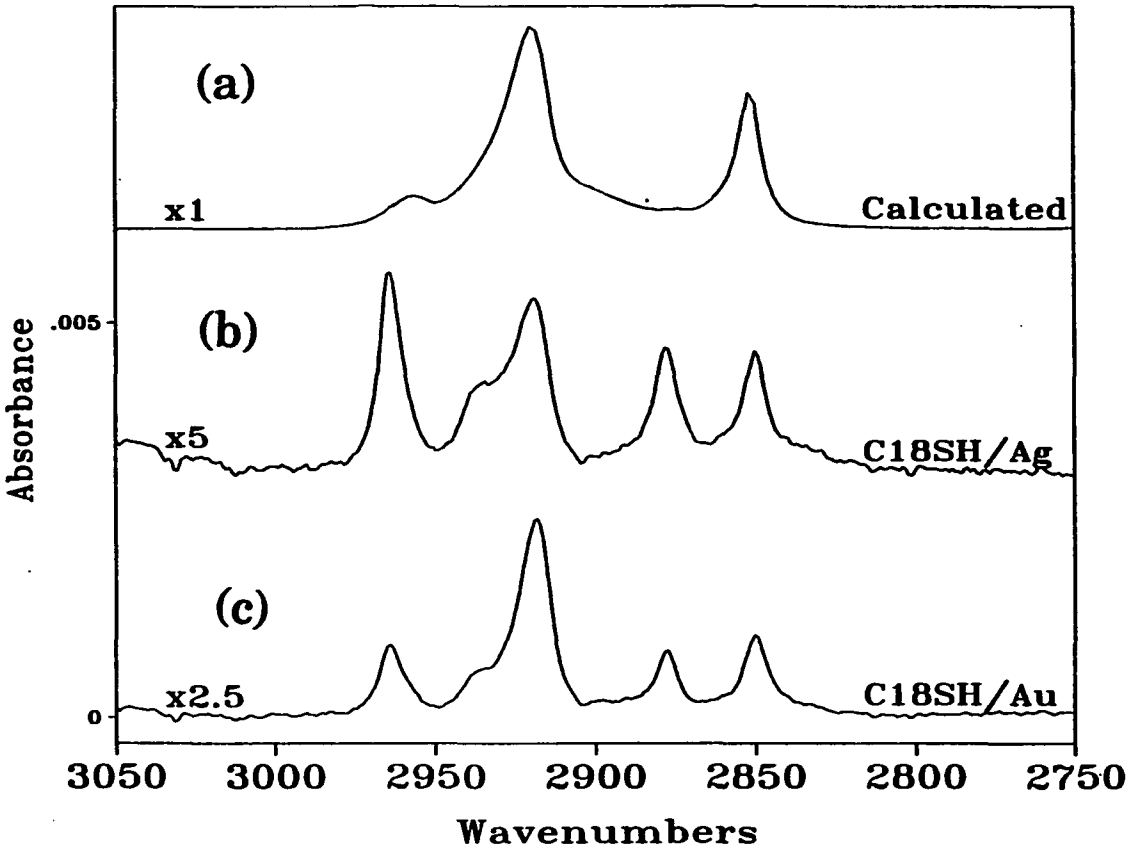

Figure I-17. **Infrared spectra of a *n*-octadecanethiol (a) calculated spectrum of a 29 Å isotropic film of a crystalline phase alkyl chain. Infrared external reflection spectra for self-assembled octadecanethiol monolayers at (b) Ag and (c) Au. The p-polarized light was incident at 80°.**

$$\frac{A_e^{\nu_i}}{3A_c^{\nu_i}} = \sin^2\theta \sin^2\phi$$

where $A_e^{\nu_i}$ and $A_c^{\nu_i}$ are the absorbances of the experimental and calculated modes of vibration ν_i, and θ is the tilt angle. The results of the orientation analysis, summarized in Table I-3, indicate, on the average, the alkyl chains are tilted 14° from the surface normal and twisted 46° around the C-C-C chain on Ag. Different models to explain average tilt of 14° are shown in Figure I-26 (vide infra).

Methyl mode analysis

Further insights concerning the orientation near the chain terminus are obtained from $\nu_a(CH_3)$ and $\nu_s(CH_3$, FR 2). The shape and peak position of $\nu_a(CH_3)$ (see Figure I-11 and Table I-2) suggest a predominant contribution from the in-plane mode. Thus, in consideration of the surface selection rule and the orthogonality of the $\nu_a(CH_3$, ip) and $\nu_a(CH_3$, op) dipoles, the $\nu_a(CH_3$, op) dipole is oriented near the surface parallel. Consideration of the orientation required to explain the absence of the $\nu_a(CH_3$, op) mode yields a conformation which is inconsistent with the appearance of the $\nu_a(CH_2)$ mode (see Table I-2), since in a fully-extended all *trans*- alkyl chain, the $\nu_a(CH_2)$ and the $\nu_a(CH_3$, op) modes are parallel to one another. This paradox can be resolved only by allowing the chain to adopt some disorder in the vicinity of the CH_3 group if the structure of the majority of the methylene portion of the chain is held in an all *trans*- highly crystalline conformation, as indicated by the $\nu_a(CH_2)$ and $\nu_a(CH_2)$ frequencies. Precedent for gauche kinks near the chain terminus comes from surface enhanced Raman studies [47] and

Table I-3. Calculated tilt (θ) and twist (ϕ) angles and calculated and observed frequencies of the $\nu_a(CH_2)$ and $\nu_s(CH_2)$ modes for long chain alkanethiols on Ag.

n	$\nu_a(CH_2)$		$\nu_a(CH_2)$		θ	ϕ
	observed	calculated	observed	calculated		
12	2921	2920	2850	2852	12.5	40.7
13	2922	2920	2849	2852	13.7	47.3
14	2923	2920	2850	2852	14.0	46.5
15	2919	2920	2851	2852	13.5	43.3
17	2918	2920	2850	2852	16.5	44.3
Averages					14.0	44.4

molecular dynamics calculations [48,49]. Enhancement of defects near the ends of the chains (more disorder near the chain terminus) has also been observed in in situ IR studies of octadecanethiol on Au in various solvents [50].

The peak positions of the three methyl modes, $\nu_a(CH_3)$, $\nu_s(CH_3, FR_1)$, and $\nu_s(CH_3, FR_2)$, are largely independent of chain length (Table I-2). However, the absorbances of the methyl modes do not increase monotonically with chain length, as the methyl modes exhibit an odd-even effect (Figure I-14 (b)). The $\nu_s(CH_3, FR_2)$ mode exhibits an unusual dependence on the number of methylene groups in the chain. We refer to this behavior as theodd-even effect caused by the difference in the intensity between a molecule with an odd or even number of methylene groups. For simplicity, we call an alkyl chain with an even number of methylene groups an *even chain* and those with an odd number of methylene groups an *odd chain*. The cause of this behavior is easily envisioned if one assumes that, for both even and odd chains, the alkyl chains tilt away from the surface normal in the same way and that the gauche kink near the end of the chain is constant (i.e., the $\nu_a(CH_3, op)$ dipole is always aligned nearly parallel to the surface). Underpotential metal deposition experiments [9] show that the evaporated Ag surface is a mixture of Ag(100) and Ag(110), and the evaporated Au is mainly Au(111). Possible structural models are illustrated in Figure I-18, in which the molecular axes of the chains are oriented 0° for Ag(100) and 32° for Ag(110) from the surface normal. On the left hand side of the figure, it can be seen that the $\nu_s(CH_3)$ dipole for an even chain length molecule on Ag(110) is oriented with a large normal component. On addition of a methylene group

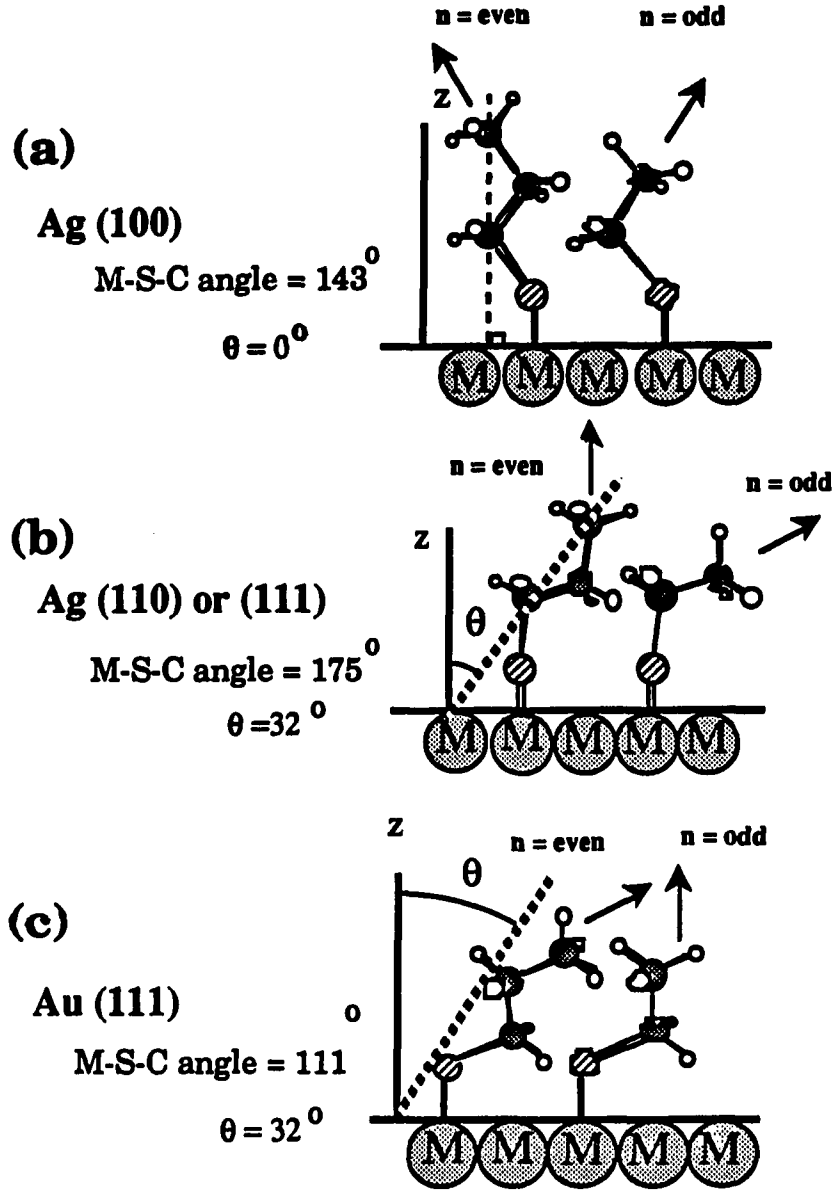

Figure I-18. Proposed model for the interaction of *n*-alkanethiol monolayers on Ag and Au surfaces: The proposed structures for (a) a thiol monolayer on Ag(100), (*b*) a thiol monolayer on Ag (110), and (c) a thiol monolayer on Au(111) for a chain with an odd (right) or an even (left) number of methylene groups in the chain. The arrows are the directions of $\nu_s(CH_3)$ dipole.

(odd chain, shown on the right hand side of Figure 18 (b)), the $\nu_s(CH_3)$ dipole is directed more parallel to the surface. When another methylene group is added to the chain (even chain), the $\nu_s(CH_3)$ dipole is again oriented as shown on the left hand side of the Figure. In this way, the addition of methylene groups to the chain can cause the odd-even effect if the overall chain orientation is fixed for all chain lengths. The model proposed in Figure I-18 predicts the observed odd-even behavior of Figure I-14 (b): the $\nu_s(CH_3, FR_2)$ band has a higher intensity for even chains because the $\nu_s(CH_3)$ dipole moment has a larger perpendicular component than for odd chains.

One would expect the odd-even behavior in other modes associated with the methyl group. The overlap between $\nu_s(CH_3, FR_1)$ and $\nu_a(CH_2)$ precludes unequivocal analysis of this methyl mode. The odd-even effect is observed for the $\nu_a(CH_3, ip)$ mode in *some* sets of sample. The odd-even effects have been observed previously for alkanoic acids on Ag surfaces [1], alkanoic acids on oxidized aluminum surfaces [51], alkanethiols on Au surfaces [1, this work], and phenyl and benzyl mercaptan on Ag surfaces [52], using contact angle measurements, infrared spectroscopy and surface-enhanced Raman spectroscopy. For the observed odd-even effect of alkanethiols on Au as shown in Figures I-10, Figure I-15 (b) can be explained with the same model in Figure I-18 (c). For Au(111), the odd-even effect appears with a methylene group offset compared to the monolayers on Ag. This offset is due to the different bond angle between Ag-S-C and Au-S-C. This head group chemistry will be discussed later. Since our Ag films are composed of Ag(110) and Ag(100), the apparent odd-even effect is more pronounced for Au, which is mainly of (111) texture.

Surface-enhanced Raman spectroscopy data provide further evidence on the alkyl chain configuration. The frequency of the C-S stretch (~700 cm^{-1}) of adsorbed hexadecanethiol on Ag indicates a predominantly all *trans*-configuration of methylene groups in the thiol region of the molecule [26].

We have also examined the C-S (600-700 cm^{-1}) and the S-H (2550-2600 cm^{-1}) stretching regions as well as the C-H bending region (1150-1500 cm^{-1}) but have not found any evidence for any of these modes in the monolayer infrared spectra. The absence of these features in the IR spectra of the adsorbed thiols may be due to inherently low intensities of these bands. Alternatively, the orientation of the ν(C-S), ν(S-H) or ν(C-H) oscillating dipoles with respect to the surface may preclude detection of these bands. On the other hand, although inherently weak, the ν(S-H) stretch may be absent due to S-H bond cleavage. As noted, surface-enhanced Raman spectroscopy results [53] indicate that S-H bond cleavage occurs when thiols adsorb on Ag surfaces and is supported by electrochemical data [12].

Monolayer characterization with electrochemistry

To assess the structure of these monolayers further, various electrochemical characterizations have been applied. The capacitance measurement of the electrode coated with non-conducting organic monolayers has been used as a probe of the average structure and integrity of the monolayer [9]. The rate of heterogeneous charge transfer at a derivatized electrode is controlled by defects within the monolayer. The underpotential deposition of metal ion onto the monolayer covered electrode can give information of the amount of defects in the covering monolayer.

Capacitance measurements not only provide information of permeability of the monolayer to simple electrolyte ions but also can be used as another measure of monolayer thickness, which complements the ellipsometric thickness. The cyclic voltammetric current response vs. applied potential for a bare Ag and octadecanethiol monolayer on Ag are shown in Figure I-19 for both 1M NaCl solution and 1mM $Ru(NH_3)_6Cl_3$ in 1M NaCl solution. For 1mM $Ru(NH_3)_6Cl_3$ in 1M NaCl on a bare Ag electrode, the shape of i-E curve shows a electrochemically reversible one-electron redox process [54]. The shape of the i-E curve for octadecanethiol monolayer is very different. Most of the current is capacitive and the current is much less. The i-E curves for 1mM NaCl only solution are quite different for a bare Ag and an octadecanethiol monolayer on Ag. The capacitance current for a octadecanethol monolayer is a lot less than that for a bare Ag.

The capacitance current is obtained as the product of the sweep rate, differential capacitance, and electrode area. The capacitance current was measured with a sweep rate of 100mV/s at -100mV (vs. Ag/AgCl/sat'd KCl) using 1M NaCl for Ag electrode. (For comparison, the capacitance current on Au was also measured at the same potential.) The capacitance currents are independent of applied potential(-0.1 to -0.5V vs. Ag/AgCl/sat'd KCl) and scan rate (10 and 100 mV/s). Our result on monolayers on Au is in good agreement with that reported previously [9], which, in turn, is similar to the model predicted by the Helmholts theory for the electrical doublelayer. It means that the monolayer can be treated as an ideal capacitor interfacing between

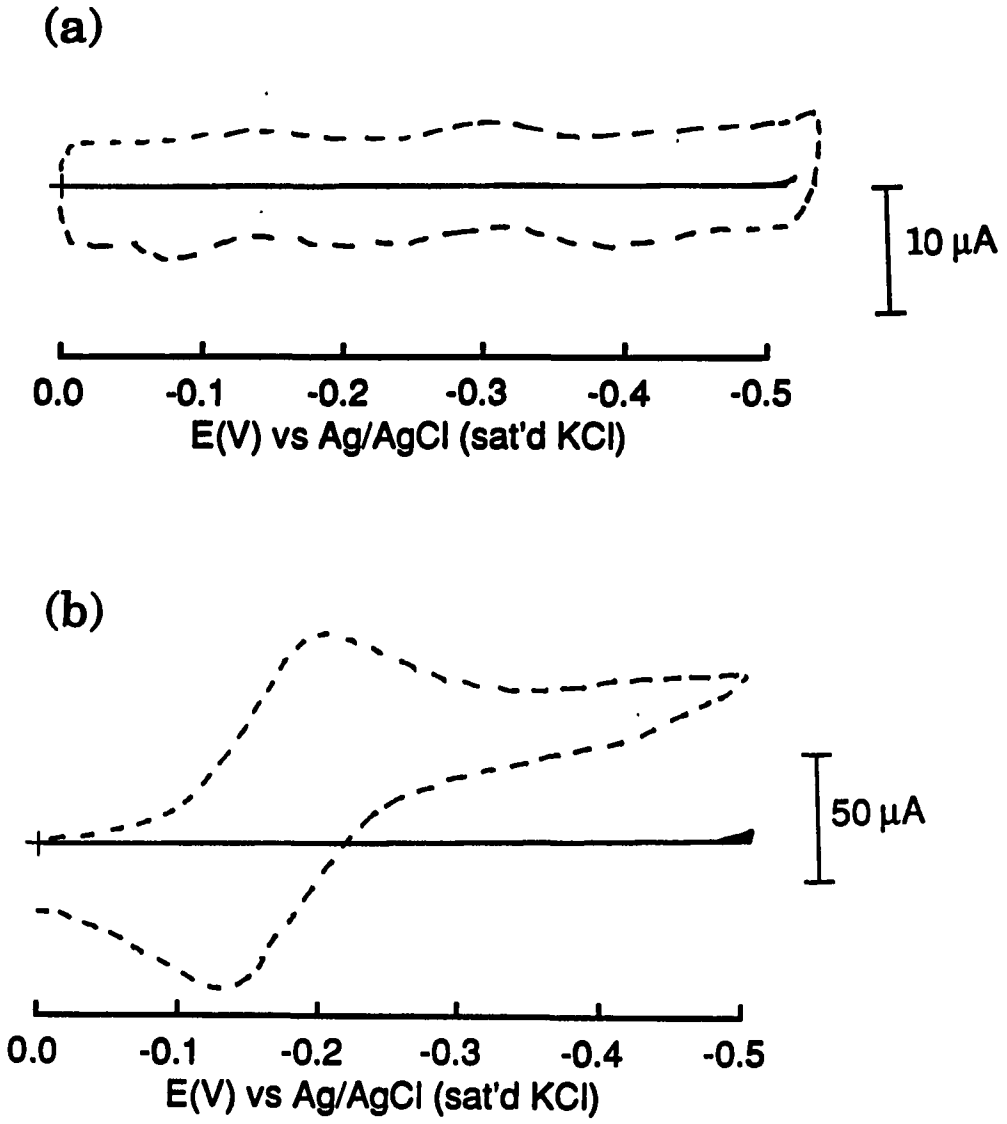

Figure I-19. Cyclic voltammetric current response as a function of applied potential for (a) 1 M NaCl only and (b) 1mM $Ru(NH_3)_6Cl_3$ in 1M NaCl. The electrodes are bare Ag (---) and octadecanethiol monolayer on Ag (—). The sweep rate is 100mV/s.

the electrolyte and electrode. The inverse capacitance dependence on chain length of alkanethiols adsorbed on Ag is shown in Figure I-20. It is observed that, in general, the monolayers become more insulating (capacitance decreases) as the chain length increases. As shown by the absolute value of inverse capacitance and slope of the curve on Figure I-20, compared to those on the reference [9], the monolayers adsorbed on Ag are more insulating than those adsorbed on Au, which indicates that the monolayers on Ag are thicker than those on Au. Interestingly, the monolayers of short alkanethiols show larger capacitance than expected on the slope of curve. This behavior might be due to the fact that the short chain alkanethiol monolayers have more defects than monolayers of long alkanethiol.

The current for the electrochemical reduction of $Ru(NH_3)_6^{3+}$ as a function of chain length of monolayers coated on Ag substrates are shown in Figure I-21. The amount of charge passed during the potential sweep as a function of chain length indicates that the monolayers form an efficient barrier to electron transfer for the long chain structures. For the shorter chain monolayers, an increasing amount of electron transfer occurs either by tunneling process through the monolayer or at defect sites. The monolayer with shorter chain certainly allows more facile electron transfer, but we do not presently understand how to separate contributions from a defects and tunneling mechanism. The increase in electron transfer with the shorter chain monolayers is consistent with infrared spectroscopy and contact angle results, providing further evidence that short chain monolayers are more disordered. For comparison, the data for monolayers on Au show that the films are barriers to electron transfer of $Ru(NH_3)_6^{3+}$ for n=12 and above.

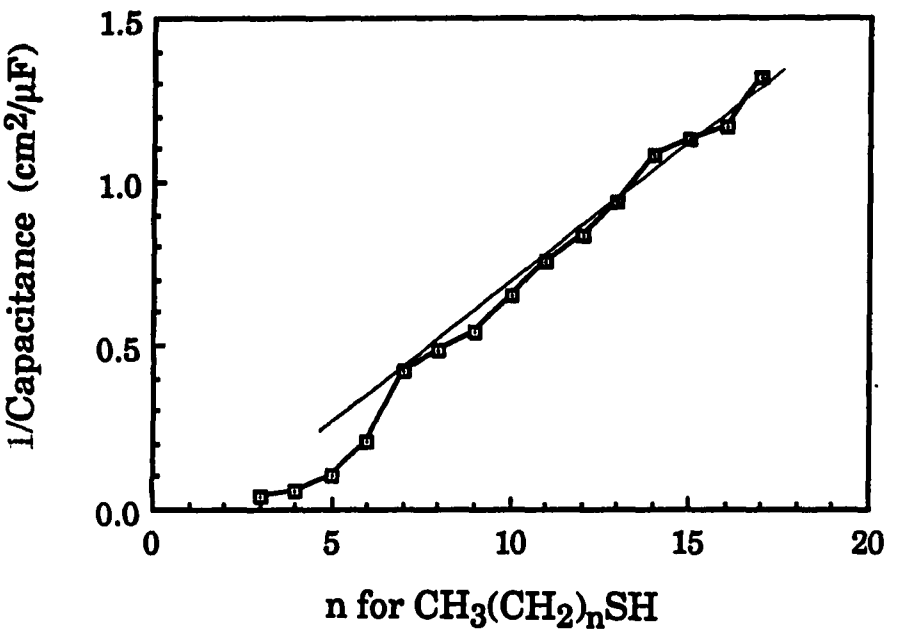

Figure I-20. Reciprocal capacitance as a function of chain length for the alkanethiol monolayers on Ag. (Electrolyte: 1M NaCl; scan rate: 100mV/s)

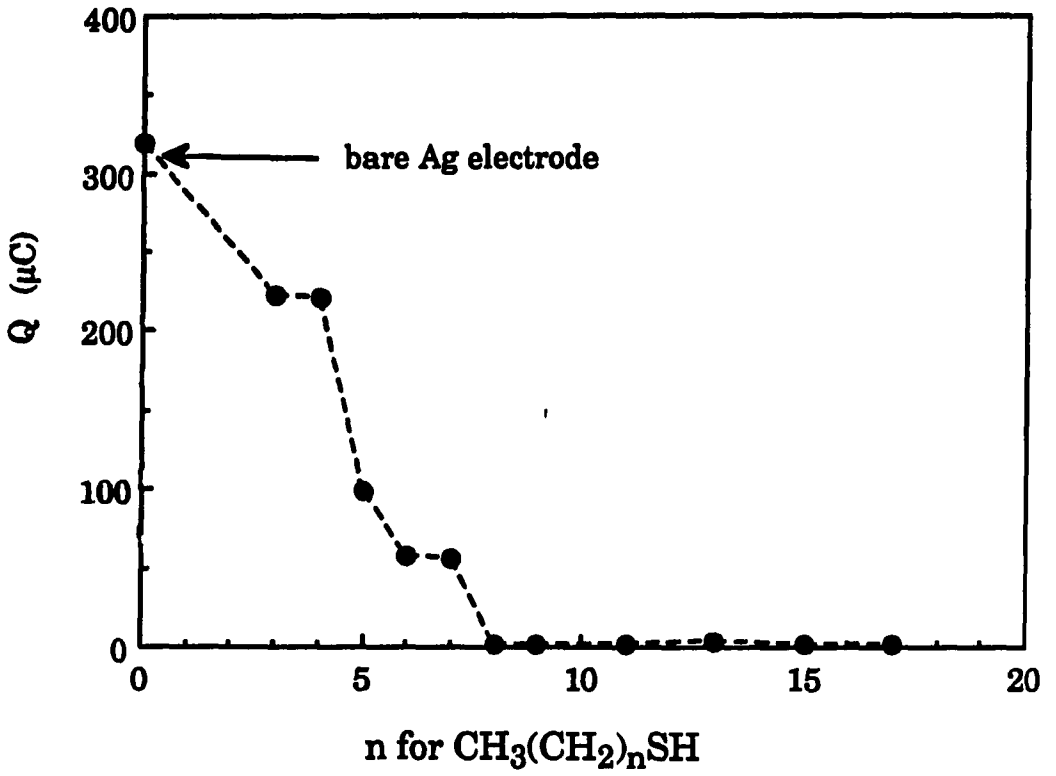

Figure I-21. Charge for the $Ru(NH_3)_6^{+3}$ reduction as a function of chain length for the alkanethiol monolayers on Ag.

Monolayers of the same chain length on Au appear to be less effective barriers to electron transfer than that on Ag, which is another indication that the monolayers on Ag are thicker or less defective than those on Au.

It is well known that metal ions can be deposited underpotentially on the surface of other metal electrode [55-59]. If an electrode is covered with a monolayer, the area available for underpotential deposition will decrease accordingly. We have observed that the currents for the deposition and desorption of lead on Ag surfaces are decreasing with increasing chain length of the monolayer [60]. We believe these indicate that the defects and/or ion penetration properties of the monolayer increases with decreasing chain length.

Microscopic Structure of Alkanethiol Monolayers at Silver

Underpotential deposition of metal ions at metal electrode can provide valuable information of underling surface crystallinity [55-59]. Depending on the underlying crystal structure, the observed UPD curve shows a different shape. Scanning tunneling microscopy can map out the surface topography on an atomic scale for conductor or semiconductor substrate. If the scanning process does not alter the surface structure, we can get, in some instances, the atomic picture of surface structure.

Roughness and crystallinity of evaporated Ag surfaces

The microscopic roughness and crystallinity of the evaporated Ag surfaces was characterized by both underpotential metal deposition (UPD) and scanning tunneling microscopy (STM). Figure I-22 shows stripping

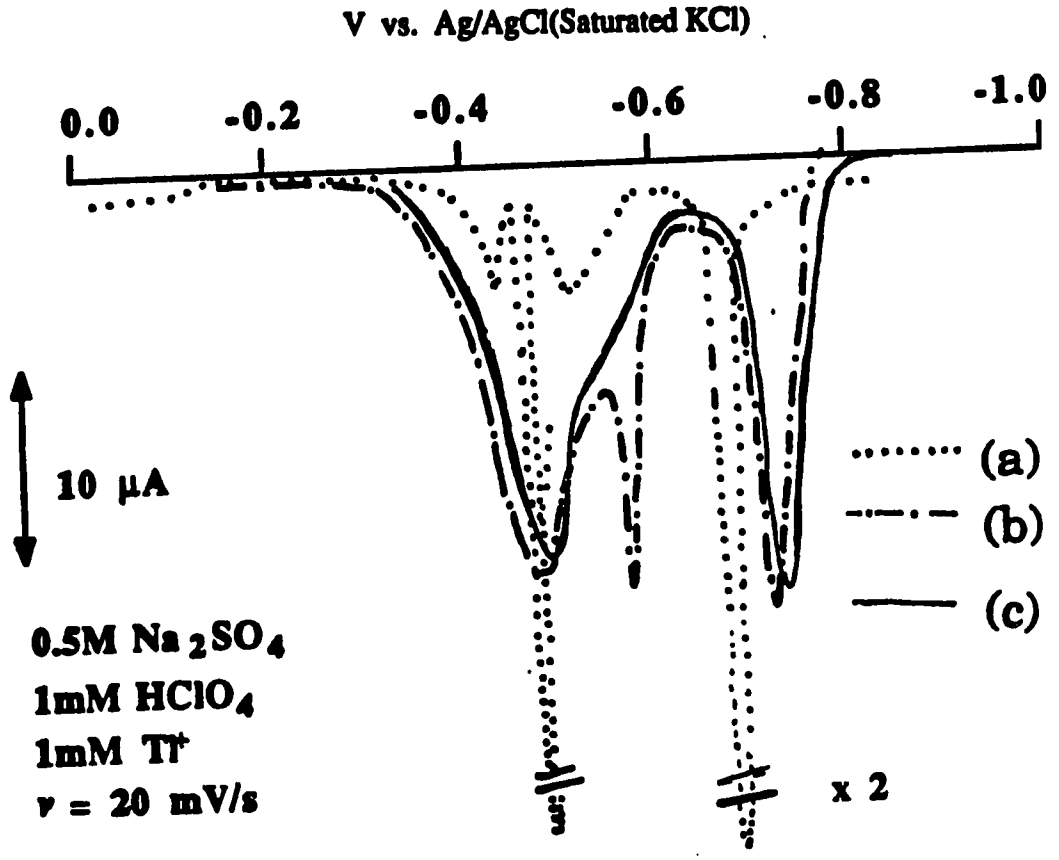

Figure I-22. UPD of Tl on (a) Ag(111), (b) Ag(100), and (c) our evaporated Ag surface.

current-potential (i-E) curves for Tl(0) at an Ag(111) surface (curve a) and at an Ag(100) surface (curve b). At Ag(111), the i-E curve exhibits two large stripping waves. Several smaller waves are also observed. The large cathodic waves (not shown) correspond to the successive deposition of two monolayers of Tl(0) at Ag; similarly, the anodic waves result from desorption of two Tl(0) monolayers.

Film crystallography was examined by comparing the voltammetric stripping curves for underpotentially deposited Tl on our vapor deposited electrodes to those obtained for single crystal surfaces [61]. Because the oxidative desorption potentials for underpotentially deposited Tl from Ag are dependent on the exposed crystal face, it may be possible to approximate the dominant crystal face, if any, in our polycrystalline samples. Representative stripping current-potential (i-E) curves shown in Figure I-22 indicate that our Ag films are largely polycrystalline. Unlike vapor deposited Au films, which are primarily Au(111), our Ag films do not grow favoring a particular crystallographic face. Analysis of the Ag films is further complicated by changes in the apparent crystallographic orientation during extended electrochemical cycling [62]. Our desorption curves were not reproducible, suggesting the proportions of the low-index planes are extreamly sensitive to deposition conditions. Similarly, a LEED and RHEED study of Ag films evaporated on glass [63] indicates that the polycrystalline surfaces have no large oriented crystallites. Silver films deposited on mica at elevated temperature are largely Ag(111), and those formed on optically polished acrylic substrates indicate a propensity toward Ag(110) orientation. Assuming that our evaporated Ag exhibits only (100) texture, a comparison of

the charge for the electrodeposition of the first Tl(0) monolayer with that observed for Ag(100) yields a roughness factor of ~1.2.

The roughness and morphology of the surface structure at a macro and microscopic level was assessed with STM. Figure I-23 is representative STM micrograph of a 250 x 250 nm area of our evaporated Au surfaces, and Ag surfaces show almost same features. The evaporated films are comprised of crystallites of ~500-1000Å diameter. The heights of the terraces are ~100Å. Based on this and other micrographs, the roughness factor of the evaporated Ag films is estimated at 1.1-1.3, which agrees with the value determined by UPD measurements above. The roughness factors calculated from the STM images assume a spherical contour for the crystallites with the above dimensions. Factors calculated from STM micrographs and measured with UPD are consistent with those reported by others [1,2] based on electrochemical measurements on evaporated films. The roughness of the underlying substrate (e.g., Si) also affects the evaporated film roughness.

An atomic-scale STM micrograph of an evaporated Ag film is shown in Figure I-24 (a). The image shows bright spots correspond to Ag atoms, which are arranged in a hexagonal lattice. The inter-atomic spacing is 3.0Å, which corresponds to the nearest neighbor distance for the Ag(111) surface.

The crystal structures of the bare Ag surface determined by STM and UPD are different. Voltage cycling in the UPD experiment may induce a rearrangement of the surface atoms. Alternatively, the images obtained with STM may be altered as a result of the tunneling process. Our current interpretation is that the STM tip perturbs the surface and that the surface

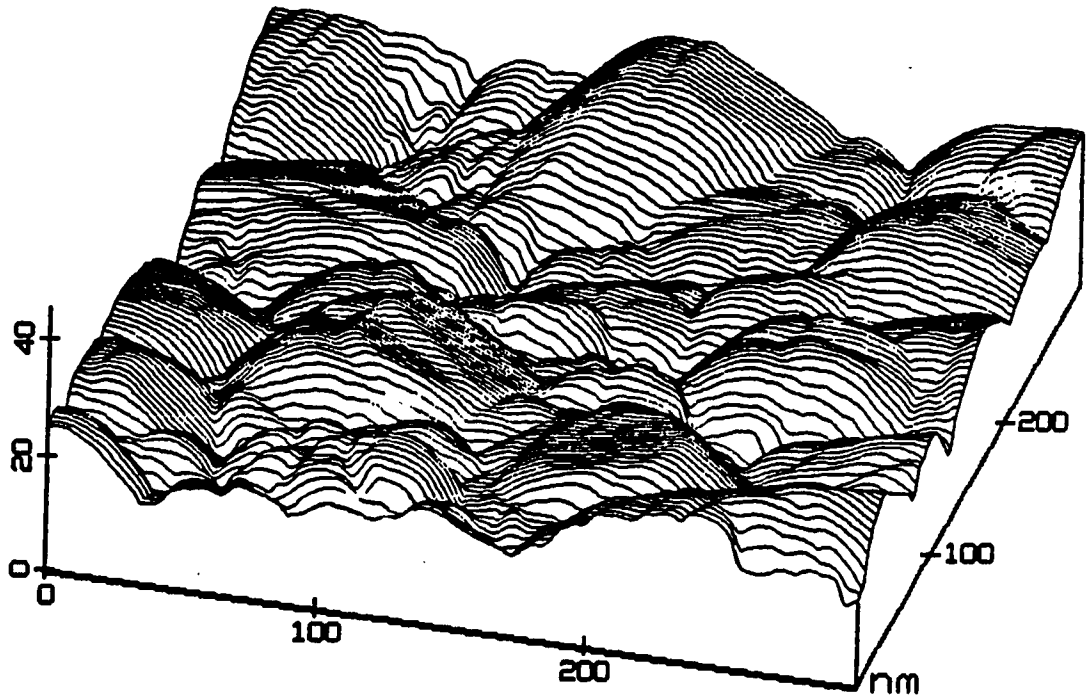

Figure I-23. STM image of Au surface 250 x 250 nm area

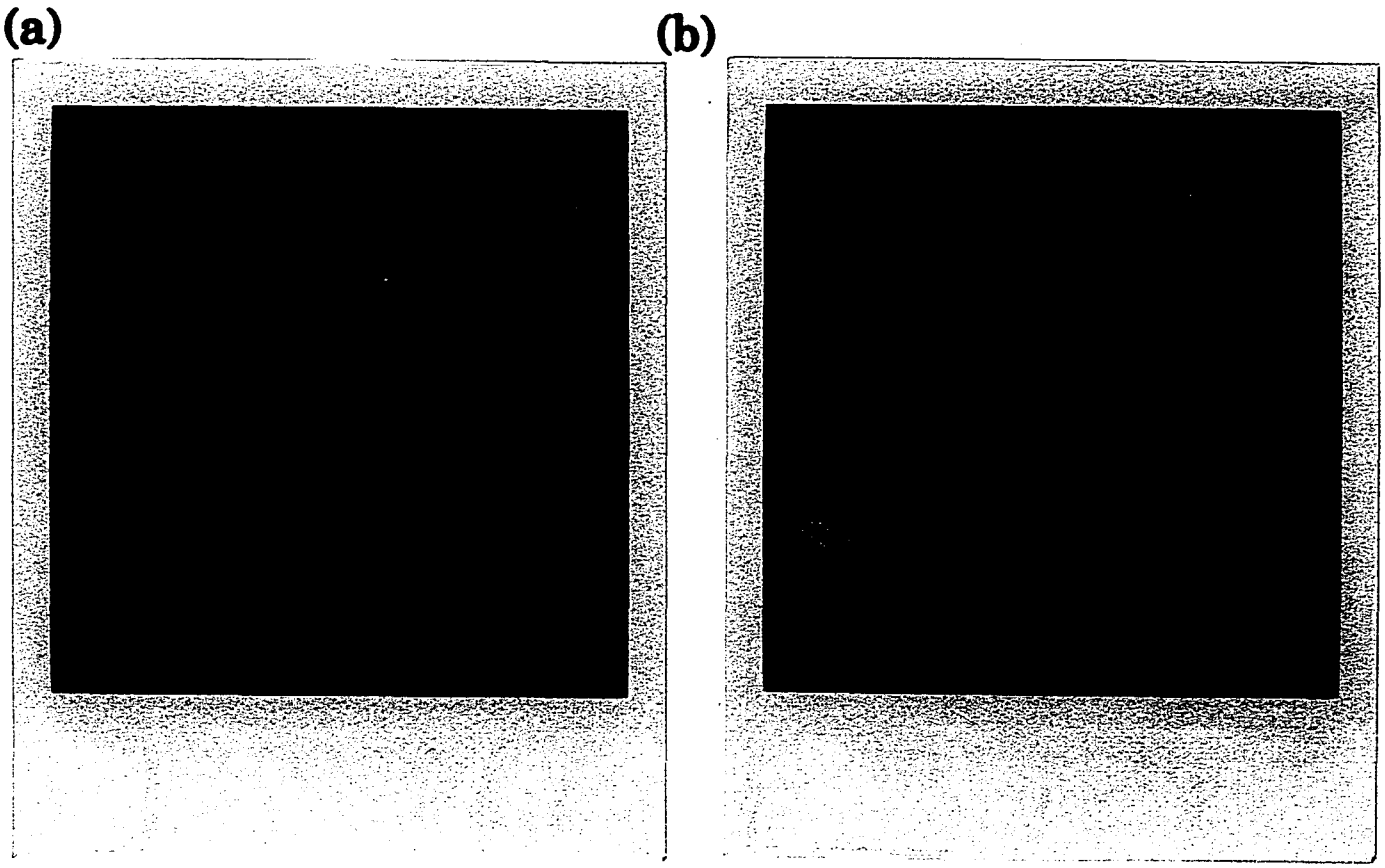

Figure I-24. **Atomic-Scale Scanning Tunneling Microscopy images of (a) bare Ag, (b) octadecanethiol on Ag. The lattice spacing for (a) corresponds to 3.0 Å, the distance between neighboring Ag atoms in the Ag(111) plane. The lattice spacing for (b) is 4.1Å, predicted for the close packed monolayer of thiol on Ag(100).**

structure determined by UPD (i.e., a predominance of Ag (100)) is representative of our evaporated Ag films).

As previously described, the chains of long alkanethiols on Au are tilted ~30° from the surface normal. In contrast, the chains on Ag exhibit tilts of ~14°, suggesting the importance of both the identity/composition (i.e., Ag vs. Au) and crystallinity (i.e., (100) vs. (111)) of the underlying surface.

Head group chemistry

The identity of the underlying substrate can influence the bonding between the thiol and the metal, which, in turn, can affect the orientation of the chains. Although not fully understood at this time, we believe that chemisorption of the alkanethiol monolayers results in the formation of a silver thiolate (R-S-Ag(I)). Evidence for this description of the head group chemistry derives from two sources. Firstly, monolayers with comparable structures can be formed from either solutions of *n*-alkanethiols or the corresponding thiolates. This result suggests that monolayers can be formed from both SH and S^- head groups. Secondly, silver surfaces exposed to the ambient environment of the laboratory are known to have ~1 monolayer of a (native) oxide.

To get information of head group chemistry between S-Au and S-Ag, we attempted to fabricate monolayers from the solution of sodium octadecanethiolate ($NaSC_{18}H_{37}$), which, we assume, exist as an ion pair (Na^+ and $C_{18}H_{37}S^-$) in anhydrous tetrahydrofuran. For the Au substrates, the ellipsometric thickness of the monolayer from ionic $C_{18}H_{37}S^-$ solution was 5 to 10Å, compared to 25Å for those from octadecanethiol. For the Ag as a substrate, ionic $C_{18}H_{37}S^-$ solution produced the same thickness of 30Å as for

a monolayer from octadecanethiol. The IR reflection spectrum of $C_{18}H_{37}S^-$ on Ag is also comparable to that of our octadecanethiol monolayer. However, the IR spectrum of monolayer prepared from the thiolate on Au was quite different from that of an octadecanethiol monolayer. The absorbances of all the modes were weaker for the ionic thiolate prepared monolayer than for the thiol prepared layer, which indicates a lower coverage of the hydrocarbons on the surface. Also the relative absorbances of the CH_2 modes over the CH_3 modes are higher at the thiolate prepared monolayers, which indicates the monolayer is less oriented or more tilted. On Ag surface, the absorbances of the CH_3 modes were comparable,with the ratio of CH_2 mode over CH_3 only slightly higher for a monolayer from the thiolate than that of a thiol monolayer;such an observation qualitatively indicates that the monolayer is slightly more tilted but the surface coverage of monolayers is almost same. This difference between Ag and Au for the ionic thiolate adsorption was not observed in ethanol solution. In ethanol, we did not observe any differences between thiol(RSH) and thiolate(RS^-) adsorption. On both Ag and Au, the thiolate made the same well-oriented monolayeras the thiol. We do not fully understand this mechanism, but postulate the following as a possibility.

For the interaction of RSH on Au, the proton is essential in the initial adsorption step. Other evidence shows that the proton is lost on the monolayer [12]. So either (1) or (2) are possible.

$$RSH + Au \rightarrow RS\text{-}Au + H \qquad (1)$$

$$RSH + Au \rightarrow \underset{\text{(physisorbed)}}{RSH\text{-}Au} \rightarrow \underset{\text{(chemisorbed)}}{RSAu} + H \qquad (2)$$

$$RS^- + Au \rightarrow N.R. \quad (3)$$

The exact nature of the species and its distribution of product "H" from the thiol is not known. However, recent experimental data show that the hydrogen peroxide is produced as a result of thiol adsorption on Au [12]. In aprotic solutions, the ionic RS^- is unreactive toward Au as shown in equation (3). In ethanolic solutions, however, the following equilibrium (4) exists which leads to the production of a protonated thiol.

$$RS^- + EtOH \rightarrow RSH + EtO^- \quad (4)$$

Since the thiol is stronger acid than ethanol, the equilibrium is expected to reside strongly on the left side of equation (4). However, if any RSH is consumed via adsorption at Au, the equilibrium will shift slightly to the right.

As noted, when anhydrous THF is used as a solvent for adsorption, above equilibrium is nonexistent because THF is aprotic solvent. However, thiol may still be produced because of the presence of adsorbed water on the Au surface. At ambient humidities, our surfaces certainly are covered with a small, but unknown amount of water; the lack of quantitative evidence for coverages of water precludes a deduction of its role.

As described in the Experimental Section, the oxide on the Ag surface is probably converted to the hydroxide as a result of exposure to ambient water vapor. The presence of the native oxide points to the existence of Ag^+ ions at the interface. Together, these facts suggest the following reaction

scheme which occurs in ethanol or hexadecane solvents (5) as well as in tetrahydrofuran or dimethylformamide (6).

$$RSH + Ag^+OH^- \rightarrow RS^-Ag^+ + H_2O \quad (5)$$

$$RS^- + Ag^+OH^- \rightarrow RS^-Ag^+ + OH^- \quad (6)$$

So, either RSH or RS^- can react with Ag surfaces. Since equation (6) does not require the presence of a thiolitic proton, the adsorption is not affected by an aprotic solvent.

The difference in the chemistry at Au and Ag implicates the importance of the oxide at Ag. Electronegativities of Ag (1.9) and Au (2.4) relative to S (2.5) suggest that the Ag-S bond has more ionic character than the Au-S bond [64, 65]. As such,the bonding of the *n*-alkanethiols at Au possesses more covalent character than ionic character, whereas *n*-alkanethiols are bonded to Ag through a bond which has more ionic character than covalent character.

From this qualitative bonding description, we can expect a bond angle of Au-S-C close to 110° and Ag-S-C close to 180°. Based on the earlier structural results, we estimate bond angles for Au-S-C of 111° and Ag-S-C of 143° for Ag(100) and 175° for Ag(110). The bond angles at Ag are consistent with the ionic nature of the binding, but require detailed calculations for a more insightful description.

The crystallinity of the substrate also influences the formation and structure of the monolayer. Surface lattice structures of transition metals, for example, are important in the growth of ice overlayers. On hexagonal

symmetry substrates (e.g., Ni(111), Ru(100), and Pt(111)), for which the lattice parameter is close to that for bulk ice, hexagonal overlayers of ice with long range periodic form. In contrast, the corrugated surfaces (e.g., Ni(110)) have a pseudo-hexagonal long range ice overlayer with a slightly distorted structure (c(2x2)) to conform to the substrate atom spacing. The importance of the substrate lattice structure on the overlayer structure is apparent. In addition to effects of substrate crystallinity, the cohesive interaction between neighboring alkyl chains may also influence the structure of monolayers formed from alkanethiols.

Figure I-25 shows the lattice structure for the three low index planes of Ag and Au, the packing of the monolayers, and the resulting tilts of the alkyl chains. Figures I-25 a, d, and g represent the (111), (100), and (110) planes. Figures I-25 b, e, and h represent the most densely packed structures of the alkyl chains. The large circles are the van der Waals radii of the chains. Figure I-25 c, f, and i illustrate the resulting tilts of the chains. The packing arrangements illustrated in Figure I-25 b, e, and h were arrived at by both placing the sulfur atoms at equivalent sites and maximizing alkyl chain density.

The tilts illustrated in Figure I-25 c, f, and i were calculated by allowing the chains positioned as in Figure I-25 b, e, and h to tilt in the direction of the nearest neighbor. If the resulting rows did not touch, the chains also tilted in the direction perpendicular to them. For example, on the (111) surface, the most densely packed arrangement of the molecules occurs for a $(\sqrt{3} \times \sqrt{3})R30°$ overlayer, as illustrated in Figure I-25 b. The nearest neighbor distance in this structure is 5.0Å. To calculate the tilt required to

achieve a packing density limited by the chain van der Waals radius, the chains first are tilted along $\vec{b_1}$ (32°) and then in the direction perpendicular to $\vec{b_1}$ (13°), for a net tilt of 35° (see Figure I-25 caption). This procedure was also followed to arrive at the descriptions of the (100) and (110) surfaces.

The tilt predicted by this model for alkanethiols at Au(111) (32°) agrees reasonably well with that experimentally determined by IR spectroscopy (31°). A hexagonal overlayer structure with interchain spacing of ~5Å has been observed by He scattering, by electron diffraction, and by STM. Since this hexagonal structure has not yet been observed with a technique sensitive to both substrate and overlayer order (e.g., Low Energy Electron Diffraction) conformation of the proposed [4,42] $(\sqrt{3} \times \sqrt{3})R30°$ structure is not possible. However, the observed interchain spacing which corresponds to what is expected for the $(\sqrt{3} \times \sqrt{3})R30°$ structure strongly infers that this is one of the predominant overlayer structures.

A similar analysis based on the diameter of a fluorocarbon chain yields a chain tilt of 0°, consistent with the angle expected for a $\begin{bmatrix} 2 & 0 \\ 0 & 2 \end{bmatrix}$ (also described in Wood notation as p(2x2)) overlayer structure. We have also observed this same spacing by STM.

This model predicts an average chain tilt of 0° from the surface normal for alkanethiols at Ag(100). A representative result of an atomic scale examination of the overlayer structure of octadecanethiol at our evaporated Ag films is illustrated with the STM micrograph in Figure I-24 (b). This figure exhibits a regular array of bright spots, which we presently attribute to tunneling through the sulfur. As a result, this technique only images the head group of the adsorbed molecules. This pattern extends over the entire

Figure I-25. Possible Packing of Alkyl Chains on Ag and Au. The topmost layer of metal atoms for the low index crystal planes of Ag or Au are illustrated in (a) (111) (b) (100) and (c) (110). The vectors $\vec{a_1}$ and $\vec{a_2}$, defining the substrate unit cells are indicated. Metal atoms are 3.0Å in diameter. Overlayer structures arising from the most densely packed arrangement of 4.24Å diameter alkyl chains on the substrate lattice (assuming equivalent sites) are illustrated in b, e and h. Refer to Table V for Matrix notation representations of these structures. Vectors defining the overlayer unit cells, $\vec{b_1}$ and $\vec{b_2}$, are indicated. Tilt angles of the alkyl chains for the three structures are illustrated in c, f and i. The angles were calculated by allowing the chains to tilt in the direction of the nearest neighbors. For a spacing d between chains and a chain diameter t, the tilt angle is given by $\cos\theta' = \frac{t}{d}$. If the rows are separated by void volume, the chains are allowed to tilt in the perpendicular direction. This tilt angle is given by $\cos\theta'' = \frac{t}{r}$ where r is the interrow spacing. The net tilt angle q is calculated by solving for the projections on the x and y axis resulting from the two tilts q' and q" using the Pthagorean Theorem.

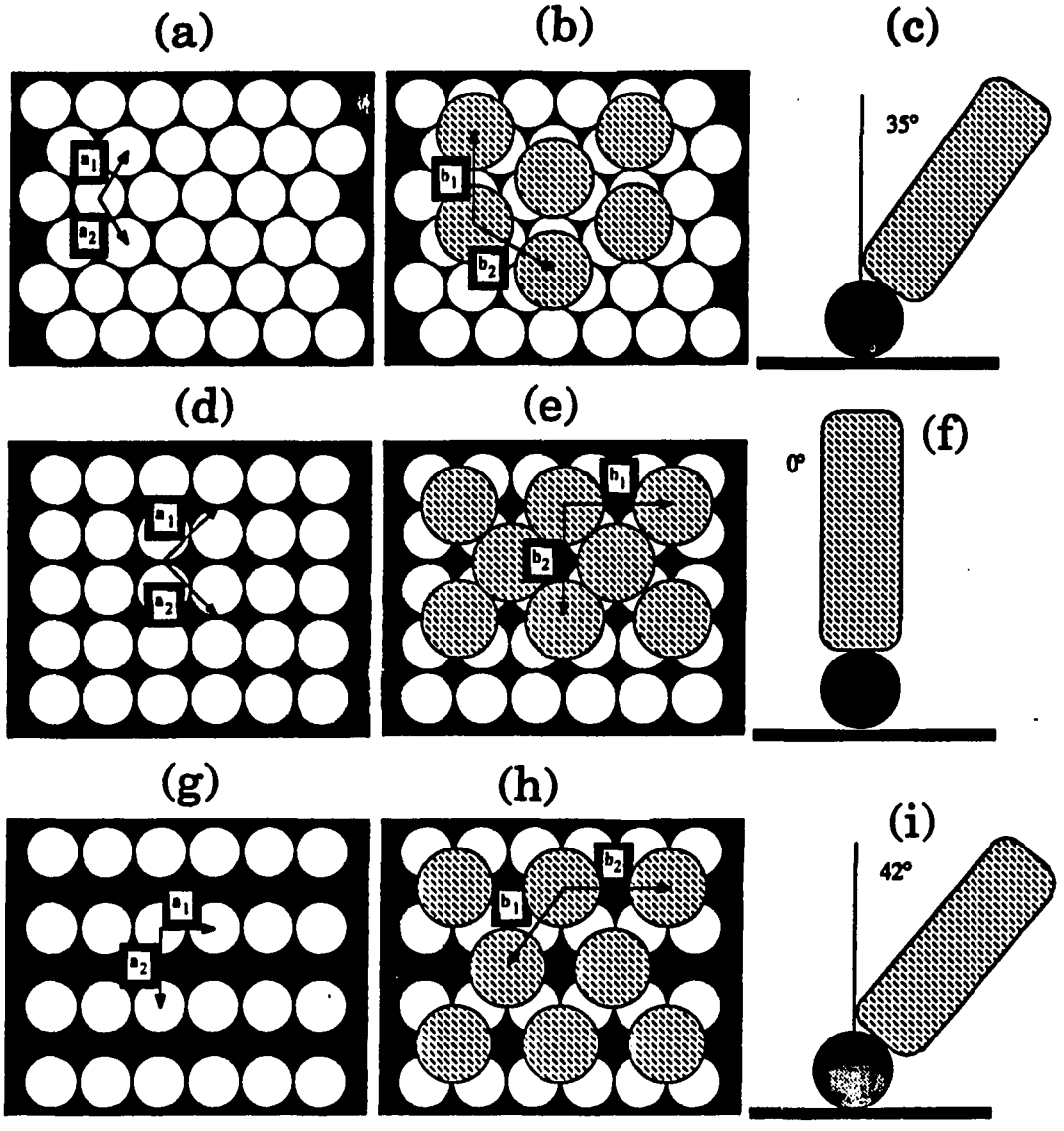
(a)
(b)
(c)
35°
(d)
(e)
(f)
0°
(g)
(h)
(i)
42°

60 x 60 Å image and has been observed by us on several samples. The spacing between a spot and its four nearest neighbors is ~4.0Å, as shown by two cross sections in Figure I-24 (b). The spacing is comparable to that expected for an alkanethiol monolayer at Ag(100), as represented by Figure I-25 e.

Although atomic scale images are not always obtained on every sample, the structure in Figure I-24 (b) is the only regular array has ever observed. This 4Å spacing represents a structure in which the alkyl chains are closely packed. Since the chains are arranged in a square lattice ($(\sqrt{2} \times \sqrt{2})R45°$), instead of the hexagonal lattice preferred by hydrocarbon chains, the substrate plays an important role in determining overlayer structure. With this overlayer structure, the alkyl chains are packed at their van der Waals radii without a tilt of the chains (0° tilt).

The chain tilt predicted for a monolayer at Ag(100) from our model of Figure I-25 (0°) is inconsistent with that determined from the orientational analysis of infrared spectroscopy (14°). Possible explanations for these differences include the presence of more than one crystal faces and a splayed structures, as illustrated in Figure I-26. Figure I-26 depicts a surface which is a composite of two crystal faces. The chains on the (100) face are directed perpendicular to the surface, while those on the (111) face are tilted 35°. The tilt of the composite surface could represent, for example, one which is ~16% (111) and ~84% (100). Figure I-26 illustrates a structure in which the head groups prefer a spacing that is less than the van der Waals radii of the chains. To alleviate strain, the chains splay away from each other as shown.

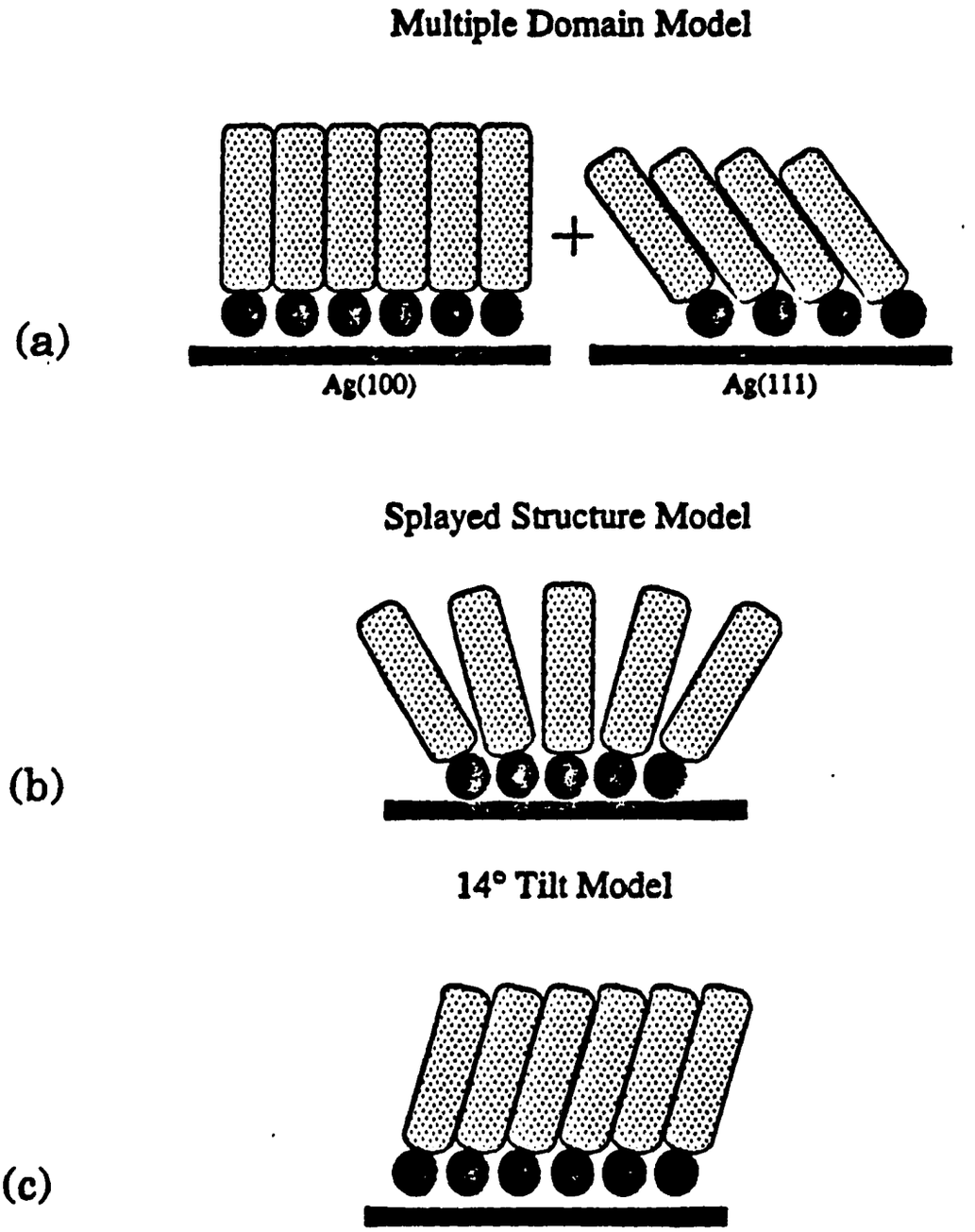

Figure I-26. Three models for the alkanethiols on Ag surface to explain 14° average tilt from the surface normal. (a) multiple domain model (b) splayed structure model (c) 14° average tilt model.

Comparison with Monolayers on Au Surfaces

The presence of the odd-even effect in both our contact angle and IR measurements and the fact that opposing odd-even behavior is demonstrated for Ag and Au surfaces suggest that the metal-sulfur ("head group") bonding geometry is different on the two substrates.

The peak position and absorbance trends in the IR spectra of *n*-alkanethiol monolayers formed on Au substrates measured in this laboratory agree with those from other laboratories [2-4] and selected parts are reproduced here. Figures I-11 and I-13 show IR spectra of the C-H stretching region of *n*-alkanethiol monolayer on Au and Ag. Qualitative comparison of the spectra on the two substrates suggests that the molecules are oriented differently. The infrared surface selection rule dictates that only vibrational modes with components of the oscillating transition dipole perpendicular to the surface are IR active`. The IR spectra in Figures I-11 and I-13 show that, on average, both the asymmetric and symmetric CH_2 dipoles have smaller perpendicular components on Ag than on Au, implying that the alkyl chains are oriented more normal to the surface on Ag. Furthermore, since the dipole moments of $\nu_a(CH_2)$ and $\nu_s(CH_2)$ are orthogonal, both modes can be IR active only if the alkyl chains deviate from the surface normal in such a way that both dipoles have a component perpendicular to the surface. Calculated tilt and twist angles for crystalline-like monolayers on Au are listed in Table I-3. Tilt angles for *n*-alkanethiols on Au agree reasonably well with those reported by others of $\theta \sim 20\text{-}30^\circ$ [1, 2] and $\theta = 40^\circ$, with Thus, the tilt of the alkyl chains for monolayers on Ag is less than on Au.

From the Tl and Pb UPD experiments on the bare Ag and Au substrates described above, we know that the evaporated Ag and Au surfaces have different surface structures: the Ag surface is a combination of Ag(100) and Ag(110) domains, while the Au substrates are primarily Au(111). We find that the most densely packed commensurate hydrocarbon phases (assuming chain diameter is 4.2Å) on the (100), (110), and (111) faces of Ag or Au (note: lattice constants are both 4.1 Å) are $\begin{bmatrix} 1 & 1 \\ -1 & 1 \end{bmatrix}$ (or $(\sqrt{2} \times \sqrt{2})R45°$), $\begin{bmatrix} 1 & 1 \\ 2 & 0 \end{bmatrix}$, and $\begin{bmatrix} 1 & -1 \\ 1 & 2 \end{bmatrix}$ (or $(\sqrt{3} \times \sqrt{3})R30°$), respectively. In these structures, the hydrocarbon chains are packed as closely as possible while maintaining substrate registry. The calculated surface coverages for these structures are 9.9, 7.0, and 7.6 x 10^{-10} moles/cm^2, respectively. If the chains are allowed to tilt just until adjacent chains touch, the predicted tilt angles are θ = 0°, 42°, and 35°, respectively.

For the Ag surfaces, which are a combination of Ag(100) and Ag(110) domains, we expect a tilt angle between 0° and 32°. The observed tilt angle of 14° can result from, to the first approximation, a surface which is 2/3 of (110) and 1/3 of (100). For the Au substrates, which are primarily (111), our calculated tilt angle of 31° agrees fairly well with the 32° expected on a (111) surface.

The odd-even effect described above for monolayers on Ag is also observed for alkanethiols on Au. Manifestation of this effect is illustrated in Figure I-15 (b) for IR and Figure I-10 for contact angle. Also Figure I-18 (c) shows the proposed structure. Comparing our data for Au and Ag shows that the trend is opposite for the two substrates. A chain length with a "high" IR absorbance or contact angle on Au has a "low" IR intensity or contact angle on

Ag. The larger magnitude of the odd-even effect on Au is consistent with a larger tilt angle for the chains: a larger difference exists between the orientation of the methyl dipole for an even and odd chain if the chains are canted further from the surface normal, as on Au.

Both the IR and contact angle measurements on Ag, illustrated in Figures I-9 and I-14 (b), show that the odd-even behavior becomes less pronounced as chain length increases. For the Au substrates, on the other hand, the effect continues throughout the series. We believe that the "dampening" effect on Ag results from interchain interactions in the tail region of the molecule which cause a slight distortion of the all *trans*-molecular skeleton at the chain terminus. The question addressing the nature of this interaction requires an answer which can, at the same time, explain the persistence of the odd-even effect on Au. An explanation which can reconcile these facts is that the surface density (coverage) of thiol on Ag is greater than on Au. Based on the crystallographic orientation and expected surface coverages described above for Ag and Au, we know the alkyl chains are, on average, more closely packed on Ag than on Au. Thus, if the chains are more closely packed on Ag, interchain interactions may favor a change in structure for longer chains, i.e., the interchain interactions may overcome the forces which favor all-*trans* configuration. The disappearance of the odd-even effect on Ag for long chains, therefore, may be attributed to interchain interactions. In other words, since the chains are, on average, more closely spaced on Ag than Au, van der Waals interactions between chains may overcome the energy gained in an extended all *trans*- configuration.

Alternatively, a higher surface coverage of thiol on Ag substrates may be due to an impurity effect. We know, from AES, that our "clean" Ag surfaces contain adsorbed Cl, O, S, and C. Adsorbates on Ag may be displaced on thiol adsorption, driven into the bulk, or remain on the surface. In the first two cases, the presence of the impurity is not expected to alter the thiol coverage. In the site blocking case, on the other hand, impurities can block adsorption sites preventing adsorption. In this case, a lower surface coverage is expected. However, since heterogeneous charge transfer experiments (Figure I-21) indicate that long chain molecules (n>8-11) are effective barriers to electron transfer for $Ru(NH_3)_6^{3+}$ and, therefore, relatively defect-free, site blocking impurities probably do not change the surface coverage of thiol. In fact, if site blocking prevents adsorption, an imperfect monolayer is predicted.

There is a possibility that our monolayers contain a high defect density. Poor monolayers could form as a result of the self-assembly process or the nature of the surface. Defect ridden structures could result if the monolayers were not immersed sufficiently long in the self-assembly solution. However, we allowed 12-24 hours for self-assembly and Bain *et al.* [8] have shown that monolayer formation is complete after a few hours. Also, our in situ ellipsometric data shows that the monolayer formation (or bilayer formation in solution phase) is complete in an hour. Defective structures could also be formed by self-assembly from solutions containing a high disulfide concentration. Our thiols were purified before use and solutions were never used for longer than ~5 days. Furthermore, IR, contact angle, and electrochemical data indicate that the long-chain monolayers are highly

ordered crystalline structures. Thus, we do not believe that the monolayers contain a large number of defects as a result of insufficient adsorption time or disulfide impurities.

Another cause of poor-quality monolayers may be the presence of an impurity on the surface which blocks thiol adsorption. There is a possibility of the diffusion of Cr from the adhesion layer to the surface causing poor monolayer formation. Since Cr does not adsorb thiols strongly and, if present on the surface, it could cause defects in the monolayer. However, capacitance current through monolayers assembled on Au films onto which no Cr adhesive layer is evaporated is a factor of 1.2 lower than the values obtained for samples with a Cr adhesive layer. Auger electron spectroscopy performed on the bare Ag and Au substrates has verified the presence of a number of impurities on the "clean" surfaces, although Cr is never observed.

To summarize, *n*-alkanethiols on Ag are oriented more along the surface normal than on Au. Monolayers formed on both substrates exhibit the odd-even effect apparent in both the IR and contact angle data. However, the trend is opposite for the two substrates, suggesting a head group is playing an important role for the orientation of alkanethiol monolayers.

CONCLUSIONS

We have utilized a multi-technique approach to unravel the structure of *n*-alkanethiols on Ag and Au. As shown with electrochemical methods and scanning tunneling microscopy results, the orientation of the alkanethiol monolayer at Ag and Au is strongly dependent on the substrate crystallinity and nature of the metal-sulfur bond. The infrared reflection spectroscopy, contact angle measurements, capacitance measurements, and ellipsometric data allow us to propose a model describing the average orientation and structure of alkanethiol monolayers on Ag and Au. The adsorbed thiolate is bonded to the Ag surface ionically, with an Ag-S-C bond angle of ~147° and an Au-S-C bond angle of ~110°, *values estimated from the tilts of the alkyl chains*. The alkyl chain extends away from the metal surface, tilted an average of 14° from the surface normal for Ag and 32° from the surface normal for Au. On Ag surfaces, this 14° arises because of contributions from portions of the monolayer assembled at Ag(100)(0°tilt) and Ag(110)(32°tilt) domains. The chain orientation is fixed for all chain lengths, giving rise to the odd-even effect observed in both the IR and contact angle measurements. The different nature of the head group chemistry between Ag-S and Au-S is also responsible for the different odd-even effect of monolayers on Au and Ag. The observed odd-even effect of methyl group orientation for alkanethiol on Ag is offset by a methylene group from that on Au. Overall, it is shown that the collective utilization of a broad range of surface characterization methods can provide more information about the interfaces than each method is applied separately. Study of the monolayers on different substrates such as

mica, silicon, and glass will provide more information about the relationship between the surface roughness and the structure of the monolayers on these substrates. More importantly, characterization of the monolayers on single crystal substrates will clarify the basic reason for the different structure of monolayers on different substrates.

The bilayer structure of organic films in solution phase is proposed with the in situ ellipsometry results. Understanding of the details of this structure may provide important insights into bio-membranes. Several in situ methods, such as in situ IR, in situ STM, and in situ ellipsometry can be developed further to study this area.

ACKNOWLEDGEMENTS

We thank K. Wolff for conducting preliminary experiments on the alkanoic acids on Ag system. We thank D. Wiederen for assistance with the ICP-AES experiments, F. Smith for assistance with the ICP-MS experiments, and Dr. A. J. Bevolo for assistance with the Auger measurements. Ames Laboratory is operated for the U.S. Department of Energy by Iowa State University under Contract No. W-7405-eng-82. This work was supported by the Office of Basic Energy Sciences, Chemical Science Division.

REFERENCES

1 W. C. Bigelow, E. Glass, and W. A. Zisman, *J. Coll. Sci.*, **1946**, 1, 563.

2 M. A. Richard, J. Deutch, and G. M. Whitesides, *J. Am. Chem. Soc*, **1981**, 100, 6613.

3 D. L. Allara and R. G. Nuzzo, *Langmuir*, **1985**, 1, 52.

4 N. E. Schlotter, M. D. Porter, T. B. Broght, and D. L. Allara, *Chem. Phys. Lett.*, **1986**, 132, 93.

5 L. C. F. Blackman, M. J. S. Dewar and H. Hampson, *J. Appl. Chem.*, **1957**, 7, 160-171.

6 L. C. F. Blackman and M. J. S. Dewar, *J. Chem. Soc.*, **1957**, 162-165.

7 L. C. F. Blackman and M. J. S. Dewar, *J. Chem. Soc.*, **1957**, 171-176.

8 C. D. Bain, E. B. Troughton, Y. T. Tao, J. Evall, G. M. Whitesides, and R. G. Nuzzo, *J. Am. Chem. Soc.*, **1989**, 111, 321-335.

9 M. D. Porter, T. B. Bright, D. L. Allara, and C. E. D. Chidsey, *J. Am. Chem. Soc.*, **1987**, 109, 3559.

10 R. G. Nuzzo, L. H. Dubois, and D. L. Allara, *J. Am. Chem. Soc.*, **1990**, 112, 558.

11 R. G. Nuzzo, B. R. Zegarski, and L. H. Dubois, *J. Am. Chem. Soc.*, **1987**, 109, 733.

12 C. A. Widrig, C. Chung, and M. D. Porter, in preparation.

13 L. Strong and G. M. Whitesides, *Langmuir*, **1988**, 4, 546-558.

14 C. E. D. Chidsey, G-Y. Liu, P. Rowntree, and G. Scoles, *J. Chem. Phys,*, **1989**, 91, 4421.

15 C. A. Widrig, C. A. Alves, and M. D. Porter, in preparation.

16 W. A. Zisman, *J. Chem. Phys.*, **1941**, 9, 534.

17 W. A. Zisman, *J. Chem. Phys.*, **1941**, 9, 729.

18 G. Rovida and F. Pratesi, *Surface Science*, **1975**, 52, 542.

19 A. M. Bradshaw, A. Engelhardt, and D. Menzel, *Ber. Bun Gesellschaft*, **1972**, 76, 500.

20 R. W. Joyner and M. W. Roberts, *Chem. Phys. Lett.*, **1979**, 60, 459.

21 C. Backx, C. P. M. De Groot, and P. Biloen, *Surface Science*, **1981**, 104, 300.

22 R. B. Grant and R. M. Lambert, *Surface Science*, **1984**, 146, 256.

23 J. S. Hammond, S. W. Gaarenstroom, and N. Winograd, *Anal. Chem.*, **1975**, 47, 2193.

24 W. Wustner and D. Menzel, *Thin Solid Films*, **1974**, 24, 211.

25 W. M. Moore and P. J. Codella, *J. Phys. Chem.*, **1988**, 92, 4421.

26 C. Au, S. Singh-Boparai, and M. W. Roberts, *J. Chem. Soc., Faraday Trans. I*, **1983**, 79, 1779.

27 L. Chau and M. Porter, private communication.

28 M. Born and E. Wolf, Principles of Optics, Pergamon Press: New York, **1965**.

29 O. S. Heavens, Optical Properties of Thin Solid Films, Dover: New York, **1965**.

30 W. N. Hansen, In Advances in Electrochemistry and Electrochemical Engineering, P. Delahey and C. W. Tobias, Eds., Wiley: New York, **1973**; Vol. 9.

31 J. D. Swalen, R. Santo, M. Tacke, and J. Fischer, *IBM J. Res. Develop.*, **1977**, 21, 168.

32 F. L. McCrackin, E. Passaglia, R. R. Stromberg, and H. L. Steinberg, *J. Res. Natl. Bureau of Standards-A.*, **1963**, 67A, 363-377.

33 W. A. Zisman, in A Decade of Basic and Applied Science in the Navy, Office of Naval Research, U.S. Government Printing Office: Washington, D.C., **1957**; p. 30.

34 P. G. de Gennes, *Reviews of Modern Physics*, **1985**, 57, 827.

35 G. M. Whitesides and P. E. Laibinis, *Langmuir*, **1990**, 6, 87.

36 R. G. Greenler, *J. Chem. Phys.*, **1966**, 44, 310.

37 L. Pauling, The Nature of the Chemical Bond, Cornell University Press: Ithaca, New York, **1960**.

38 Handbook of Chemistry and Physics, Ed., R. C. Weast, CRC: Boca Raton, FL, **1981**.

39 J. Gun, J. Sagiv, *J. Colloid Interface Sci.*, **1986**, 112, 457.

40 H. W. Fox and W. A. Zisman, *J. Colloid Sci.*, **1952**, 7, 428.

41 S. R. Cohen, R. Naaman, and J. Sagiv, *J. Phys. Chem.*, **1986**, 90, 3054.

42 R. G. Snyder, H. L Strauss, and C. A. Ellinger, *J. Phys. Chem.*, **1982**, 86, 5154.

43 I. R. Hill and I. W. Levin, *J. Chem. Phys.*, **1979**, 70, 842.

44 R. G. Snyder, S. L Hsu, and S. Krimm, *Spectrochim. Acta, Part A*, **1978**, 34, 395.

45 E. Sabatani, I. Rubinstein, R. Maoz, and J. Sagiv, *J. Electroanal. Chem.*, **1987**, 219, 365.

46 E. B. Wilson, Jr., J. C. Decius, and P. C. Cross, Molecular Vibrations, McGraw-Hill: New York, 1955; p. 285.

47 C. J. Sandroff, S. Garoff, and K. P. Leung, *Chem. Phys. Lett.*, 1983, 96, 547.

48 W.J.-P. Ryckaert, M. L. Klein, and I. R. McDonald, *Phys. Rev. Lett.*, 1987, 58, 698.

49 J.-P. Ryckaert and M. L. Klein, *J. Chem. Phys.*, 1986, 85, 1613.

50 S. M. Stole and M. D. Porter, *Langmuir*, in press

51 D. L. Allara and R. G. Nuzzo, *Langmuir.*, 1985, 1, 45.

52 T. H. Joo, K. Kim, and M. S. Kim, *J. Phys. Chem.*, 1986, 90, 5816.

53 C. J. Sandroff and D. R Herschbach, *J. Phys. Chem.*, 1982, 86, 3277.

54 A. J. Bard, L. R. Faulkner, Electrochmical Methods: Fundamentals and Applications, Wiley: New York, 1980.

55 J. W. Schultze and D. Dickertmann, *Surface Sci.*, 1976, 54, 489-505.

56 D. Dickertmann, F. D. Koppitz, and J. W. Schultze, *Electrochemica Acta*, 1976, 21, 967-971.

57 A. Hamelin, A. Katayama, G. Picq, and P. Vennereu, *J. Electroanal. Chem.*, 1980, 113, 293-300.

58 D. M. Kolb, *Adv. Electrochem.*, 1978, 11, 125-271.

59 K. Engelmann, W. J. Lorenz, and E. Schmidt, *J. Electroanal. Chem.*, 1980, 114, 11-24.

60 C. Chung and M. D. Porter, in preparation.

61 A. Bewick and B. Thomas, *J. Electroanal. Chem.*, 1975, 65, 911.

62 R. I. Tucceri and D. Posadas, *J. Electroanal. Chem.*, 1989, 270, 415.

63 C.M. S. Zei, Y. Nakai, G. Lehmpfuhl, and D. M. Kolb, *J. Electroanal. Chem.*, 1983, 150, 201.

64 A. Itaya, M. Van der Auweraer, and F. C. DeSchryver, *Langmuir*, 1989, 5, 1123.

65 C. E. Mortimer, Chemistry A Conceptual Approach, 4th ed., Van Nostrand: New York, 1979.

PART II. MOLECULAR RECOGNITION BY SPONTANEOUSLY ADSORBED MONOLAYERS OF SULFUR-BEARING CYCLODEXTRIN DERIVATIVES ON GOLD AND SILVER SURFACES

ABSTRACT

As an example of functional interfaces, molecular recognition interfaces are fabricated by the spontaneous adsorption of sulfur-bearing organic compounds on Au and Ag surfaces, and properties of the interfaces are studied.

Sulfur-bearing cyclodextrin derivatives are synthesized and monolayers of these compounds are fabricated onto the evaporated Au and Ag substrates by the spontaneous adsorption from ethanol solution. Compounds studied are hexakis(6-thio-6-deoxy)-α-cyclodextrin, hexakis(6-ethylthio-6-deoxy)-α-cyclodextrin, hexakis(6-dodecylthio-6-deoxy)-α-cyclodextrin, heptakis(6-thio-6-deoxy)-β-cyclodextrin, heptakis(6-ethylthio-6-deoxy)-β-cyclodextrin, and heptakis(6-dodecylthio-6-deoxy)-β-cyclodextrin.

Optical ellipsometry, infrared reflection spectroscopy, contact angle measurement, and electrochemical measurements show that these molecules make monolayers both on the Au and the Ag surfaces. For the thiols adsorbed on Au/mica substrates, surface coverages are measured by electrochemical desorption in 0.5M potassium hydroxide solution. The surface coverages are about 90% for both hexakis(6-thio-6-deoxy)-α-cyclodextrin and heptakis(6-thio-6-deoxy)-β-cyclodextrin. Contact angle measurements, electrochemical desorption, infrared reflection spectroscopy, and ellipsometry show that the hydroxyl groups of cyclodextrin thiols are exposed on the monolayer surfaces. It is also found that the monolayers of these compounds have more defects, compared to the alkanethiols adsorbed on either gold or silver. Molecular recognition of cyclodextrin derivatives

monolayer, evidenced with infrared spectroscopic data and electrochemical results, as well as potential applications of these monolayers are discussed.

INTRODUCTION

This section describes the fabrication, characterization, and application of the molecular recognition monolayer films on the noble metal surfaces. This is a part of the broad ranging program to fabricate the organic thin films in which we can control the structure of film at a molecular level. Such control of surface structure can contribute enormously to the exploration of interfacial phenomena such as wetting [1], adhesion [2], corrosion [3], artificial bioorgans [4], and lubrication [5]. The work reported here focuses on the fabrication of monolayers composed of cyclodextrin moieties and to translate the size exclusion effect and/or the "molecular recognition" discrimination based on the cyclodextrin cavity bound to an interface.

It is now firmly established that the organic compounds with sulfur moiety adsorb strongly and spontaneously onto Au [6-8] and Ag [9] to form monolayers. Alkanethiol monolayers both on Au and Ag have been well characterized. Dialkyl sulfide and dialkyl disulfide monolayers have also been studied [10]. "Two component" monolayers (two different end groups) have been studied to assess the scope of flexibility in controlling interfacial properties [11]. Monolayers formed by spontaneous adsorption offer unique opportunities as model systems for organic surface research: they are easily fabricated; they do not require a Langmuir-Blogett trough; they are a single molecular thick (a structure is simple compared to that of a polymer interface). Theoretically, if we can carefully synthesize a molecule with specific targeted properties and functionalize it with a sulfur moiety, we can fabricate monolayers with a specific function. The potential areas of

application of interest to us include photo-switches, molecular recognition devices, and biocompatible membranes.

Of these potential areas, molecular recognition devices constitute the focus of this research. Molecular recognition is the ability to recognize and respond accordingly to a specific component (e.g., a molecule or an ion) in the presence of other species. An example of a molecular recognition structure membrane is the biomembrane. For example, activity, communication, and regulation in living organisms are mostly governed by a bilayer cell membrane, which has a molecular recognition function. By utilizing the experience of the monolayers of targeted moieties, we can produce molecular recognition monolayers on metal surfaces. These layers can serve as model systems for biomembrane studies, and as a sensor membrane which can increase the specificity in electrochemical analysis. Such monolayers can also potentially perform a selective electrochemical synthesis because of different complexation constants toward different geometric or optical isomers.

To characterize organic monolayers, many different methods can be applied according to the specific property we want to study. In this study, we have applied a variety of surface sensitive methods to characterize the interface structure. Optical ellipsometry was used to measure a monolayer thickness and/or surface density. Infrared reflection spectroscopy was used for information of surface composition, spatial orientation, surface coverage, and reactivity of the surfaces. Contact angle measurement provided us the hydrophobicity of the surface, giving structural information indirectly. Electrochemical measurements gave information about reactivity, true surface area, surface texture, and defects on the monolayer.

In this work, we synthesized the cyclodextrin derivatives, hexakis(6-thio-6-deoxy)-α-cyclodextrin, hexakis(6-ethylthio-6-deoxy)-α-cyclodextrin, hexakis(6-dodecylthio-6-deoxy)-α-cyclodextrin, heptakis(6-thio-6-deoxy)-β-cyclodextrin, heptakis(6-ethylthio-6-deoxy)-β-cyclodextrin, and heptakis(6-dodecylthio-6-deoxy)-β-cyclodextrin , all of which contain sulfur as a binding site onto the Au and the Ag surfaces. A variety of surface sensitive techniques have been applied to characterize the monolayers fabricated by the spontaneous adsorption method.

We are exploring the potential for constructing molecular recognition interfaces. Selective binding of a specific compound by a cyclodextrin monolayer is studied. Possible follow-up studies are also discussed.

ABBREVIATIONS

The following abbreviations were used throughout the Part II of this dissertation.

ADCA	Adamentane carboxylic acid
α-CD	α-cyclodextrin
α-CDBr	hexakis(6-bromo-6-deoxy)-α-cyclodextrin
α-CDSH	hexakis(6-thio-6-deoxy)-α-cyclodextrin
α-$CDSC_2$	hexakis(6-ethylthio-6-deoxy)-α-cyclodextrin
α-$CDSC_{12}$	hexakis-6-dodecylthio-6-deoxy)-α-cyclodextrin
β-CD	β-cyclodextrin
β-CDBr	heptakis(6-bromo-6-deoxy)-β-cyclodextrin
β-CDSH	heptakis(6-thio-6-deoxy)-β-cyclodextrin
β-$CDSC_2$	heptakis(6-ethylthio-6-deoxy)-β-cyclodextrin
β-$CDSC_{12}$	heptakis(6-dodecylthio-6-deoxy)-β-cyclodextrin
CTAB	Cetyl trimethylammonium bromide
FCA	Ferrocene carboxylic acid
SDS	Sodium dodecyl sulfate

LITERATURE REVIEW

Monolayers Formation

The organization of organic monolayer assemblies at smooth surfaces provides a rational approach for fabricating interfaces with a well-defined atomic and molecular level control in composition, structure, and thickness [12]. These monolayer assemblies with controlled structure can serve as model systems to probe the fundamental chemical and physical interactions at a variety of technologically important interfaces and material. Applications of these include corrosion control [3], wetting [1], adhesion [2], tribology [5], and biocompatibility [4]. Some monolayer assemblies are also similar to the components of the cell wall of biological membranes. So, the study of these monolayer systems can provide insights into structure-reactivity relationships of these important membranes.

LB films and spontaneously assembled films

Organic monolayer films can be obtained mainly by two methods. One is using the Langmuir-Blogett (LB) film method and the other is using the spontaneous adsorption method. In the LB film method [13-16], as shown in Figure II-1, a small volume of dilute solution of organic compounds is dispersed on the liquid (normally aqueous) subphase contained in a Teflon trough (step a in Figure II-1). While the surface pressure is monitored with either a Wilhelmy plate or a Langmuir-Blogett film balance, the film is compressed until a compact layer is formed (step b in Figure II-1). Then, the compressed film is transferred onto the substrate (step c in Figure II-1). This LB method can produce crystalline multilayer structures, especially with

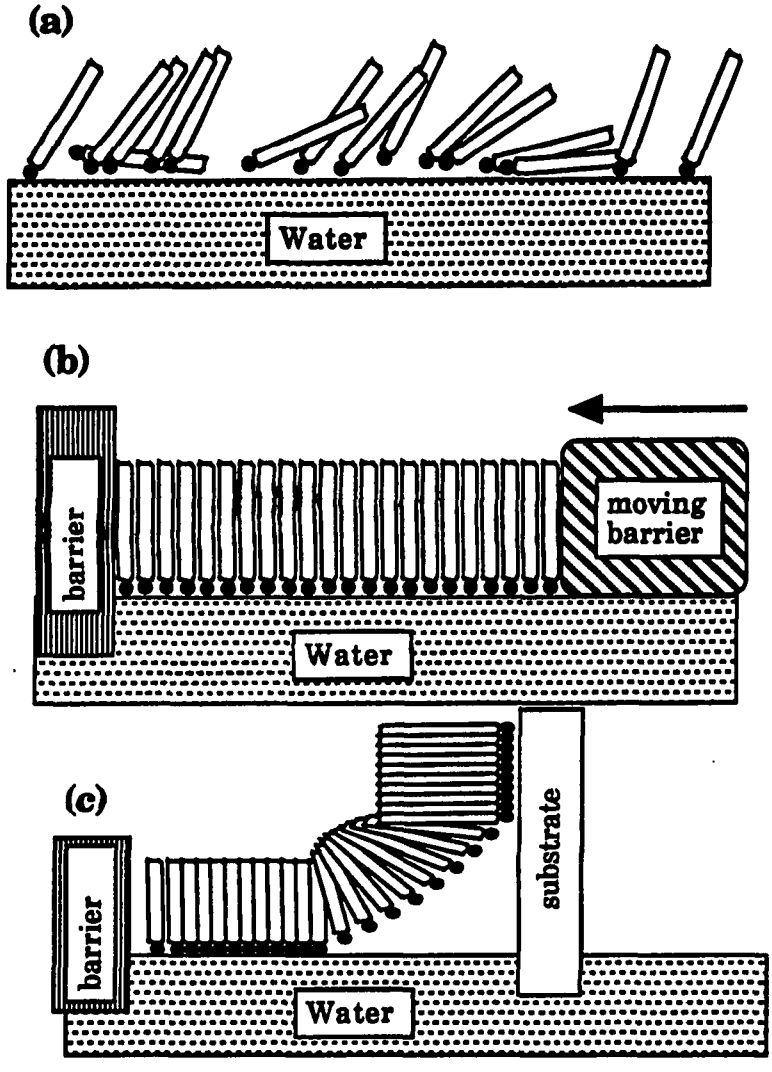

Figure II-1. Formation of Langmuir-Blogett films. (a) a drop of dilute solution of a organic compound is dispersed on the surface of water. (b) The film is compressed until compact layer is obtained. (c) The film is transferred onto a substrate.

amphiphilic compounds with a long alkyl chain as a tail group. Since the LB film is first a compressed film on a water-air interface, the stability of the structure of the compounds at this interface plays a major role in their formation with transferred monolayer assemblies often described as being metastable [17].

In the spontaneous adsorption method shown in Figure II-2, the metal substrate is immersed into a dilute solution of the desired compound. After the compound is spontaneously adsorbed, the substrate is emersed and rinsed to remove residual material. This method is easy to use and can avoid many complexities and limitations of the LB film method. The studies of compatibility of films produced by the LB method and by the spontaneous adsorption have shown that the structures of both are comparable [18-20].

Spontaneously adsorbed monolayer assemblies can be fabricated with carboxylic acids [21-23], silanes [24], and organosulfur compounds at a variety of metallic and nonmetallic surfaces to produce stable, highly oriented, and sometimes polyfunctional structures. Among these systems, monolayers of organosulfur compounds at Au are particularly attractive as the bare surface is zero valent and relatively unreactive. This low level of reactivity facilitates the handling and formation of surface films in the laboratory ambient.

Properties of Cyclodextrin

General properties

Cyclodextrins have been a focus of various fields of research [25]. Cyclodextrins are doughnut shaped oligosaccharides produced by the action of

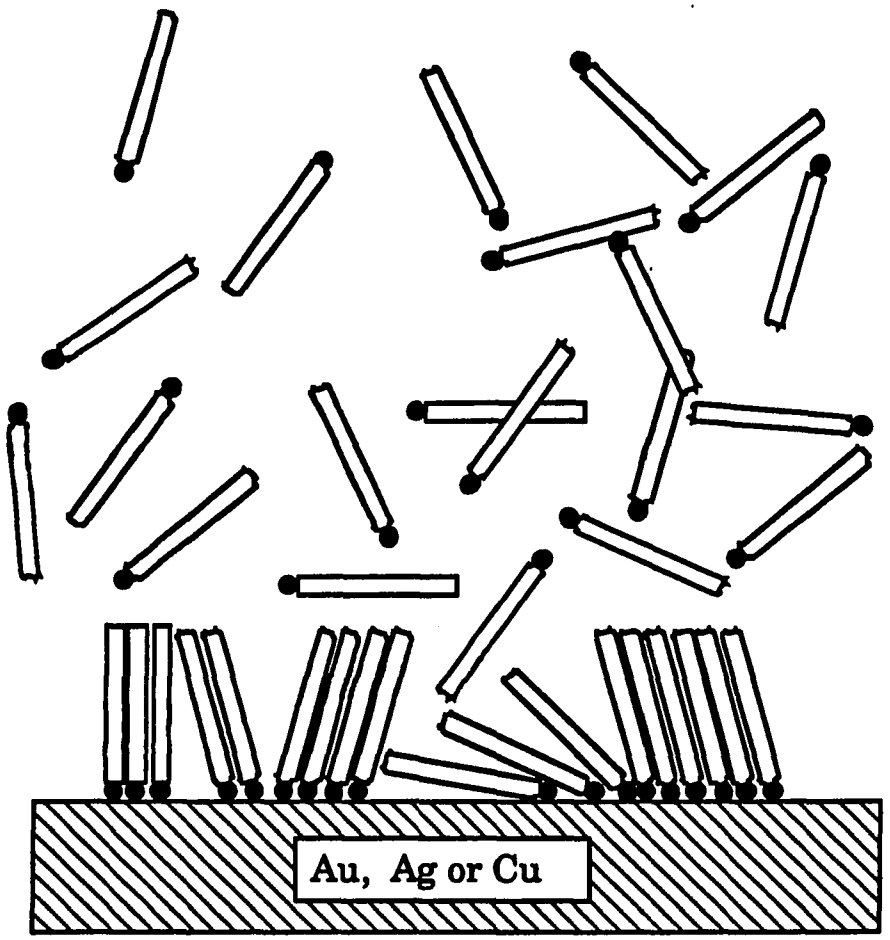

Figure II-2. Formation of spontaneously adsorbed monolayers.

the amylase of *Bacillus macerance* on starch and related compounds. Depending on the number of glucose units (6,7,8,...), the cyclodextrins are designated by Greek letters: α- , β-, γ- ,...., respectively. Other common names are cyclohexaamylose or cyclohexaglucan(α-1,4) for α-cyclodextrin, cycloheptaamylose or cycloheptaglucan(α-1,4) for β-cyclodextrin, and cyclooctaamylose cyclooctaglucan(α-1,4) for γ-cyclodextrin. Their structures and physical properties have been well characterized both as a solid and in aqueous solutions by nuclear magnetic resonance, infrared spectroscopy, optical rotatory dispersion spectroscopy, and X-ray crystallography [26]. Important properties of cyclodextrins are listed in Table II-1. Figure II-3 shows the structure and shape of the three most common cyclodextrins.

Inclusion complexation

The most important characteristic of cyclodextrins is their ability to form inclusion complexes with various compounds, in which a guest compound is included into the cavity of a cyclodextrin (host). Guest compounds range from acids, amines, ions such as ClO^{4-}, SCN^-, halides, to aliphatic, alicyclic [27], and aromatic hydrocarbons, and even to rare gases. In most cases, the complexation constant is well correlated with the size of the substrate and contour of the cavity of the cyclodextrin. Complexation constants have been measured with various methods including UV-VIS absorption spectroscopy, nuclear magnetic spectroscopy [28], electron spin resonance spectroscopy [29], fluorescence spectroscopy, and electrochemistry [30,31].

Cyclodextrins catalyze many organic reactions, and, in some ways, mimic enzyme reactions. Furthermore, cyclodextrins exhibit a certain

Table II-1. Physical and chemical properties of cyclodextrins [32]

Properties	α-cyclodextrin	β-cyclodextrin	γ-cyclodextrin
Number of glucose residues	6	7	8
Molecular weight (calculated)	972	1135	1297
Molecular size (Å)			
inside diameter	5.7	7.8	9.5
outside diameter	13.7	15.3	16.9
height	6.7	7.0	7.0
Specific rotation $[\alpha]_D^{25}$	+150.5	+162.5	+177.4
Color of iodine complex	Blue	Yellow	Yellow
Solubility in water (g/100ml) 25 °C			
Distilled water	14.50	1.85	23.20
Saturated solution of guest compounds			
Cyclohexane	0.22	0.01	0.45
Bromobenzene	2.45	0.04	0.01
Fluorobenzene	1.08	0.06	0.03
p-Cymene	2.74	0.06	0.17
Diethyl ether	3.80	0.61	0.28

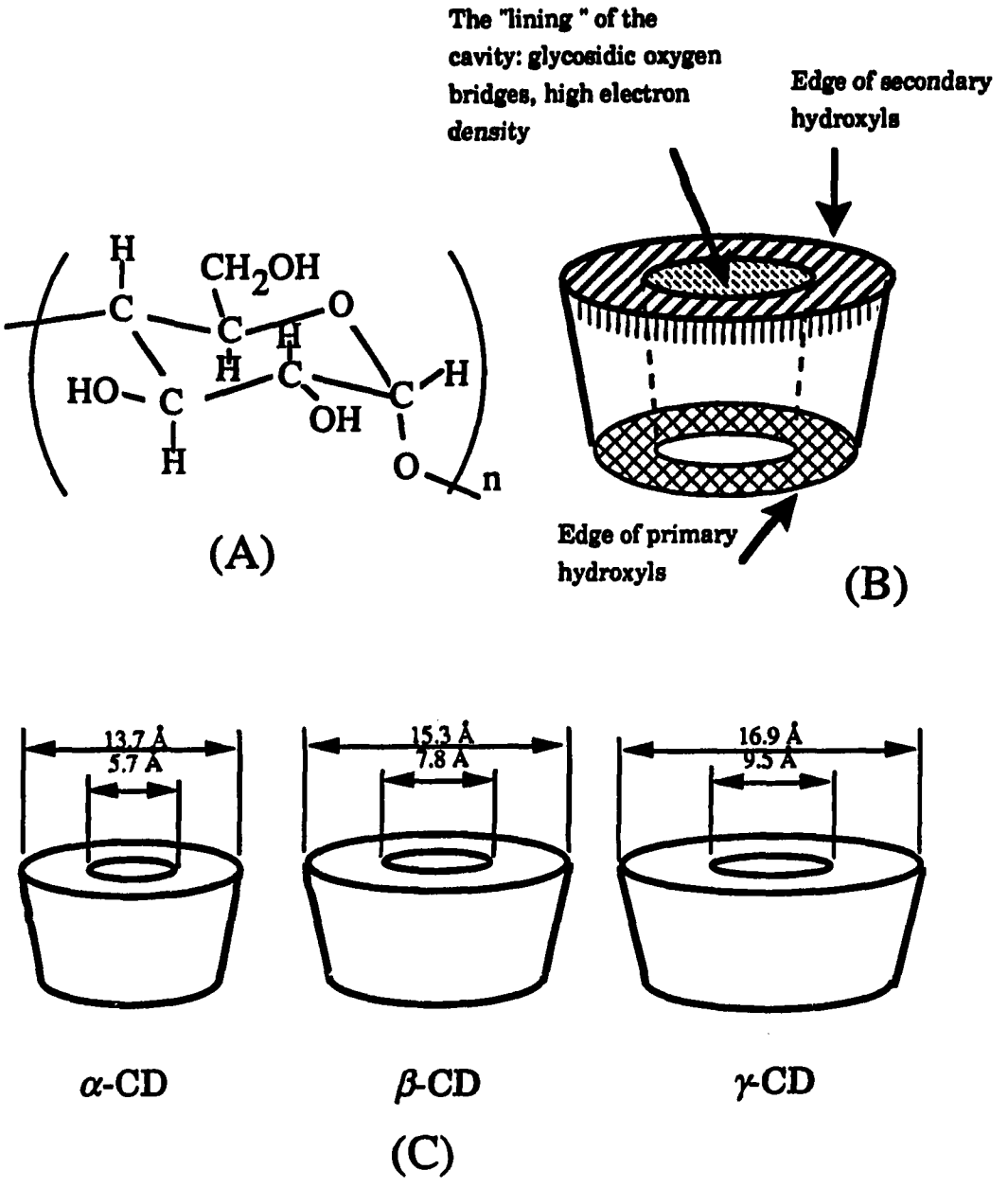

Figure II-3. Structure and size of the cyclodextrins. (a) Chemical structure of individual glucose unit of a cyclodextrin. (b) Functional group characteristics of a cyclodextrin. (c) sizes of cyclodextrins.

amount of stereospecificity. These catalytic powers and stereospecificity, along with its simple structure, have made cyclodextrins ideal candidates as model compounds for studying enzyme reactions [33]. Most enzymes have molecular weights of 20,000-30,000 daltons, but cyclodextrins have molecular weights of ~1000 daltons. Thus, the cyclodextrins bridge the gap between simple organic compounds and larger, more complex enzymes.

To improve or re-direct the catalytic ability of a cyclodextrin, its covalent and noncovalent modifications have been tried in different ways. To increase binding toward a targeted compound, reactive moieties other than hydroxyl groups have been introduced at the rim of a cyclodextrin cavity [34]. Others have capped the cavity, changing its hydrophobicity [35,36].

Analytical application of cyclodextrin

Inclusion properties of cyclodextrins have been utilized extensively in analytical chemistry. Applications in chromatographic separations have been the most prominent area [37]. Cyclodextrins have been used in HPLC [38], TLC [39-41], and gas chromatography [42], mostly as a stationary phase but sometimes as an additive in a mobile phase [43-45]. Recent work in this field has included the covalent bonding of cyclodextrins to a column packing material like silica [46-48]. Not only geometric isomer separation [44] but also stereo isomer including enantiomer separation have been achieved 49,50].

In electrochemistry, only limited amount work has done with cyclodextrins. The adsorption behavior of α- and β- cyclodextrin on dropping mercury electrode has been studied [51-53]. Inclusion complexation reactions between cyclodextrins and other organic guest molecules have also been

investigated [54]. A chromatographic method usually has a large theoretical number of plates for the separation, so requires only a small complexation constant difference to achieve an effective separation. On the other hand, electrochemistry uses a small number of the theoretical plate, which means a huge difference of a complexation constant difference needed to get an effective analysis. One of the early applications of cyclodextrin in electrochemistry appeared in the analysis of *o*- and *p*-nitrophenol mixtures. It has been shown that the *para* isomer complexes preferentially with α-cyclodextrin when α-cyclodextrin is added into a mixture of *o*- and *p*-nitrophenol. Because of complex formation, the apparent diffusion constant of the *para* isomer decreases which, in turn, contributes more negative cathodic peak current potential in a cyclic voltammetry experiment. Without addition of cyclodextrin, a separation in the cathodic peaks between *o*- and *p*-nitrophenol was too small to be observed [55].

Attachment of cyclodextrin moiety on an electrode was also explored with simple adsorption and covalent bonding. Glassy carbon electrodes were oxidized with chromic acid and then, the cyclodextrin was either physically adsorbed by dipping an electrode into α-cyclodextrin solution or by chemical attachment with ester linkage to the electrode surfaces. Selective reduction of *o*-nitrophenol in the presence of *p*-nitrophenol was tested by using these modified monolayers [56]. Regioselective anodic chlorination of anisol was also tested [57], but with only limited success.

Langmuir-Blogett films of cyclodextrins

Langmuir-Blogett film preparations have also been used to incorporate cyclodextrins at surfaces to achieve molecular recognition. Mixed, insoluble

monolayers of amphiphilic cyclodextrins and cholesterol have been studied at the air-water interface. Results showed that cholesterol can be included into only the γ-cyclodextrin cavity [58]. Cis-azobenzene derivatives have been found to be stabilized by amphiphilic cyclodextrins on Langmuir-Blogett trough [59]. Recently, voltammetric sensors responsive to anionic guests were constructed based on LB films deposited on glassy carbon electrodes [60].

Molecular recognition by monolayers

Several groups have attempted to utilize spontaneously adsorbed monolayers to achieve molecular recognition or size exclusion. The Rubinstein group has used an organic sulfide ligand to complex selectively metal ions [61]. They synthesized the 2,2'- thiobisethyl acetoacetate which can complex with Cu^{++}, but not Fe^{+++}, then built an organic monolayer by immersing a gold film into a solution of this compound. By making a mixed monolayer of this compound with octadecanethiol, they observed the selective response of Cu^{++} in the presence of Fe^{+++}. Co-adsorbing octadecanethiol was used to reduce structural defects, which were prevalent if only the 2,2'-thiobisethyl acetoacetate was used to fabricate the monolayer.

The Regen group has published the results of their work on a spontaneously adsorbed assembly of phosphatidylcholine monolayers on gold as a biomembrane model [62]. They extended the permeability studies of lipid bilayers from synthesized phosphocholins. They made several phosphatidylcholine molecules which contain either thiol moiety or the disulfide moiety to be adsorbed via the chemisorption of sulfur onto the gold surface. They found that the monolayer could be formed out of these

compounds and that the layers are densely packed, macroscopically uniform, strongly hydrophilic, and oriented so that the polar head groups extended outward from the surface and the sulfur moieties are in intimate contact with gold [63]. They also prepared various calixarene-derivative monolayers on the air-water interface by the Langmuir-Blogett film method. They carried out water evaporation experiments which revealed the resulting calixarene monolayer maintains a porous structure [64,65].

Another way of cyclodextrin membrane preparation is using an oriented polymer [66]. There is also an unsuccessful report of cyclodextrin membrane-modified electrodes as sensor material [67]. Surprisingly, they reported a -4mV shift on cyclic voltammogram of *p*-nitrophenol at this electrode, whereas no shift was observed in the case of *o*-nitrophenol.

EXPERIMENTAL

General

Solvent

Deionized water was obtained from a Milli-Q purification system (Millipore Products, Bedford, MA). Absolute ethanol (Midwest Grain, Pekin, IL) and hexane (HPLC grade, Fisher Scientific, Pittsburgh, PA) were used as received. Hexadecane (Aldrich Chemical Co., Milwaukee, WI) was passed twice through an activity 1 α-alumina column before use and passed the Zisman test [68,69]. Pyridine (Fischer) was refluxed with and distilled from KOH. Tetrahydrofuran (Fisher) was purified according to the reference [70].

Other chemicals

Sodium hydride (Aldrich, 60% in oil suspension) was rinsed with hexane several times just before use. α-Cyclodextrin and β-cyclodextrin were either purchased from Aldrich or donated by Amazo company, and were freeze dried at -15 ^{o}C (dry ice-acetonitrile bath) for 24 hours before use. No difference was found between material from two sources during the experiments. *o*-Nitrophenol was recrystallized twice from methanol and once from water. 1,4-hydroquinone (Aldrich), 2,3-dimethyl hydroquinone (Aldrich) and catechol (Sigma) were recrystallized from benzene twice.

Synthesis of Chemicals

Methyl sulfonyl bromide

Methyl sulfonyl bromide was synthesized based on the reference [71]. 102 g of zinc powder was suspended in 150g of ice and 150g of deionized

water. Cooled in our ice and sodium chloride bath, 80ml of methyl sulfonyl chloride was added slowly to the Zn powder solution for 2 hours with stirring. The temperature was kept below 5°C throughout the addition. The unreacted zinc was filtered with Buchner funnel, followed by washing with ice water. To the filtered solution, 50 ml of bromine was added while the temperature was kept below 5° C. The product was extracted with chloroform, followed by washing successively with sodium bicarbonate solution and deionized water. After drying over anhydrous sodium sulfate, chloroform was removed in a rotary evaporator. Any remaining oil was vacuum distilled. Measured bp was 74-76°C at 18 mmHg (Reference [70] value: 72-73°C at 14 mmHg).

α-CDBr [72]

Since the synthetic routes to the α-Cyclodextrin and β-cyclodextrin derivatives are similar to each other, only synthesis of β-cyclodextrin derivatives will be described.

To the anhydrous DMF solution of β-cyclodextrin (1 g β-cyclodextrin / 15 ml DMF), six equivalents (for glucose unit of cyclodextrin) of methyl sulfonyl bromide were added dropwise for an hour at 60°C. After the addition, the solution was constantly stirred for 20 hours at room temperature, and the resulting yellow solution was concentrated and coevaporated with toluene with a rotary evaporator. The remaining thin pale yellow syrup was dissolved in methanol and neutralized with 3 M sodium methoxide in methanol. The mixture was poured into an ice water mixture with vigorous stirring. The precipitate was filtered and dried. Measured mp for α-CDBr was 195-196°C (decomp), and mp for β-CDBr was 205-206°C (decomp) which are the same as the reference values [71].

α-CDSH and β-CDSH

All the process below were done under a flushing argon atmosphere. β-CDBr (1.1 g) was dissolved in anhydrous DMF (solution A). In another flask, sodium hydride (140 mg) was suspended in 5 ml of dry DMF and thioacetic acid (400 µl) was added with stirring (solution B). Solution A was added dropwise to the solution B, followed by stirring for 24 hours at room temperature. The solution was poured into 200 ml of a sodium hydroxide solution in an ice bath, stirred vigorously for 5 hours at 40°C, and then cooled in an ice bath. A white precipitate formed upon acidification with 2N hydrochloric acid. After cooling for 4 hours at 0 °C, the white precipitate was filtered and rinsed thoroughly with chilled deionized water. The powder was recrystalized twice and dried at 40 °C in vacuum.

Others

Heptakis-(6-O-mesitylsulfonyl)-β-cyclodextrin was synthesized from a 2,4,6-trimethylphenylsulfonyl chloride and pyridine solution of β-CD according to the reference [64].

The synthesis of β-$CDSC_2$ and β-$CDSC_{12}$ from β-CDBr was performed according to the reference [65].

The synthesis of β-$CDSC_2$ and β-$CDSC_{12}$ from heptakis-(6-0-mesitylsulfonyl)-β–cyclodextrin is described below for β-$CDSC_{12}$. α-$CDSC_2$ and α-$CDSC_{12}$ were synthesized similarly.

100ml of anhydrous DMF was deoxygenated with argon. 1.2 equivalent of sodium hydride was suspended in DMF with stirring. Dodecanethiol 1.0 equivalent was added, followed by addition of 2.89g heptakis-(6-0-mesitylsulfonyl)-β-cyclodextrin. The yellow solution was stirred

at room temperature for 24 hours. The mixture was poured into ice-water and the precipitate was filtered and recrystallized.

Monolayer Preparation

Metal substrate preparation

Metal substrates were prepared by resistive evaporation of 15-20 nm of Cr (0.2 nm/s), followed by 250-300 nm (2.5-3.0 nm/s) of Ag (or Au, 0.6 nm/s) onto 2 inch diameter polished p-type silicon (111) wafers (Virginia Semiconductors, Inc., Fredricksburg, VA). For electrochemical desorption experiment, green mica substrates(1 inch x 3 inch) were used instead of silicon wafer, with Au or Ag evaporated without a Cr layer. The pressure in the cryopumped E360A Edwards Coating System during the evaporation was $<9 \times 10^{-5}$ Pa (7×10^{-7} Torr). After about 45 minutes cooling time, the evaporator was back-filled with purified N_2 and the substrates were removed.

Cyclodextrin monolayer preparation

Cyclodextrin derivatives monolayers were spontaneously adsorbed from dilute (0.01-0.1 mM) solutions in absolute ethanol or tetrahydrofuran onto freshly evaporated Ag or Au substrates on Si. Prior to immersion, the films on mica were annealed in a muffle furnace at 220 °C for 12 hours after the metal deposition. After cooling to room temperature, the metal coated mica was immersed into a chromic acid solution for 15 minutes. The samples were then emersed and rinsed thoroughly with deionized water and ethanol successively. These substrates were then immersed into the dilute solution of cyclodextrin derivatives to make the monolayers. After 24 hours, the samples were emersed, rinsed with absolute ethanol or tetrahydrofuran accordingly,

and spun dry on a photoresist spin-coater (Headway Research, Inc., Garland, TX). We found that the monolayers formed slowly compared to alkanethiols and monolayer density (surface coverage) depended on immersion time up to 10 hours.

Characterization of Monolayers

Ellipsometric measurements of film thickness

Monolayer thicknesses were determined by optical ellipsometry with a computer-interfaced Gaertner Model L-116B Auto Gain ellipsometer operating at a wavelength of 6328Å (He-Ne laser). We assumed that the refractive index of 1.45 [73] to determine the monolayer thicknesses. This value was selected as representative of hydrocarbon phases. Refractive indices between 1.43 and 1.46 resulted in differences less than 3%.

Contact angle measurements

Contact angles between hexadecane or deionized water drops and the monolayer films were obtained in air with a Rame-Hart Model 100-00 goniometer. A 2μL droplet was formed on the substrate (with the needle of a syringe in the droplet) and the volume of the droplet increased slowly. When the boundary between the liquid and substrate advances across a "dry" film, the contact angle measured is an advancing contact angle, θ_a. Receding contact angles, θ_r, are measured when the boundary withdraws as the volume of the droplet decreases. The hysteresis of contact angle (θ_a-θ_r) gives qualitative information on surface roughness and defects. Hysteresis values as large as 30° were observed.

Infrared absorption spectroscopy

Infrared spectra were acquired with a Nicolet 740 FT-IR (Nicolet Analytical Instruments, Madison, WI) spectrometer optimized for grazing angle reflection using p-polarized light incident at 80°. The spectrometer was purged with liquid N_2 boil-off. Spectra were obtained by coaddition of 1024 sample to background scans at 2 cm^{-1} resolution (zero filled) and Happ-Genzel apodization with a liquid N_2 cooled InSb or MCT detectors. All spectra are reported as $-\log(R/R_0)$ where R is the reflectivity of the sample and R_0 is the reflectivity of the bare Au reference substrate.

The bare Au reference wafers were immersed in 1:3 30% H_2O_2:con. H_2SO_4 solution (piranha etch) for 5-10 minutes, rinsed in deionized water and in 30% H_2O_2 successively, and spinned on the photoresist spinner. The nearly-dry reference wafer was placed directly into the spectrometer and allowed to dry completely in the N_2-purged chamber for a few minutes before recording the reference spectrum. An alternative reference which we found successful was the deutrated octadecanethiol monolayer on Au (see Part I of this dissertation). The advantage of this particular method is the elimination of the harsh "piranha etch" solutions, with the reference used reliably for ~2 weeks without further treatment.

Electrochemical measurements

Cyclic voltammetry was performed with either a CV-27 potentiostat (Bioanalytical Systems, Inc., W. Lafayette, IN) or a CYSY-1 Computer Controlled Electroanalytical System (Cypress Systems, Lawrence, KS). The monolayer coated metal substrates were mounted in a conventional three-electrode cell with an exposed electrode area of 0.24 cm^2. Solutions were

deoxygenated with water saturated Ar (Air Products, Allentown, PA) or N_2 (Air Products) for 30 minutes. All potential measurements are reported with respect to a Ag | AgCl | sat'd KCl electrode.

RESULTS AND DISCUSSIONS

Monolayer Formation of Cyclodextrin Derivatives

The general procedure for the synthesis and monolayer formation of the cyclodextrin derivatives is given in Figure II-4. Only α-cyclodextrin derivatives are shown, but the preparation of the β-cyclodextrin derivatives follows the same path. Cyclodextrin derivatives were synthesized with either mesitylsulfonate or bromide as an intermediate. Monolayers were fabricated with the spontaneous adsorption method from ethanol or tetrahydrofuran solutions with cyclodextrin concentrations of 0.1-0.01 mM.

Synthesis of compounds

Generally, mono or multiple tosylates of cyclodextrins were used as the intermediates of synthesis of cyclodextrin derivatives [74]. However, the production of poly(6-O-tosyl)-cyclodextrin in high purity was very difficult as it was always contaminated with by-products such as poly(2,6-di-O-tosyl)-cyclodextrin, poly(3,6-di-O-tosyl)-cyclodextrin or poly(2,3,6-tri-O-tosyl)-cyclodextrin. Therefore, this method inevitably requires column chromatography or other complicated purification techniques. Another disadvantage of this method is that the intermediate poly(6-O-tosyl)-cyclodextrin is partially decomposed by the elevated temperature required in the following step. Generally we found that a high percentage of this intermediate decomposed to give the starting material. To avoid these problems, we used a route in which poly(6-O-mesitylsulfonyl)-cyclodextrin was used as an intermediate to the synthesis of cyclodextrin derivatives. This method [75] did not require separation of an intermediate.

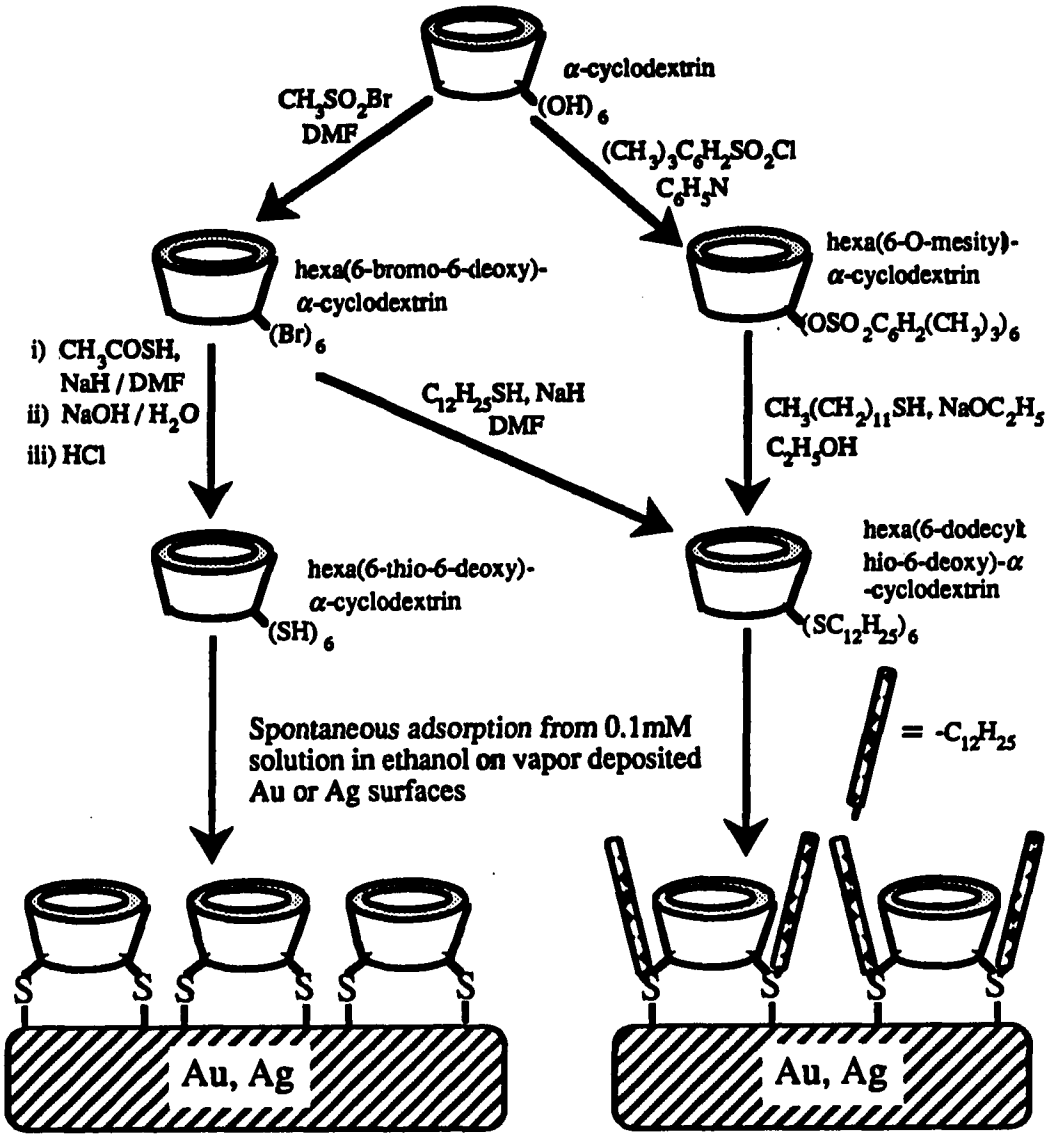

Figure II-4. General strategy to fabricate the monolayers of cyclodextrin derivatives.

The following reaction was used to produce hexakis(6-alkanethio-6-deoxy)hexaglucan(α-1,4), with a similar route for the synthesis of heptakis(6-alkylthio-6-deoxy)hepta-glucan(α-1,4). Treatment of 1 equivalent of dodecanethiolate reacted with hexakis(6-mesitylsulfonyl)hexaglucan(α-1,4) in anhydrous DMF produced hexakis(6-dodecanethio-6-deoxy)hexaglucan(α-1,4). The yield was about 85%.

We also tried to produce the α-CDSH and β-CDSH via the same intermediate, but, were unsuccessful. Meanwhile, Takahashi *et al.* published the synthesis of heptakis(6-alkylthio-6-deoxy)-β-cyclodextrin using β-CDBr as an intermediate [76]. Since this intermediate reacted at very mild conditions and was more versatile for subsequent derivitizations, we switched and used this as an intermediate to other cyclodextrin derivatives. α-$CDSC_{12}$ was produced according to reference [65] and infrared spectra of compounds made of two different intermediates were compared with each other. These spectra were virtually identical. The elemental analysis values were also the same. With α-CDBr intermediate, α-$CDSC_2$, α-$CDSC_{12}$, β-$CDSC_2$ and β-$CDSC_{12}$ were prepared.

We also prepared α-CDSH and β-CDSH using the same intermediate as described below. Thioacetic acid reacted with a stoiochiometric equivalent of sodium hydride in anhydrous DMF solution to produce thioacetate. Addition of 1 glucose unit equivalent of β-CDBr produced the thioacetate of β-cyclodextrin, but no attempt was made to isolate these species. Addition of sodium hydroxide decomposed the thioacetate to produce the cyclodextrin thiolate (β-CDS$^-$Na$^+$) and sodium acetate. The clear solution became turbid with β-CDSH as the solution was acidified with aqueous hydrochloric acid.

The precipitation was completed with cooling in an ice bath for several hours. (These products should not be stored in acidic solution for extended period because of decomposition).

Characterization of reaction product

For the characterization of the reaction products, infrared transmission spectroscopy and elemental analysis were used. The infrared spectrum (KBr pellet) of the α-CD is shown in Figure II-5 (a) along with IR spectra of α-CDSH (Figure II-5 (b)), α-$CDSC_2$ (Figure II-5 (c)), and α-$CDSC_{12}$ (Figure II-5 (d)). Infrared spectra of derivatives of β-cyclodextrin show the same features as those of α-cyclodextrin derivatives. The absorption band at around 2900 cm^{-1} represents the C-H stretching modes of the cyclodextrin. The series of peaks at 1200 cm^{-1} to 900 cm^{-1} correspond to the C-O stretching bands of inter-ring and intra-ring ether linkage of the cyclodextrin unit and to the C-O stretching modes of the primary and secondary alcohols band; however, a more exacting peak assignment is complicated by extensive overlap. All of the cyclodextrin derivatives have retained the C-O stretching modes from 1200 cm^{-1} to 900cm^{-1} region which again shows that the cyclodextrin moiety remains intact. For the alkylthiocyclodextrins (α-$CDSC_2$, α-$CDSC_{12}$, β-$CDSC_2$ and β-$CDSC_{12}$), the increased intensities at 3000 cm^{-1} to 2800 cm^{-1} indicate the inicorporation of the targeted alkyl chain is also incorporated. For the α-CDSH and β-CDSH, there are features representing a SH stretching mode at 2500cm^{-1}. In Figure II-5 (b), this SH mode is shown as a small peak. However, in expanded scale, it is observed as an obvious peak of SH mode.

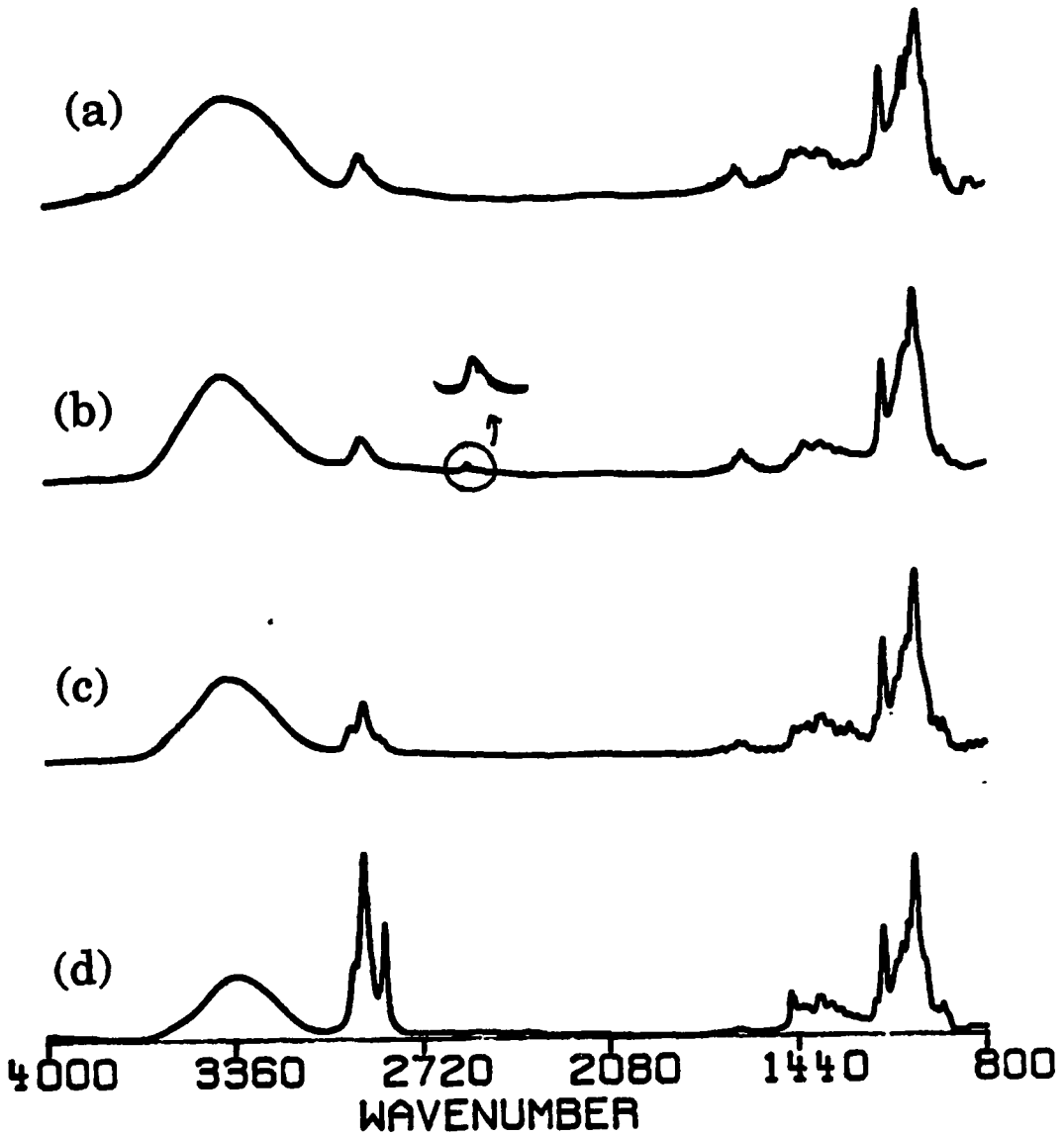

Figure II-5. Infrared spectra of cyclodextrin and derivatives. (a) KBr pellet spectrum of α-cyclodextrin. (b) KBr pellet spectrum of α-CDSH. (c) KBr pellet spectrum of α-$CDSC_2$. (d) KBr pellet spectrum of α-$CDSC_{12}$.

Elemental analysis was performed at the Schwarzkopf Microanalytical Laboratory (Woodside, New York) for the compounds α-CDSH, α-$CDSC_{12}$, β-CDSH, and β-$CDSC_{12}$. The results are listed in Table II-2. The elemental analysis of sulfur results shows a little discrepancy with the calculated value: the experimental values of sulfur contents are a little less than the expected values for the corresponding compounds. There is a possibility that some of the primary hydroxyl groups are not substituted to thiols but remain as alcohols, which will result in less contents of sulfur. Other than sulfur atom, the experimental results agree well with the calculated values.

Characterization of the Monolayer of CD

Ellipsometric characterization

Monolayer fabrication was performed in ethanolic solutions of the compounds studied. The concentration of the compounds in ethanol were extremely low (0.01mM), so at least 24 hours of immersion time was used to insure film formation. Even though a careful study was not performed to examine relationship between the immersion time and monolayer density (coverage), thicknesses for monolayers immersed for less than for 12 hours indicated a more defective structure. Immersion times of 12 to 48 hours did not show any observable thickness differences. To increase the solution concentration, anhydrous tetrahydrofuran (THF) was also used as an adsorption media, which facilitated monolayer formation and required shorter immersion times. Concentrations in THF solution were 0.05mM. The thicknesses of the monolayer films measured with optical ellipsometry are listed in Table II-3. Thicknesses of simpler films are also given for

Table II-2. Elemental analysis results

Compound	Molecular formular	Molecular Weight	% of element found (calculated)			
			C	H	O	S
α-CDSH	$(C_6H_{10}O_4S)_6$	1069.2	40.38 (40.44)	5.73 (5.66)	34.70 (35.91)	15.11 (17.99)
β-CDSH	$(C_6H_{10}O_4S)_7$	1247.4	40.50 (40.44)	5.78 (5.66)	35.64 (35.91)	15.20 (17.99)
α-$CDSC_{12}$	$(C_{18}H_{34}O_4S)_6$	2079.2	62.65 62.39	9.80 (9.89)	19.02 (18.47)	8.92 (9.25)
β-$CDSC_{12}$	$(C_{18}H_{34}O_4S)_7$	2425.7	62.01 (62.39)	9.78 (9.89)	20.10 (18.47)	8.70 (9.25)

Table II-3. Advancing contact angle and ellipsometric thickness of different monolayers.

Monolayer	Adv. Contact Angle $\theta_a(H_2O)$	$\theta_a(C_{16}H_{34})$	Ellipsometric Thickness (Å)
$CF_3(CF_2)_5(CH_2)_2SH/Au$	118	71	---
$CH_3(CH_2)_{11}SH/Au$	111	44	13
$HO(CH_2)_{11}SH/Au$	<10	<10	12
$-CH_2-$ (Polyethylene)	110	<10	---
α-CDSH/Au	35	<10	11
α-CDC_2/Au	73	<10	10
α-CDC_{12}/Au	95	<10	13
β-CDSH/Au	45	<10	10
β-CDC_2/Au	73	<10	8
β-CDC_{12}/Au	95	<10	13
α-CDSH/Ag	23	<10	8
α-CDC_2/Ag	73	<10	10
α-CDC_{12}/Ag	47	<10	13
β-CDSH/Ag	35	<10	8
β-CDC_2/Ag	73	<10	11
β-CDC_{12}/Ag	67	<10	13

comparison. For the monolayers of cyclodextrin derivatives, a refractive index of 1.45 (representative of bulk hydrocarbons) was assumed to calculate the film thickness. Since we do not know the exact refractive index of the films, the reported thicknesses are not absolute, but only approximate. We also built a CPK model of these cyclodextrin derivatives and measured the thickness of the film assuming the molecular axis of the cavity was normal to the surface. Height of the cyclodextrin cavity of the CPK models was 8Å. Comparisons of the values in Table II-3 point to the formation of a surface film that is one molecular layer thick, confirming the formation of a monolayer. In some instances, we found abnormally large thicknesses of cyclodextrinthiols at silver, indicating multilayer formation; we also observed such phenomena for the short chain alkanethiols (C_2H_5SH and C_3H_7SH) at Ag. Multilayer formation was also confirmed by the reflected infrared spectra of these monolayers. Absorption of these layers showed 2 to 10 times higher intensity than that of a "normal" monolayer. These process may result from the corrosion of the silver layer by the thiol moieties but its exact nature is not yet understood.

Infrared spectra of the monolayers

Infrared spectra of the representative cyclodextrin derivative adsorbed at Au and Ag are shown in Figure II-6. The presence of the CO stretching bands between 1250 cm^{-1} and 900 cm^{-1} indicates that the cyclodextrin moiety is adsorbed on the metal surface. α-$CDSC_{12}$ and β-$CDSC_{12}$ show high intensities of CH_2 stretching modes at 2929 and 2850 cm^{-1} on both the Au surface and the Ag surfaces, whereas the intensities of the methyl group stretching modes at 2960 and 2880 cm^{-1} are relatively low. These indicate

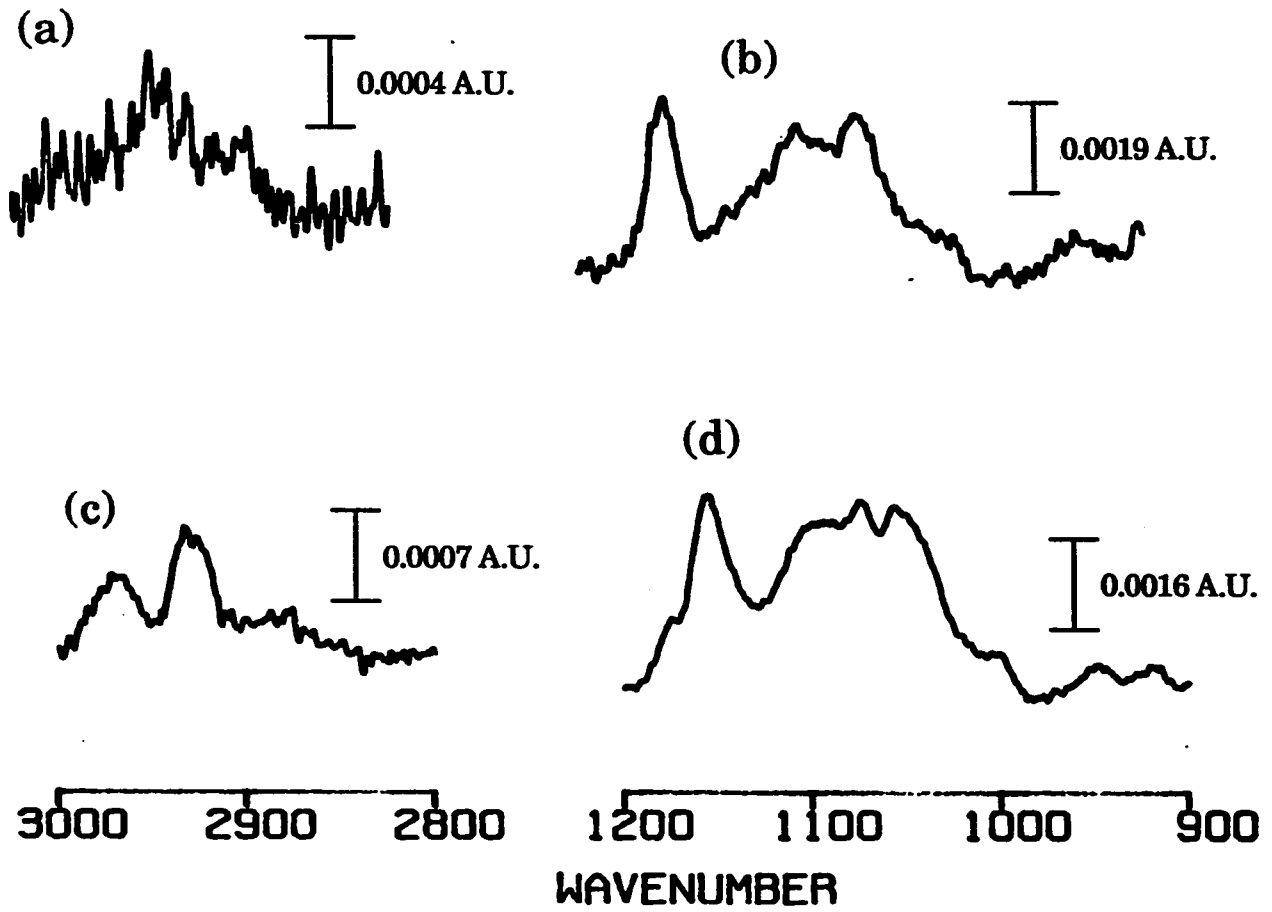

Figure II-6. Infrared reflection spectra of cyclodextrin monolayers. (a) and (b) α-CDSH on Ag, (c) and (d) β-CDSC$_2$ on Au.

that the side alkyl side chains around the cyclodextrin cavity are tilted from the surface normal.

Differences between infrared reflection spectra of α-$CDSC_{12}$ and β-$CDSC_{12}$ on gold surface were also observed. For the α-$CDSC_{12}$ on Au, the CH_3 symmetric stretching mode is much more intense than that of the β-$CDSC_{12}$ on Au. Also the peak position of the CH_2 mode at 2920 and 2869 cm^{-1} for the monolayer of α-$CDSC_{12}$ is down shifted compared to that of the β-$CDSC_{12}$ on Au. These observations can be explained only if we assume that α-$CDSC_{12}$ monolayers are packed better than β-$CDSC_{12}$ monolayers on Au.

Sometimes, when a monolayer was formed in tetrahydrofuran, the reflection infrared spectra indicated the partial retention of the solvent molecules, but extensive rinsing with ethanol removed these peaks. Otherwise, no difference was observed among the different solvents.

Contact angle comparison with other monolayer

Contact angles can be used to probe the hydrophobicity and the roughness of these surfaces, as well as qualitatively indicate composition. For the monolayers of cyclodextrin derivatives, contact angles are tabulated in Table II-3. For comparison, the Table also contains the contact angles for other monolayers. Both α-CDSH and β-CDSH on Au and Ag have very low contact angles. In contrast to the ω-hydroxy thiols, however, the advancing contact angle with water is larger at these two surfaces. This might be due to the fact that the cyclodextrin has the cavity and the inside rim of the cavity is hydrophobic which will increase the contact angle with water. It is also noted that the advancing contact angle increases with the length of alkyl side chain, which is consistant with the intended strucrure of the monolayers.

Electrochemical desorption of thiols

It has been found that *n*-alkanethiols spontaneously adsorbed on gold film that have been evaporated on mica can be desorbed electrochemically in potassium hydroxide solution [77]. Surprisingly, the same compounds adsorbed on gold films on silicon wafers or slide glass substrates, however, do not exhibit this desorption; an observation we do not understand. Figure II-7 shows a representative electrochemical desorption current-potential curve for a thiol on Au/mica substrates. Octadecanethiol (Figure II-7 (a)) shows a sharp peak at -1.2 V vs. Ag/AgCl electrode. For the cyclodextrin thiols adsorbed on mica substrates, the thiol desorption peak (Figure II-7 (b)) is much broad compared to the alkanethiols. If the cyclodextrin thiol monolayer was immersed into a octadecanethiol solution, we also observed that the cyclodextrin thiol was replaced by the octadecanethiol. Figure II-7 (c) and (d) indicate that the octadecanethiol is continually replacing the cyclodextrin thiol film: after 30 min. of immersion in octadecanethiol, there are a desorption peak at -1.0V corresponds to the cyclodextrin thiol, and another peak at -1.1V corresponds to octadecanethiol((Figure (c)); after 2 hours of immersion, the peak of octadecanethiol has been increased and the peak of cyclodextrin has been decreased(figure (d)). The displacement was also found to be largely irreversible. When the octadecanethiol monolayer was immersed into the cyclodextrin thiol solution, there was no difference in the desorption of octadecanethiol monolayer from Au/mica substrate. This is probably a kinetic effect as the displacement of several alkanethiols must occur concertedly to accommodate an incoming cyclodextrin thiols. Since

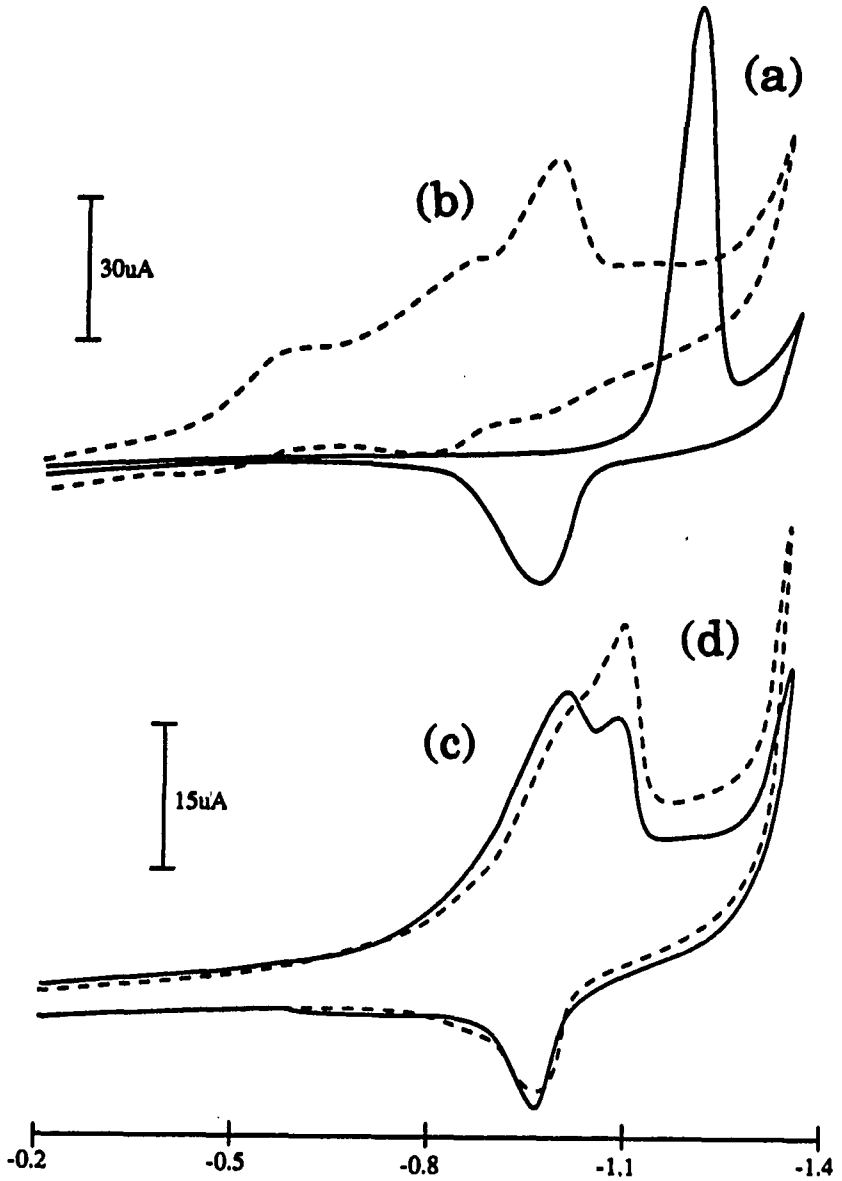

Figure II-7. Cyclic voltammograms (first sweeps) of electrochemical desorption of thiols. (a) octadecanethiol/Au/mica (b) α-CDSH/Au/mica (c) β-CDSH/Au/mica after 30 min. in a octadecanethiol solution (d) β-CDSH/Au/mica after 2 hours in a octadecanethiol solution

octadecanethiols form a defect-free monolayer, this further prevents the approach of cyclodextrin thiol molecule to a "bare" Au surface.

If we assume the one electron transfer reduction is the mechanism of the desorption process for the CD thiols, we can estimate their surface coverage. Integration of the desorption i-E curves indicates coverages between 80 to 100% for the α-CDSH and β-CDSH. Similar attempts have been made for monolayers at silver evaporated mica. As a result of the different head chemistry, the reductive desorption of these monolayers at Ag are negative of solvent reduction, which precluded a coverage estimation.

Orientation and Molecular Recognition of Monolayers

Ellipsometric result for structure of monolayer

To obtain insights into the structure of our cyclodextrin monolayers, the following ellipsometric experiment was performed. If cyclodextrin thiols are oriented with secondary hydroxyl group exposed at the air/film interface and sulfur moiety bound to the metal surface, the secondary hydroxyl group is available to hydrogen bond with other molecular species. If the cyclodextrin is largely tilted from the surface normal, the interface will behave more like a hydrocarbon bearing material. We used a mercaptoetanol monolayer as a model system which presents hydroxyl groups at the air/film interface and dodecanethiol and octadecanethiol which exposes a hydrocarbon moiety at this interface.

α-CDSH, β-CDSH, mercaptoethanol, dodecanethiol, and octadecanethiol monolayers on Au and bare Au were immersed into 0.5 M ethanol solutions of *o*-nitrophenol, *p*-nitrophenol, o- and *p*-nitrophenol

mixture and ADCA. After 1 hour, the substrates were emersed slowly and allowed the remaining solution on the surface to desorb. Ellipsometric thickness differences before and after the immersion were measured, and are listed in Table II-4. At bare gold, the dodecanethiol monolayer and the octadecanethiol monolayer, there was no observable retention of the phenol species. On the other hand, the mercaptoethanol monolayer retained *p*-nitrophenol and ADCA, but not *o*-nitrophenol. α-CDSH and β-CDSH monolayers behave the same as mercaptoethanol monolayer. This retention of *p*-nitrophenol and ADCA is not considered to be solely the result of inclusion complexation. We feel these thicknesses of the retained probe molecules are too large to be explained by 1 to 1 complexation. Furthermore, mercaptoethanol does not form an inclusion complex with *p*-nitrophenol or the adamentane carboxylic acid. Our thickness data show that when there is a hydroxyl group on the surface, the adamentane carboxylic acid and *p*-nitrophenol can be adsorbed on the surface, a result that can be explained by hydrogen bonding between surface hydroxyl groups of monolayer and probe molecules. *o*-Nitrophenol forms an intramolecular hydrogen bond in ethanol, with interactions with monolayer surface hydroxyl groups markedly deminished. However, ADCA and *p*-nitrophenol can not intramolecularly hydrogen bond, and therefore, interact with the surface hydroxyl group of the α-CDSH, β-CDSH, and mercaptoethanol monolayers. The absence of hydroxyl groups with the alkanethiol monolayers precludes binding with the probe molecules. Figure II-8 illustrates the hydrogen bonding in the nitrophenols.

Table II-4. Difference [a] of the ellipsometric thickness

Monolayer	*o*-NP [b],Å	*p*-NP [b],Å	ADCA [c],Å
α-CDSH/Au	0	+10	+7
β-CDSH/Au	+1	+12	+9
$C_{18}H_{37}SH$/Au	0	0	+1
Mercaptoethanol	+1	+16	+17
Bare Au	+1	+2	+2

[a] [Thickness after emersion] - [Monolayer thickness]
[b] *o*-Nitrophenol, *p*-Nitrophenol, 0.5 mM in EtOH
[c] Adamantanecarboxylic acid, 0.5 mM in EtOH

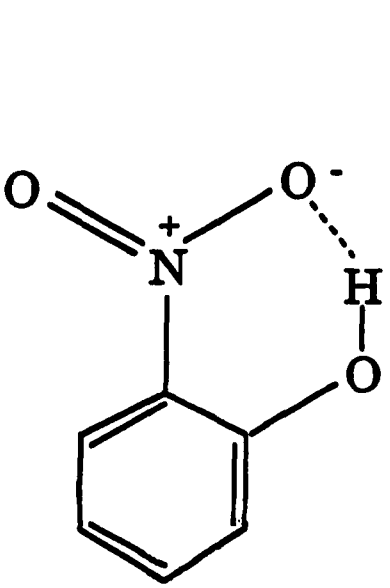

o-nitrophenol

(a)

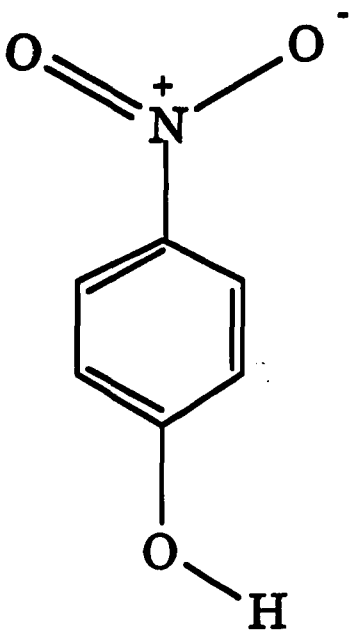

p-nitrophenol

(b)

Figure II-8. Hydrogen bonding of nitrophenols. (a) *o*-Nitrophenol has intramolecular H-bonding. (b) *p*-Nitrophenol has OH group available for intermolecular H-bonding with cyclodextrins.

Athough this experiment does not confirm the presence of molecular recognition of monolayers, it provides valuable information about the orientation of the cyclodextrin monolayers. The retention of the *p*-nitrophenol and ADCA suggests that the α-CDSH and β-CDSH is oriented with its secondary OH group exposed at the air/film interface and that the thiol moiety bound to the metal substrate; this is a structural arrangement, which is consistent with electrochemical desorption data.

Infrared spectroscopic evidence for the selective *p*-nitrophenol adsorption

The complexation of α-cyclodextrins with nitrophenols is well known [28,78]. To test the selective adsorption of *p*-nitrophenol by cyclodextrin monolayers, we obtained the infrared reflection spectra of the monolayers before and after immersion in solutions of *p*-nitrophenol, *o*-nitrophenol, and mixtures of the two. Difference spectra of representative samples are shown in Figure II-9. For comparison, KBr pellet spectra of *o*-nitrophenol and *p*-nitrophenol are shown in Figure II-9 (a) and (b), respectively; the y-axis scale is not shown for these two spectra because it depends on the concentration of KBr pellet. For α-CDSH/Au, as shown in Figure 9 (c) and (d), only p-nitrophenol was retained by the monolayer surface after immersion into separate nitrophenol isomer solutions. The β-CDSH/Au monolayer shows the same behavior. This behavior is consistent when either of these monolayers are immersed into the mixture of two nitrophenol isomers, as the difference spectrum in Figure II-9 (c). The absorbances of the peaks in Figure II-9 (c) are 5-10 times stronger than those expected for a monolayer, which suggests the participation of the hydrogen-bonding mechanism discussed in the above ellipsometric data, and so it is not retained by the cyclodextrin cavity. As

Figure II-9. Infrared difference spectra of monolayers taken after emersed from a nitrophenol solution referenced to the spectrum taken before the dipping. (a) KBr spectrum of *o*-nitrophenol. (b) KBr spectrum of *p*-nitrophenol. (c) difference spectrum of α-CDSH/Au emersed from *p*-nitrophenol/ethanol. (d) difference spectrum of α-CDSH/Au emersed from *o*-nitrophenol/ethanol. (e) difference spectrum of α-$CDSC_{12}$/Ag emersed from *p*-nitrophenol/ethanol. (f) difference spectrum of α-$CDSC_{12}$/Ag emersed from *o*-nitrophenol/ethanol. (g) difference spectrum of $C_{18}H_{37}SH$/Au emersed from *o*- and *p*-nitrophenol mixture /ethanol.

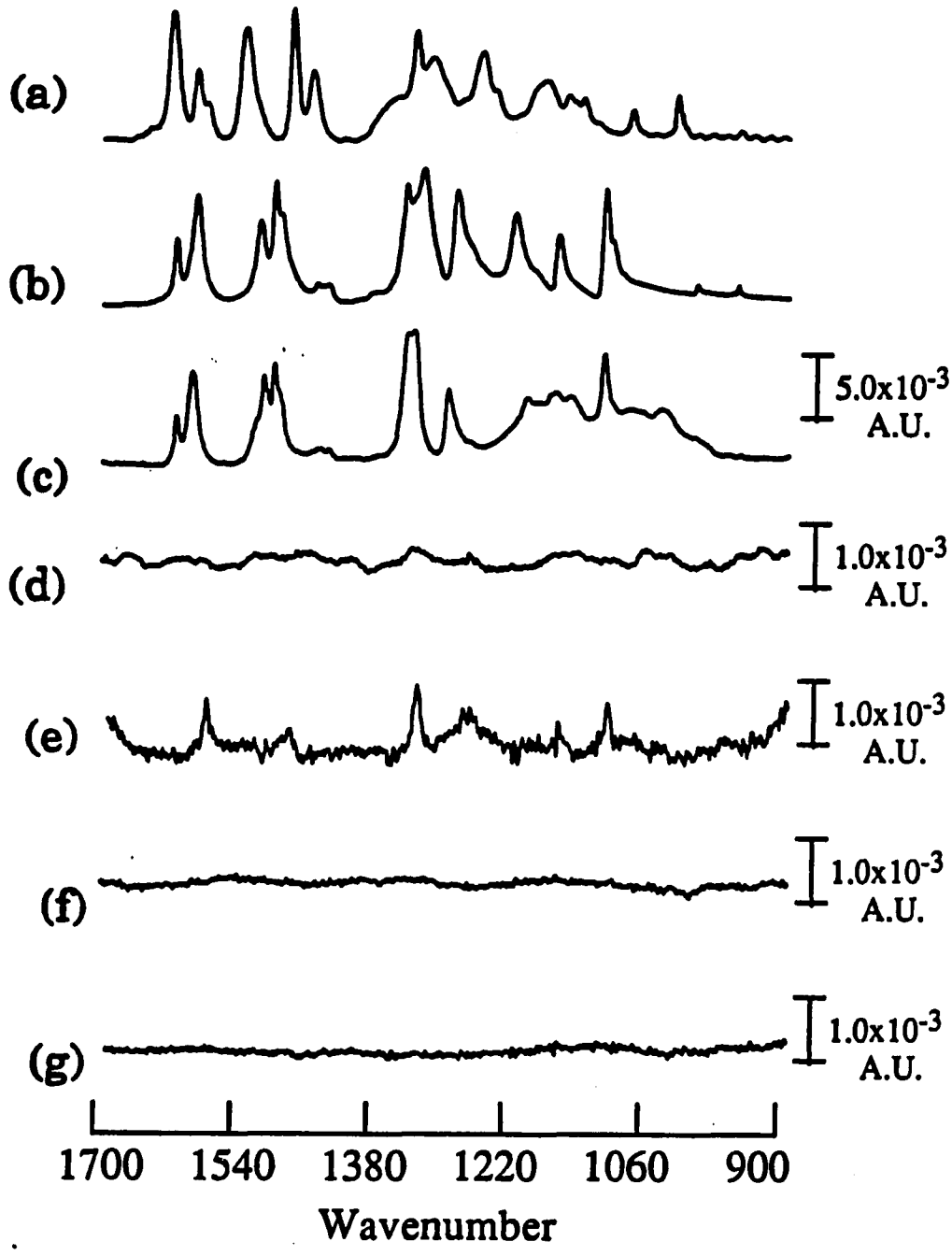
(a)
(b)
(c)
(d)
(e)
(f)
(g)
5.0x10-3 A.U.
1.0x10-3 A.U.
1.0x10-3 A.U.
1.0x10-3 A.U.
1.0x10-3 A.U.
1700
1540
1380
1220
1060
900
Wavenumber

explained before with ellipsometric results, the intramolecular hydrogen bonding of *o*-nitrophenol prohibits retention at the OH terminated interfaces. We believe that *p*-nitrophenol is retained on α-CDSH/Au or β-CDSH/Au monolayers primarily by intermolecular hydrogen bonding. Both nitrophenols are not retained on the alkanethiol monolayers ranging from hexadecanethiol to eicosanethiol. A representative octadecanethiol monolayer difference spectrum is shown in Figure II-9 (g) before and after dipping into the nitrophenol mixture. No observable retention of either nitrophenol isomer was formed. The same result was obtained with dipping into a solution of *p*- or *o*-nitrophenol alone. Surprisingly, nitrophenol was not retained on bare Au surface. The infrared difference spectrum taken after dipping into each of the isomers of nitrophenol is comparable to that in Figure II-9 (g), which also fails to exhibit any observable retention.

The adsorption of *p*-nitrophenol on α-$CDSC_{12}$/Ag, as evidenced by the spectra in Figure II-9 (e) and (f), displays a different behavior. Some of the vibrational modes disappear with several of the peak maxima shifted. To investigate this effect in detail, we calculated the expected spectrum of *p*-nitrophenol as randomly oriented monolayer on the surface based on a KBr spectrum of the compound with average thickness of 2 Å thickness and compared with the experimentally obtained monolayer spectrum. Figure II-10 (a) shows the experimental spectrum of *p*-nitrophenol adsorbed on α-$CDSC_{12}$/Ag monolayer and Figure II-10 (b) shows the calculated spectrum of *p*-nitrophenol. In Figure II-10 (a), we can see that the NO_2 asymmetric vibration mode decreases compared to that of the symmetric NO_2 stretching mode. The C-O stretching modes are preserved. If we consider the structure

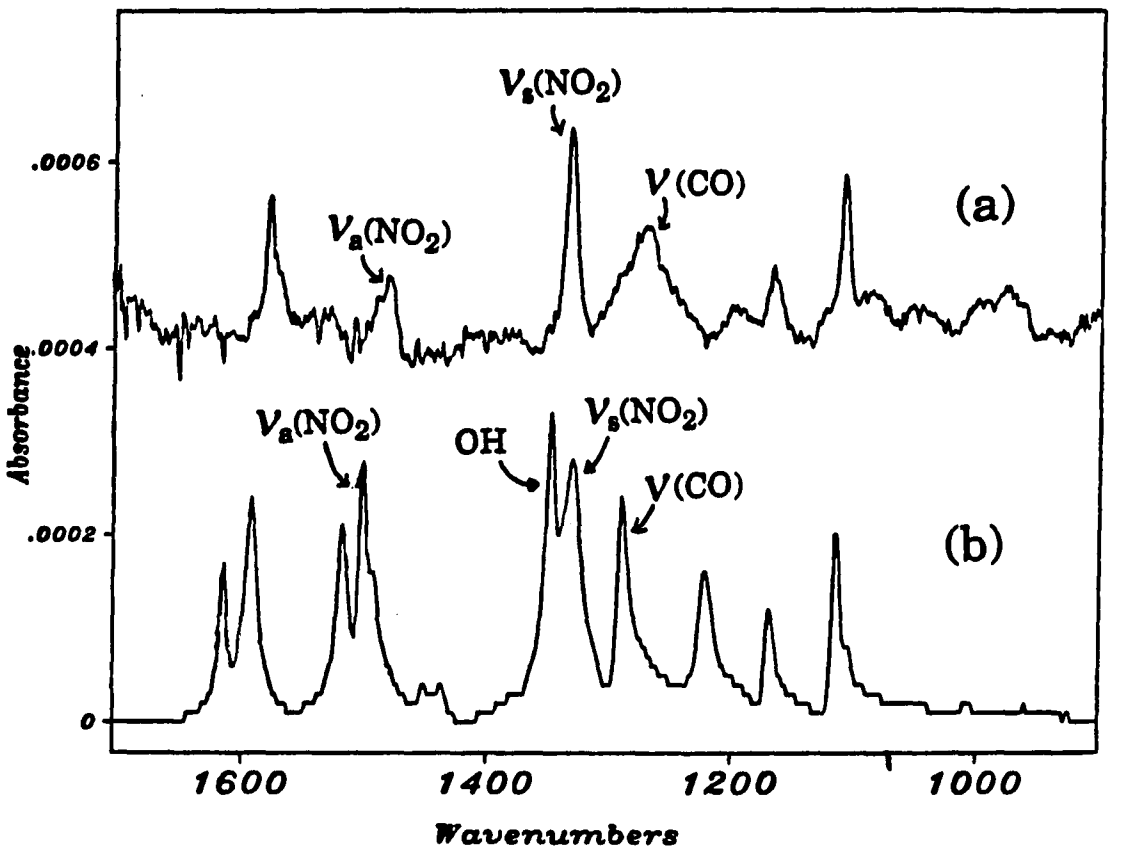

Figure II-10. Calculated and experimental spectrum of *p*-nitrophenol. (a) experimental spectrum on α–$CDSC_{12}$/Ag monolayer. (b) calculated spectrum.

of *p*-nitrophenol in Figure II-11, we note that the transmission dipole moment of the observed peaks is parallel to the molecular axis of the molecule. The disappearance or at least decreased absorbance of the NO_2 asymmetric mode can, therefore, be explained by the infrare surface selection rule [79]. We postulate that the *p*-nitrophenol molecule on α-$CDSC_{12}$/Ag monolayer is oriented with its molecular axis perpendicular to the surface. The same orientation of p-nitrophenol was observed when it was complexed with a α-cyclodextrin in solution [78]. We ascribe the peak shifts to lower energy to complexation in the low dielectric environment of the cavity of α-cyclodextrin.

Electrochemical evidence for the molecular recognition.

Several electrochemical experiments were performed to probe about the properties of our cyclodextrin monolayers. First, we studied the heterogeneous electron transfer of the probe molecules such as $Ru(NH_3)_6^{+3}$, $Fe(CN)_6^{-3}$, and ferrocene carboxylic acid. The results are shown in Figures II-12 and II-13. Properties of the probe molecule are listed in Table II-5. Figure II-12 shows the reversible redox reaction of three probes on bare gold electrode. Figure II-13 shows the behavior of the probe molecules on the α-$CDSC_{12}$/Au electrode. We observed that the electron transfer for the $Ru(NH_3)_6^{+3}$ (Figure II-13 (c)) and $Fe(CN)_6^{-3}$ (Figure II-13 (b)) were inhibited, whereas FCA (Figure II-13 (c)) was relatively uneffected by the presence of the monolayer. As shown in Table II-5, FCA can form an inclusion complex with β-cyclodextrin, whereas $Ru(NH_3)_6^{+3}$ and $Fe(CN)_6^{-3}$ do not. We think this result shows the selective interaction of β-cyclodextrin with FCA. However, since $Ru(NH_3)_6^{+3}$ and $Fe(CN)_6^{-3}$ are highly charged inorganic species and FCA is organic molecule, these results can be explained with the

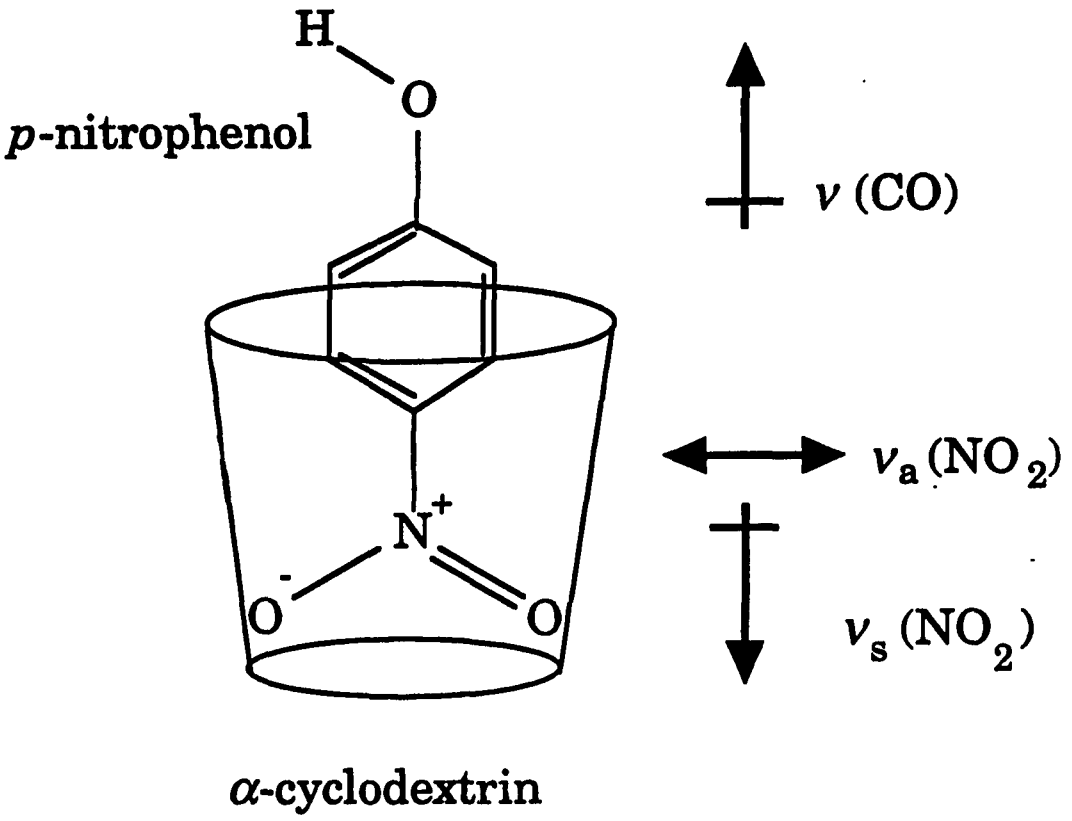

Figure II-11 Orientation of a *p*-nitrophenol molecule in a α-cyclodextrin cavity and the directions of dipole moments of *p*-nitrophenol.

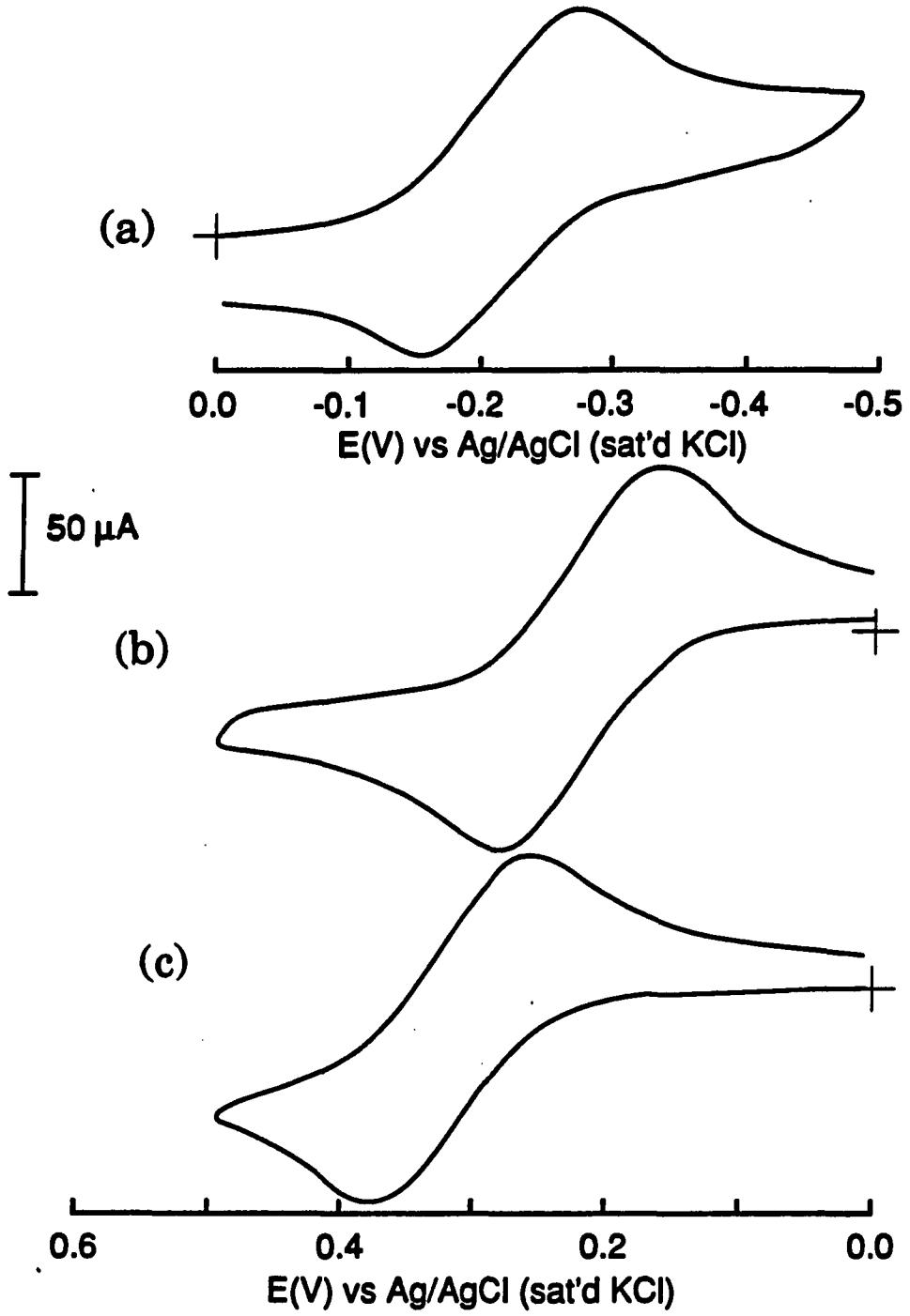

Figure II-12. Cyclic voltammetric current responds vs. applied potential for bare Au. The solutions are (a) 1mM $Ru(NH_3)_6Cl_3$, (b) 1mM $K_3Fe(CN)_6$ and (c) 1mM FCA in 0.1 M Phosphate buffer at pH 6.9

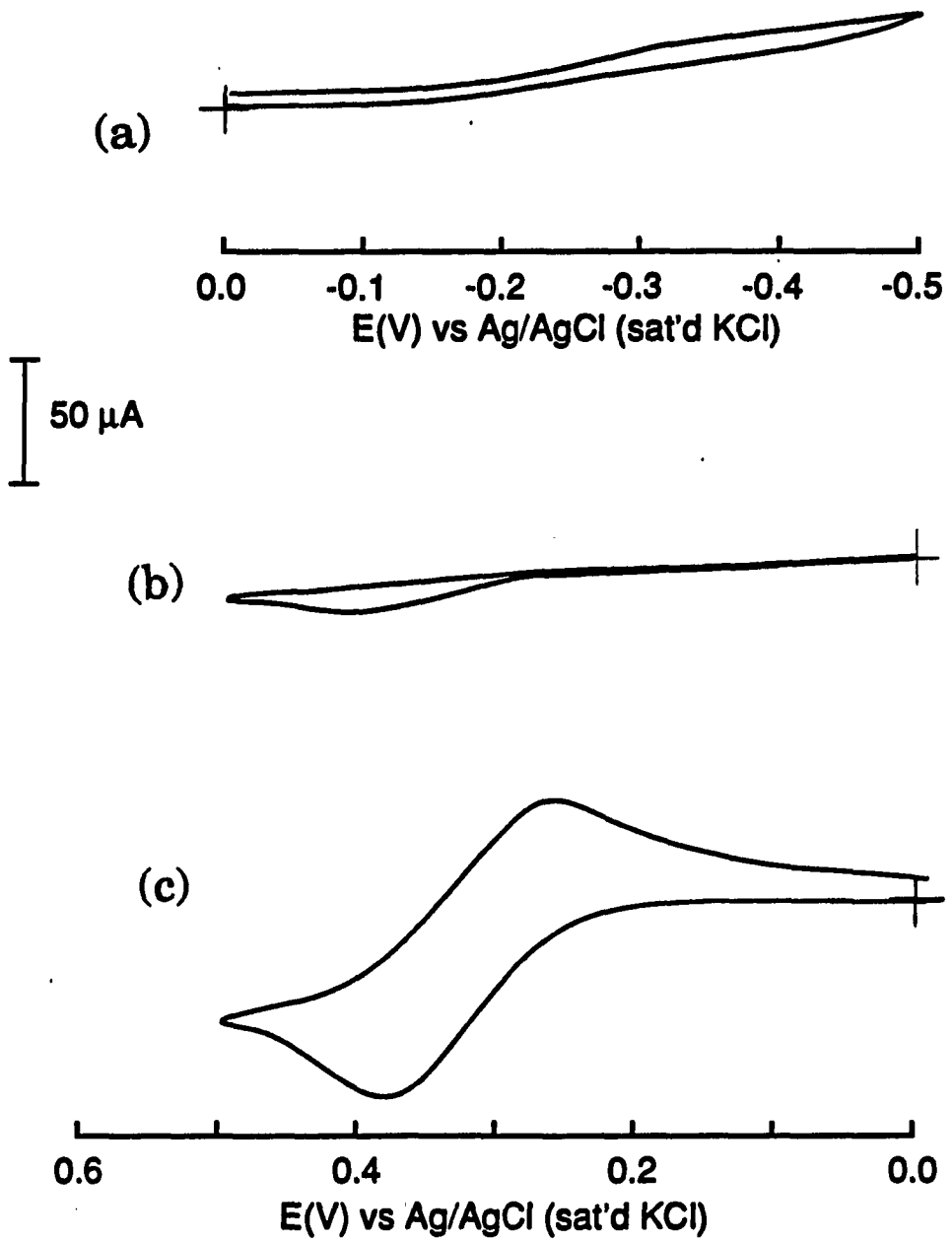

Figure II-13. Cyclic voltammetric current responds vs. applied potential for α-$CDSC_{12}$/Ag electrode. The solutions are (a) 1mM $Ru(NH_3)_6Cl_3$, (b) 1mM $K_3Fe(CN)_6$ and (c) 1mM FCA in 0.1 M Phosphate buffer at pH 6.9

Table II-5. Chemical Probes for Molecular Recognition

Compound	Kf(1/M) [a, b]	Mol.Size	pH
FCA	2100	6.0Å(Cp) [c]	9.2, 7.0
FCA^+	<20		9.2, 7.0
CTAB	$2x10^5$	5.1Å(Alkyl)	sl. basic
SDS	1600	5.1Å(Alkyl)	sl. basic
$Ru(NH_3)_6^{3+}$	d	7.0Å	9.2
$Fe(CN)_6^{3-}$	d	8.8Å	9.2

[a] Kf is a complexation constant.

[b] Kf values are from the references 53,76, and 77.

[c] Cp-Fe-Cp axis is parallel to the axis of CD cavity (6.8A).

[d] No inclusion was observed with UV-VIS spectrometry.

hydrophobic interactions between FCA and β-cyclodextrin. Therefore, we tried the same probe molecules on alkanethiols/Au electrodes. Monolayers of dodecanethiol or longer thiols are insulating to the electron transfer of all three species. Both FCA and $Ru(NH_3)_6^{+3}$ penetrate the thiol monolayers of hexanethiol and shorter thiols. Another interesting result was obtained when we added the surfactant CTAB into the solution of FCA. As shown in Figure II-14 (b), the electron transfer of the FCA probe is not affected up to 3μM of CTAB, but it is gradually prohibited at the CTAB concentration of 5μM or higher. Figure II-14 (c) shows the cyclic voltammogram of FCA in the presence of 0.2 mM CTAB (below the critical micelle concentration of CTAB). CTAB is known to have a larger complexation constant (K_f = 200,000) [53] toward β-cyclodextrin than FCA does (K_f = 2100) [80,81]. At this concentration of CTAB, most of the cyclodextrin cavity will be occupied with CTAB, preventing the penetration of FCA. Unfortunately the reproducibility of these electrochemical experiments was low (~30%). A large percentage (~70%) of the monolayers behave like a bare Au electrode.

We think that the reason behind this low reproducibility is the presence of defects in the monolayer structure. Infrared spectroscopic data is normally give the information about the average structure in the monolayer. In electrochemical experiments, however, diffusion of the analyte in a microelectrode fashion amplifies the presence of structural defects.

Another set of the electrochemical experiments was performed with *ortho-* and *para-* nitrophenols, which are reduced on Ag electrodes covered with α-CDC_{12} and β-CDC_{12}. As shown in Figure II-15 (a), the reduction potential of *o*-nitrophenol was shifted for both α-CDC_{12}/Ag and β-CDC_{12}/Ag

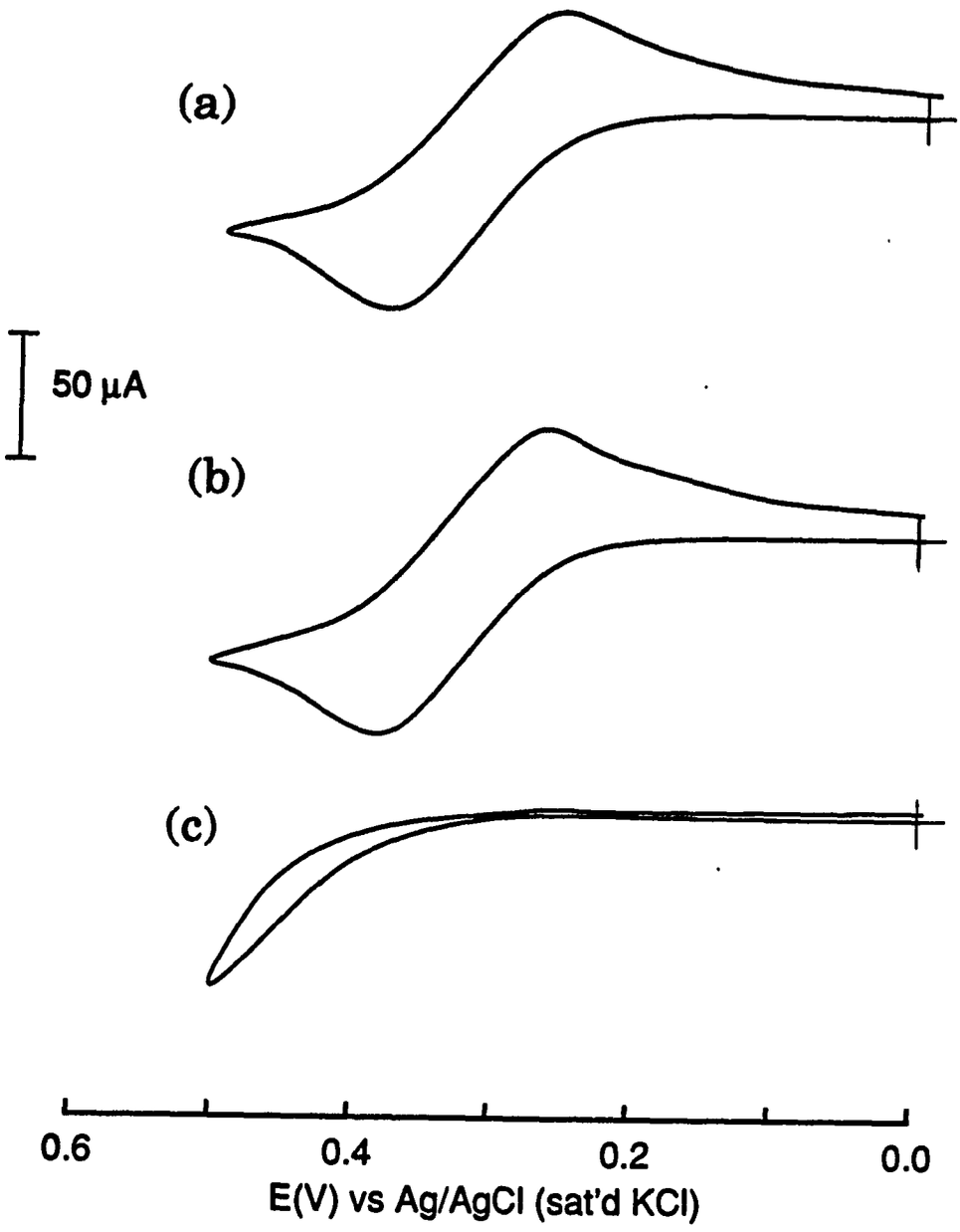

Figure II-14. Effect of CTAB on current responds vs. applied potential for α-$CDSC_{12}$/Ag electrode. (a) 1mM FCA only, (b) 1mM FCA with 3 μM CTAB, (c) 1mM FCA with 0.2 mM CTAB.

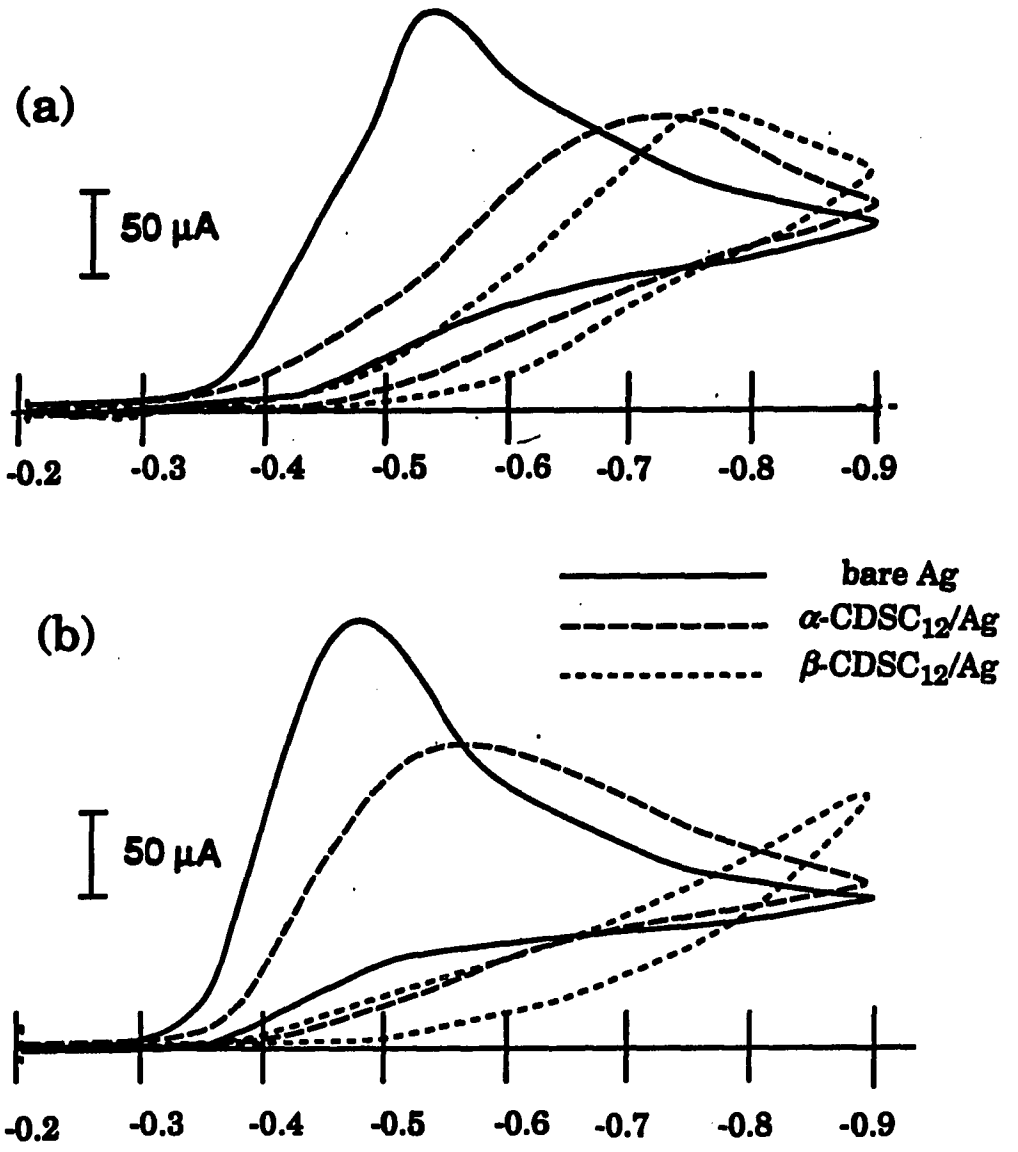

Figure II-15. Cyclic voltammetry of nitrophenols on bare Ag, α-$CDSC_{12}$/Ag and β-$CDSC_{12}$/Ag electrodes. (a) *o*-nitrophenol. (b) *p*-nitrophenol.

electrodes. The reduction peak shift of the *p*-nitrophenol is drastically different on α-CDC_{12}/Ag electrode and β-CDC_{12}/Ag electrode, as shown in Figure II-15 (b). It is thought that both α-CDC_{12}/Ag and β-CDC_{12}/Ag electrodes are acting as a thin barrier to the electron transfer of *o*-nitrophenol reduction. This is the same for the *p*-nitrophenol reduction on β-CDC_{12}/Ag electrode. A strong binding of the α-cyclodextrin with *p*-nitrophenol produces an inclusion complex which is known to be electrochemically inactive [52]. This complex will act as a thicker barrier to the electron transfer of *p*-nitrophenol reduction, producing further peak shift for α-CDC_{12}/Ag electrode. Similar phenomena were reported with a cyclodextrin epitaxial polymer electrode [64].

Electrochemical evidence for the size selectivity

Cyclodextrin has different size cavity depending on the number of glucosidic units. To investigate the size selectivity between α-cyclodextrin and β-cyclodextrin monolayers, electrochemical reduction-oxidation reactions of 1,4-hydroquinone, catechol, and 2,3,-dimethyl hydroquinone were studied with bare Au, α-CDC_{12}/Au, β-CDC_{12}/Au, and octadecanethiol/Au electrodes. For 1,4-hydroquinone (Figure II-16), catechol (Figure II-17), and 2,3-dimethyl-hydroquinone (Figure II-18), the α-CDC_{12}/Au electrode was a more efficient electron transfer barrier than β-CDC_{12}/Au electrode. Monolayers of alkanethiols with comparable film thickness were insulating to the electron transfer of the three probe molecules. Representative electrochemical responses of an octadecanethiol/Au electrode are shown in each Figure as a reference. These results suggest the following explanation. The cyclodextrin monolayers are porous. It is not known if the electrochemical redox reaction

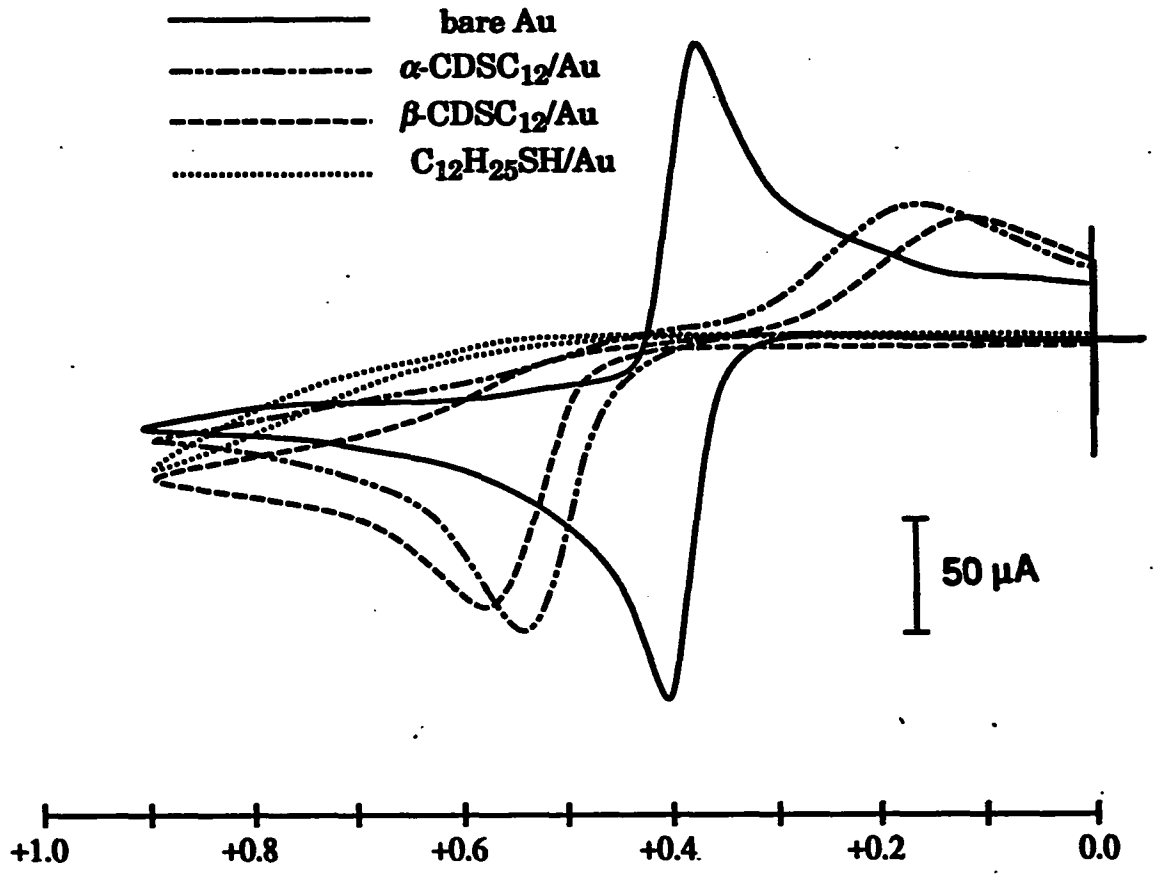

Figure II-16. Electrochemical response of 1,4-hydroquinone on bare Au, α-$CDSC_{12}$/Au, β-$CDSC_{12}$/Au and dodecanethiol/Au electrodes.

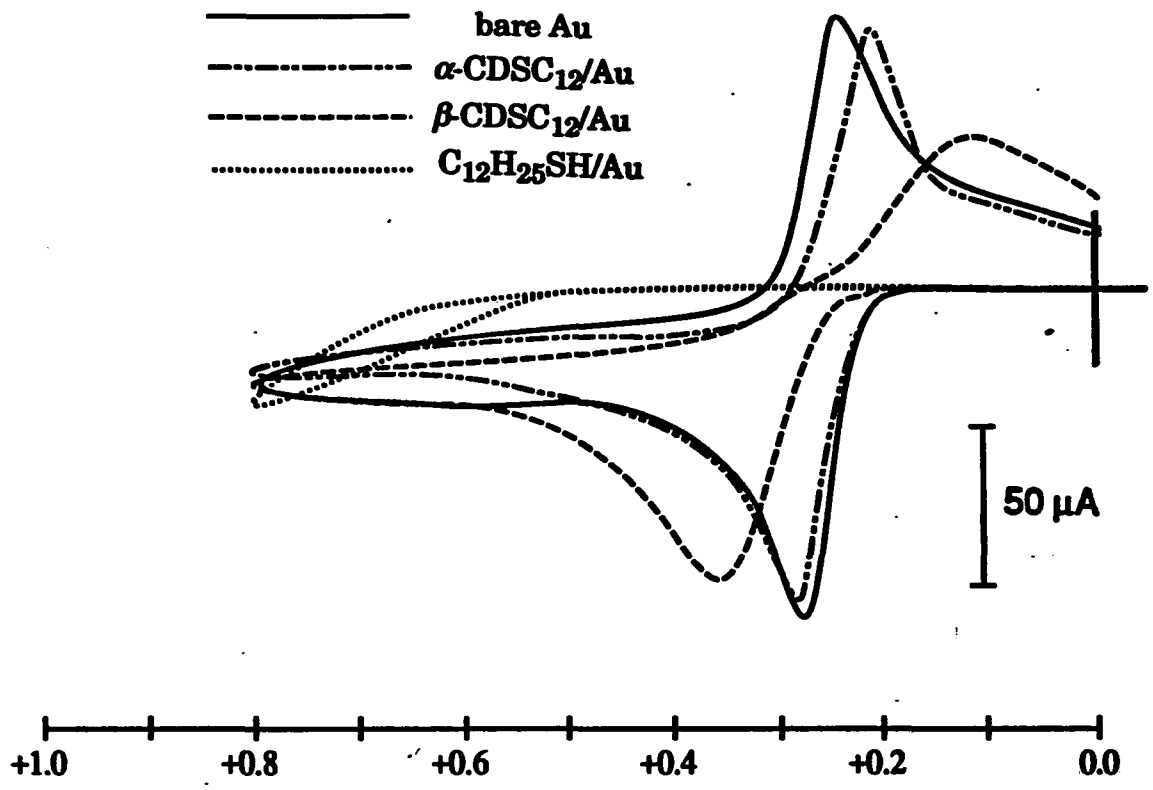

Figure II-17. Electrochemical response of catechol on bare Au, α-$CDSC_{12}$/Au, β-$CDSC_{12}$/Au and dodecanethiol/Au electrodes.

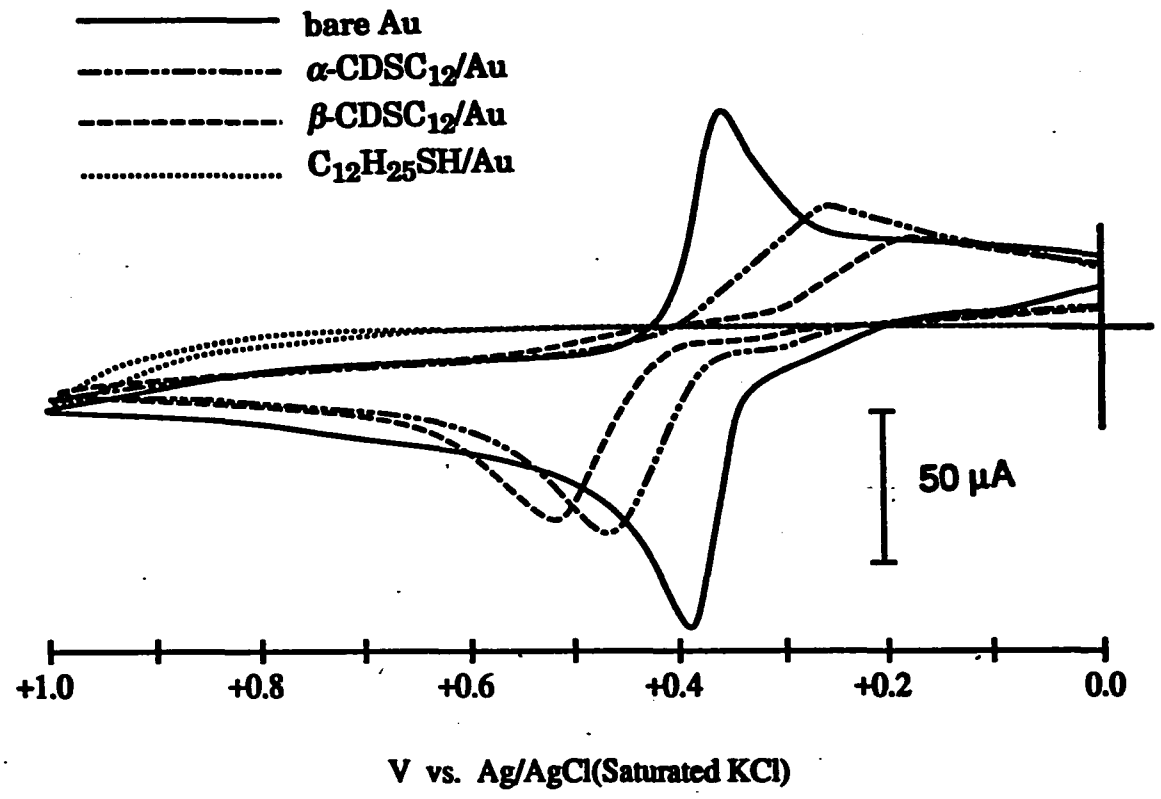

Figure II-18. Electrochemical response of 2,3,-dimethylhydroquinone on bare Au, α-$CDSC_{12}$/Au, β-$CDSC_{12}$/Au and dodecanethiol/Au electrodes.

occurs through random defect sites between the cyclodextrin molecules or the throgh cyclodextrin cavity. α-CDC_{12}/Au electrode has a smaller cavity compared to the β-CDC_{12}/Au electrode, so it is more difficult for the probe molecules to approach the electrode surface of the α-CDC_{12}/Au electrode than to the β-CDC_{12}/Au electrode. This trend was also observed with other probe molecules such as naphtoquinone (not shown). UV-VIS spectroscopy and electrochemistry were used to measure the complexation constant between α-cyclodextrin and probe molecules, 1,4-hydroquinone, catechol, and 2,3,-dimethyl hydroquinone. Since none of the above compounds show complexation in solution phase with α-cyclodextrin or β-cyclodextrin, the above phenomena is thought to be the size selectivity of the cyclodextrins. For a β-cyclodextrin monolayers with a larger cavity, the probe molecules can approach closer to the electrode surfaces than for a α-cyclodextrin monolayers with a smaller cavity.

Comparison with Other Monolayers

Experimental results support the monolayer formation of the six compounds studied in this work both on gold and silver surfaces. In case of alkanethiol studied in the Part I, the monolayers behaved quite differently on gold and silver surfaces. No significant difference was observed for the cyclodextrin monolayer on gold and silver surfaces. One of the reason for this might be that the reproducibility of cyclodextrin monolayer is significantly lower than the case of the alkanethiols. We can easily expect that the alkanethiol makes very densely packed monolayer. For the cyclodextrin derivatives, their bulky structures and binding mechanisms prevent densely packed monolayer formation. For α-$CDSC_{12}$ and β-$CDSC_{12}$ monolayers, alkyl

side chains are tilted from the surface rather than normal to the surface. The relatively low intensity of the CO stretching mode and the large absorbance of the CH_2 mode in the IR spectra of monolayers support this assumption. In case of the cyclodextrin thiol monolayers, we can assume that both the α- and β-CDSH are densely packed. The electrochemical desorption data support this conclusion. This result shows that α-CDSH and β–CDSH on gold evaporated mica substrate are near monolayer coverage. Although we could not desorb the α-CDSH and β-CDSH on silver surfaces, we believe our assumption of monolayer coverage because the IR absorbance of the monolayers on gold and silver are comparable within experimental error.

Emersion experiments using infrared spectroscopy and optical ellipsometry support that the structure of cyclodextrin thiol is such that the secondary hydroxyl group of the cyclodextrin is exposed on the surface and thiol group is sticking on the surface. The head group interactions with metal surfaces are also proved by electrochemical desorption, which can be explained only in case where at least 5 thiol groups should interact with gold surface to give the experimental desorption charge density.

In this work, the presence of molecular recognition is more evident in infrared spectroscopic results compared to electrochemistry. Electrochemical measurement shows a degree of molecular recognition. The reproducibility of these latter experiments, however, is very low. Though both infrared spectroscopy and electrochemistry can provide information about the surface coverage of monolayer, the detailed information can be quite different. Infrared spectroscopy is not sensitive to a small quantity of defects of the monolayer because it probes only the majority of the monolayer. On the other

hand, electrochemistry is sensitive to small amounts of monolayer defects. For example, if there is 5 % of a defect in the monolayer, the IR response will be 95% of the perfect layer. Diffusion of the analyte in a microelectrode fashion amplifies defects in the electrochemistry experiments.

CONCLUSIONS

We have synthesized several sulfur-bearing cyclodextrin derivatives. We have fabricated spontaneously adsorbed monolayer films of these compounds on silver and gold surfaces. Characterization of these monolayers was performed by use of optical ellipsometry, infrared reflection spectroscopy, contact angle measurement, and electrochemistry. It has been found that these compounds are spontaneously adsorbed by sulfur atom with the cavity axis normal to the surfaces For α-CDSH and β-CDSH on Au/mica, surface coverages were determined to be 80-100 %. These coverage was calculated by electrochemical reductive desorption experiments. The specific orientation of *p*-nitrophenol on the cyclodextrin monolayers and selective adsorption of *p*-nitrophenol over *o*-nitrophenol onto the cyclodextrin molecules indicate the molecular recognition due to the cyclodextrin cavity. This molecular recognition is also supported by the electrochemical measurements. Size exclusion is also demonstrated with an electrochemical method. The lack of reproducibility of electrochemical measurements also shows that the cyclodextrin monolayers have defects.

Further improvement for the molecular recognition by the cyclodextrin derivatives or any other monolayers should utilize the defect-free monolayers. The study of cross-linking among the monomer molecules or the proper mixed monolayers may be useful to improve the quality of these layers.

Substitution of the secondary hydroxyl group of cyclodextrins derivatives monolayer with carboxylic acid or amine could control the

complexation behavior of the cyclodextrin cavity depending on solution pH, so it might be possible to make chemical amplifiers based on these compounds. Also, a Langmuir-Blogett film has different characteristics compared to the spontaneously adsorbed monolayers, such an approach may prove useful.

To achieve the molecular recognition, the proper orientation of the cyclodextrin on the surface is essential. To improve the packing of the cyclodextrin moiety, atomically smooth surface will be beneficial. Also adding a long "leg" between the cyclodextrin and sulfur moiety will facilitate cyclodextrin packing on the metal surfaces.

REFERENCES

1 A. W. Adamson, Physical Chemistry of Surfaces, 4th ed., Wiley: New York, 1982; Chapter 10.

2 W. A. Zisman, In Handbook of Adhesives; I. Skeist, Ed., Van Nostrand: New York, 1977; Chapter 3.

3 J. I. Bregman, Corrosion Inhibitors, Macmillan: New York, 1963; pp. 197-212.

4 B. D. Ratner, In Biomaterials: Interfacial Phenomena and Applications, S. L. Cooper and N. A. Cooper, Eds., Advances in Chemistry 199, American Chemical Society: Washington, D. C., 1982; pp. 9-23.

5 F. P. Bowden and D. Tabor, The Friction and Lubrication of Solids, Part II., Oxford University Press: London, 1968; Chapter 19.

6 R. G. Nuzzo and D. L. Allara, *J. Am. Chem. Soc.*, 1983, 105, 4481-4483.

7 M. D. Porter, T. B. Bright, D. L. Allara, and C. E. D. Chiedsey, *J. Am. Chem. Soc.*, 1987, 109, 3559-3568.

8 R. G. Nuzzo, F. A. Fusco and D. L. Allara, *J. Am. Chem. Soc.*, 1987, 109, 2358-2368.

9 M. W. Walczak, C. Chung, S. M. Stole, C. A. Widrig, and M. D. Porter, in preparation.

10 E. B. Troghton, C. D. Bain, and G. M. Whitesides, *Langmuir*, 1988, 4, 365-385.

11 C. D. Bain and G. M. Whitesides, *Science*, 1988, 240, 62-63.

12 E. Sabatani, I. Rubinstein, R. Maoz and J. Sagiv, *J. Electroanal. Chem.*, **1987**, 219, 365.

13 G. L. Gaines, Insoluble monolayers at liquid-gas interfaces, Wiley-Interscience: New York, **1966**.

14 T. Ohnishi, A. Ishitani, H. Ishida, N. Yamamoto, and H. Tsubomura, *J. Phys. Chem.*, **1978**, 82, 1989.

15 D. L. Allara and J. Swallen, *J. Phys. Chem.*, **1982**, 86, 2700.

16 J.F. Rabolt, F. C. Burnes, N. E. Schlotter, and J. D. Swallen, *J. Chem. Phys.*, **1983**, 78, 946.

17 P.-A. Choller, *Thin Solid Films*, **1978**, 52, 343.

18 R. Maoz and J. Sagiv, *J. Coll. Interface Sci.*, **1984**, 100, 465.

19 N. E. Sclotter, M. D. Porter, T. B. Bright, and D. L. Allara, *Chem. Phys. Lett.*, **1986**, 132, 93-98.

20 J. Gun, R. Iscovici and J. Sagiv, *J. Coll. Interface Sci.*, **1984**, 101, 201.

21 W. C. Bigelow, D. L. Pickett, and W. A. Zisman, *J. Coll. Interface Sci.*, **1946**, 1, 513.

22 E. E. Polymeropoulos and J. Sagiv, *J. Chem. Phys.*, **1978**, 69, 1836.

23 D. L. Allara and R. G. Nuzzo, *Langmuir*, **1985**, 1, 52.

24 P. R. Moses, L. Wier, and R. W. Murray, *Anal. Chem.*, **1975**, 47, 1882.

25 M. L. Bender and M. Komiyama, Cyclodextrin Chemistry, Springer-Verlag: New York, **1978**.

26 P. C. Manor and W. Saenger, *J. Am. Chem. Soc.*, **1974**, 96, 3630-3639.

27 M. R. Eftink, M. L. Andy, K. Biystrom, H. D. Perlmutter and D. S. Kristol, *J. Am. Chem. Soc.*, **1989**, 111, 6765-6772.

28 Y. Inoue, T. Okuda, F.-H. Kuan, and R. Chujo, *Carbohydr. Res.*, **1984**, 129, 21-32.

29 Y. Kotake and E. G. Janzen, *J. Am. Chem. Soc.*, **1989**, 111, 5138-5140.

30 T. Osa, T. Matsue, and M. Fujihara, *Heterocycles*, **1977**, 6, 1833-1839.

31 T. Matsue, T. Osa, and D. H. Evans, *J. Inclusion Phenomena*, **1984**, 2, 547-554.

32 Marketing Briefs from Amazo company.

33 R. Breslow, *Science*, **1982**, 218, 532-537.

34 Y. Kitaura and M. L. Bender, *Bioorg. Chem.*, **1975**, 4, 237.

35 I. Tabushhi, K. Shimokawa, N. Shimizu, H. Shirakata, and K. Fujita, *J. Am. Chem. Soc.*, **1976**, 98, 7855-7856.

36 J. Emert and R. Breslow, *J. Am. Chem. Soc.*, **1975**, 97, 670-672.

37 W. L. Hinze, *Separation and Purification Methods*, **1981**, 10, 159-237

38 A-E.Hamid, N. Ahmed, and S. M. El-Gizawy, *Analyst*, **1989**, 114, 571-573.

39 W. L. Hinze and D. W. Amstrong, *Anal. Lett.*, **1980**, 13, 1093-1104.

40 D. W. Amstrong and G. Y. Steine, *J. Am. Chem. Soc.*, **1983**, 105, 2962-2964.

41 A. Alak and D. W. Armstrong, *Anal. Chem.*, **1986**, 58, 582-584.

42 W. A. Konig, P. Mischnick-Lubbecke, B. Brassat, S. Lutz, and G. Wenz, *Carbohydr. Res.*, **1988**, 183, 11-17.

43 K. Fujimura, T. Ueda, M. Kitagawa, H. Takayanagi, and T. Ando, *Anal. Chem.*, **1986**, 58, 2668-2674.

44 J. Debowski and D. Sybilska, *J. Chromatogr.*, **1986**, 353, 409-416.

45 J. Zukowski, D. Sybilska, and J. Jurczak, *Anal. Chem.*, **1985**, 57, 2215-2219.

46 K. Fujimura, T. Ueda, and T. Ando, *Anal. Chem.*, **1983**, 55, 446-450.

47 M. Tanaka, Y. Kawaguchi, and T. Shono, *J. Chromatogr.*, **1983**, 267, 285-292.

48 D. W. Amstrong and W. DeMond, *J. Chromatogr. Sci.*, **1984**, 22, 411-415.

49 W. L. Hinze, T. E. Riehl, D. A. Amstrong, W. DeMond, A. Alak, and T. Ward, *Anal. Chem.*, **1985**, 57, 237-242.

50 D. A. Amstrong, W. DeMond, and B. P. Czech, *Anal. Chem.*, **1985**, 57, 481-484.

51 Y. Matsui, H. Sawada, K. Mochida, and Y. Date, *Bull. Chem. Soc. Jpn.*, **1975**, 48, 3446-3449.

52 Z. Borkowska, *J. Electroanal. Chem.*, **1988**, 246, 423-431.

53 R. Jaworski, M. Goledzinowski, and Z. Galus, *J. Electroanal. Chem.*, **1988**, 252, 425-440.

54 R. Palepu, J. E. Richardson, and V. C. Reinsborough, *Langmuir*, **1989**, 5, 218-221.

55 T. Matsue, M. Fujihara, and T. Osa, *Anal. Chem.*, **1981**, 53, 723-726.

56 T. Matsue, M. Fujihara, and T. Osa, *J. Electrochem. Soc.*, **1982**, 129, 1681-1685.

57 T. Matsue, M. Fujihara, and T. Osa, *J. Electrochem. Soc.*, **1981**, 128, 1473-1478.

58 S. Taneva, K. Ariga, and Y. Okahata, *Langmuir*, **1989**, 5, 111-113.

59 H. Niino, A. Yabe, A. Ouchi, M. Tanaka, Y. Kawabata, S. Tamura, T. Miyasaka, W. Takaki, H. Nakahara, and K. Fukuda, *Chem. Lett.*, **1988**, 1227-1230.

60 S. Nagase, M. Kataoka, R. Naganawa, R. Komatsu, K. Odashima, and Y. Umezawa, *Anal. Chem.*, in press.

61 I. Rubinstein, S. Steinberg, Y. Tor, A. Shanzer, and J. Sagiv, *Nature*, **1988**, 332, 426.

62 J. Stefely, M. A. Markowitz, and S. L. Regen, *J. Am. Chem. Soc.*, **1988**, 110, 7463-7469.

63 W. Fabianowsky, L. C. Coyle, B. A. Weber, R. D. Granata, D. G. Castner, A. Sadownik, and S. L. Regen, *Langmuir*, **1989**, 5, 35-41.

64 M. A. Markowitz, R. Bielski, and S. L. Regen, *J. Am. Chem. Soc.*, **1988**, 110, 7545-7546.

65 M. A. Markowitz, R. Bielski, and S. L. Regen, *Langmuir*, **1989**, 5, 276-278.

66 H. Hirai, M. Komiyama, and H. Yamamoto, *J. Inclusion Phenom.*, **1984**, 2, 655.

67 M. Komiyama, *Angewandte Macromolekulare Chemie* , **1988**, 163, 205-207.

68 W. A. Zisman, *J. Chem. Phys.*, **1941**, 9, 534.

69 W. A. Zisman, *J. Chem. Phys.*, **1941**, 9, 729.

70 D. D. Perrin, W. L. F. Armarego, and D. R. Perrin, Purification of laboratory chemicals, 2nd Ed., Pergamon Press Ltd.: New York. **1980**.

71 G. Sieber, *Ann.*, **1960**, 631, 180-184.

72 K. Takeo, T. Sumimoto, and T. Kuge, *Staerke,* **1974**, 26, 111-118.

73 Handbook of Chemistry and Physics, Ed., R. C. Weast, CRC: Boca Raton, FL, **1981**.

74 S. Umezawa and K. Tatsuta, *Bull. Chem. Soc. Jpn.,* **1968**, 41, 464-468.

75 H. Kurita and M. Kawazu, *U.S. Patent,* **1976**, 3,974,274.

76 H. Takahashi, Y. Irinatsu, M. Tsujimoto, S. Kozuka, and W. Tagaki, *Nippon Kagaku Kaishi,* **1987**, 293-299.

77 C. A. Widrig, C. Chung, and M. D. Porter, in preparation.

78 Y. Inoue, T. Okuda, Y. Miyata, and R. Chujo, *Carbohydr. Res.*, **1984**, 125, 65-76.

79 R. G. Greenler, *J. Chem. Phys.*, **1966**, 44, 310.

80 T. Matsue, D. H. Evans, O. Osa, and N. Kobayashi, *J. Am. Chem. Soc.*, **1985**, 107, 3411.

81 T. Matsue, M. Suda, I. Uchida, T. Kato, U. Akiba, and T. Osa, *J. Electroanal. Chem.*, **1987**, 234, 163.

CONCLUSIONS

We have utilized a multi-technique approach to unravel the structure of *n*-alkanethiols and sulfur-bearing cyclodextrin derivatives on Ag and Au.

The orientation of the monolayer at Ag and Au is strongly dependent on the substrate crystallinity and nature of the metal-sulfur bond. The infrared reflection spectroscopy, contact angle measurement, capacitance measurement, and ellipsometric data allow us to propose a model describing the average orientation and structure of alkanethiol monolayers on Ag and Au.

Fabrication and characterization of several cyclodextrin derivatives were studied. Potential application of cyclodextrin derivatives monolayer, such as size exclusion and molecular recognition, is demonstrated with several probe molecules.

Further development of in situ technique is expected to characterize the detailed structure in the solution phase during the spontaneous adsorption process. Refinement of the defect free monolayers is also expected to achieve better molecular recognition.

ACKNOWLEDGEMENT

I have been quite lucky to have many people around me to offer the kinds of help that I needed. So this acknowledgement has to be a lengthy one.

I thank Dr. Marc Porter for his guidance and patience throughout my stay in the group not only for the academic achievement but also for the personal life. His sincere concern made all of the transition from one group to another tolerable, which might have been a disaster.

Dr. Dennis Johnson deserves special thanks for his guidance and encouragement as a co-major advisor. Thanks are extended to the other committee members, Drs. Sam Houk, Walter Trahanovsky and David Lewis for their advice.

I thank my dear group members (Cindra, Scott, Mary, Tom, Carla, Darwin, Chau, Wu, Earl, and Randy). Without their help and discussions, this work would have not been possible.

My high school teacher, Dr. In-Kil Lee, drove me to this career as a chemist, and Dr. Tae-Young Lee guided me through undergraduate and graduate school at Seoul National University. I really appreciate their guidance.

All the friends both in Korea and in Ames deserve acknowledgement. Especially, the members of the Society of Korean Studies kept me awake in social conscience throughout the graduate work.

It might be true that the expectation of a large family (Grandpa, Grandma, Dad, Mom, Chinsook, Chinsung, all the uncles, and aunts) could be

more pressure than encouragement, but their moral support throughout this period is really appreciated. Most of all, I owe a great deal of thanks to my wife, Eunkyung, and son, Jooyoung.